ULTRA-THIN MULTIBAND LINEAR AND CIRCULAR POLARIZATION CONVERTER BASED ON METAMATERIAL

Fadi ALAHMED ALBASRY

Master of Science Thesis
Department of Electrical and Electronics Engineering
Asst. Prof. Gokhan OZTURK
2022

R.T.
ATATURK UNIVERSITY
INSTITUTE OF SCIENCES
DEPARTMENT OF ELECTRICAL AND ELECTRONICS ENGINEERING
ELECTROMAGNETIC FIELDS AND MICROWAVE TECHNIQUE DEPARTMENT

ULTRA-THIN MULTIBAND LINEAR AND CIRCULAR POLARIZATION CONVERTER BASED ON METAMATERIAL

(Metamalzeme Temelli Ultra Ince Çok Bantli Lineer ve Dairesel Polarizasyon Dönüştürücü)

Master of Science Thesis

Fadi ALAHMED ALBASRY

Supervisor: Asst. Prof. Gokhan OZTURK

Erzurum
August, 2022

FEN BİLİMLERİ ENSTİTÜSÜ
Graduate School of Natural and Applied Sciences

T.R.
ATATÜRK UNIVERSITY
Graduate School of Natural and Applied Sciences Diretorate
THESIS ACCEPTANCE AND APPROVAL REPORT

Ultra-thin Mutliband Linear and Circular Converter Based on Metamaterial

This study, prepared by Fadi Alahmed Albasry under the supervision of Asst. Prof. Gokhan Ozturk, was accepted by the following jury on 07/09/2022 as a Master of Science thesis in the department of Electrical and Electronics Engineering, on the field of Electromagnetic Fields and Microwave Techniques, with unanimous / majority of votes (3/3).

Chairman of the Jury:	Asst. Prof. Muhammed Fatih Corapsiz *Ataturk University*	Aslı Islak İmzalıdır
Advisor:	Asst. Prof. Gokhan Ozturk *Ataturk University*	Aslı Islak İmzalıdır
Jury Member:	Asst. Prof. Yunus Kaya *Bayburt University*	Aslı Islak İmzalıdır

The Institute's
Administrative Board
..../.../.... date and
decision number......

I certify that this thesis fulfills the conditions specified in the relevant articles of Atatürk University Graduate Education Regulation.

Prof.Dr. Saltuk Buğrahan CEYHUN

Enstitü Müdürü

Aslı Islak İmzalıdır

FEN BİLİMLERİ ENSTİTÜSÜ
Graduate School of Natural and Applied Sciences

T.R.
ATATÜRK UNIVERSITY RECTORATE
GRADUATE SCHOOL OF NATURAL AND APPLIED SCIENCE DIRECTORATE

ETHİCAL STATEMENT AND PLAGIARISM REPORT FORM

As a master of science thesis, we declare that the study titled " Ultra-thin Multiband Linear and Circular Converter Based on Metamaterial ", presented under the consultancy of Asst. Prof. Gokhan Ozturk, was written by us in accordance with scientific ethical principles, that the works benefited from are shown in the bibliography, that the Turnitin Program similarity rates determined by the Institute of Science are not exceeded, and that they are at the following rates.

Parts of Thesis	Thesis Similarity Rate (%)	Maximum Acceptable Rate (%)
Introduction	6%	**30**
Theoretical Foundations	4%	**30**
Material and Method	11%	**35**
Research Findings and Discussion	0%	**20**
Conclusions and Recommendations	0%	**20**
General Thesis	6%	**25**

Note: *Similarities up to seven words and Title, Bibliography, Table of Contents, Acknowledgments, Index and Appendices can be excluded fromo the turnitin report. In addition to the maximum similarity rates given above, the similarity rates from a single source must not be greater than 5%.*

We declare that the information provided is correct and we accept the legal responsibilities that may arise otherwise.

Writer of the Thesis (Student)	Advisor of the Thesis
Fadi Alahmed Albasry	Asst. Prof. Gokhan Ozturk
07.09.2022	07.09.2022
Sign: Aslı Islak İmzalıdır	Sign: Aslı Islak İmzalıdır

* If there is an obstacle for the thesis to be published in YÖKTEZ, please fill in the field below.

☐ Submitted patent application related with the thesis / due to the continuation of the patent process, access to the thesis was blocked for 2 (two) years by the Institute's Administrative Board …./…/…. date and ………….. number decision.

☐ Access to the thesis was blocked for 6 (six) months by the Institute's Administrative Board …./…/…. date and ………….. number decision.

ACKNOWLEDGEMENTS

First and foremost, I like to sincerely thank my supervisor Asst. Prof. Gokhan Ozturk for his constant support of my master’s study and research, as well as for his tolerance, inspiration, passion, and vast knowledge. His advice was helpful to me throughout the entire research and thesis-writing process process. For my master’s study, I could not have asked for a greater advisor and mentor. I also wish to thank my committee members Asst. Prof Fatih Corapsiz and Asst. Prof. Yunus Kaya for giving my defense a pleasant experience.

Additionally, I want to thank my colleagues M.E Fatih Tutar and M.E Ahmad Nusari for their support, advices and suggestions. Further, I wand to thank all the assistant professors and professors at Ataturk university for their efforts to graduate highly qualified engineers.

My mother and my father, as well as my family as a whole, deserve the major thanks for their unwavering support and patience as I undertaked and wrote my porject. You prayed for me, and that’s what got me this far.

I wouldd want to end by thanking Allah for steering me through all of the difficultie.

Fadi ALAHMED ALBASRY

ABSTRACT

MASTER OF SCIENCE THESIS

ULTRA-THIN MULTIBAND LINEAR AND CIRCULAR POLARIZATION CONVERTER BASED ON METAMATERIAL

Fadi ALAHMED ALBASRY

Supervisor: Asst. Prof. Dr. Gokhan OZTURK

Purpose: The goal of this work is to achieve maximum polarization efficiency in multi-frequency bands within the minimum volume of a metamaterial converter.

Method: CST Microwave Studio and MATLAB programs were used as simulation programs to calculate the polarization converter techniques within the scope of this thesis. Polarization conversion ratio was computed analytically using the S parameters obtained with the simulation results.

Findings: Two metamaterial-based polarization converters are proposed in this study. The first one could perform both linear and circular polarization conversion in the X and Ku bands. The other could provide linear and circular polarization conversion in the K and Ka bands. Both of the proposed converters are designed to be ultra-thin in thickness.

Results: The polarization converters proposed in this study literally have both ultra-thin thickness and wide angle performance than other polarization converters in the related operating bands. They also show higher performance in terms of cost-effective bandwidth.

Keywords: Metamaterials, Stoke’s Parameters, circular polarization, linear polarization, wave polarization.

August 2022, 87 pages

ÖZET

YÜKSEK LİSANS TEZİ

ULTRA İNCE ÇOK BANTLI DAİRESEL VE LİNEER METAMALZEME POLARİZASYON DÖNÜŞTÜRÜCÜ

Fadi ALAHMED ALBASRY

Danışman: Dr. Öğr. Üyesi Gökhan ÖZTÜRK

"Elektromanyetik dalga polarizasyonu" terimi, uzayda sabit bir noktada salınan elektrik alan bileşeninin zamanı hesaba katarak oryantasyonunu karakterize eder. EM dalgasının yönü, bir polarizasyon dönüştürücüsü ile değiştirilebilir. Askeri sistemlerde radar kesitinin en aza indirilmesi, anten tasarımı, yarım ve çeyrek dalga plakaları dahil, mikrodalgadan terahertz domain EM dalga polarizasyon dönüştürücülerinin sayısız kullanımı, onların önemini gösterir. Bir radyo bağlantısının sonucu olarak antenler doğal olarak polarizasyona meyilli olduklarından, polarizasyonu bozucu veya bozucu olmayan dikey yönde hareket ettirerek polarizasyonu arttırılabilir veya azaltılabilir. Aynı zamanda hem iletim hem de alım için tek bir anten kullanan monostatik radarlar için de kullanılırlar. Polarizasyon dönüştürücüler mükemmel polarizasyon gerektiren sensörler, anten, radar, optik iletişim dahil olmak üzere çeşitli endüstrilerde kullanılmaktadırlar.

Geleneksel olarak elde edilen polarizasyon dönüşümü, doğal olarak oluşan kristallerde çift kırılma olgusunun yardımıyla gerçekleştirilir ve moleküler düzeyde anizotropi mevcuttur. Bu kristallerin zayıf anizotropisi, büyük hacmi, açıya bağlı polarizasyon tepkisi ve önemli güç kaybı geleneksel yöntemlerin pratik uygulamalarda kullanılmalarını engeller. Ek olarak, bu teknikler, faz hesaplaması ve büyük yayılma mesafeleri için özel ekipman gerektirir. İki yarıya ayrılan ışık ışınları, kelimenin tam anlamıyla çift kırılma olarak adlandırılır. Çift görüntü görünümü veren bu ayırma, çift kırılmalı malzemelerde doğal olarak oluşur. Dielektriklerde dönüşüm optiği kullanılarak oluşturulan bir cihaz yapıldığında, çift kırılma sıklıkla istenmeyen bir yan etki olarak ortaya çıkar. Dielektriklerde, polarizasyon tipik olarak bu dezavantajların dikkate alınmadığı durumlarda uygulanır. Son yıllarda polarizasyon dönüştürücüler, bu dezavantajların üstesinden gelmek için metayüzey yapıları kullanılarak gerçekleştirilmektedir. Metayüzeyler, dar hacimlere sahip dalga altı periyodik bir yapıları ile dikkatleri üzerinde çekmektedir. Metayüzey polarizasyon dönüştürücüler mikrodalga, terahertz, kızılötesi ve görünür ışık bandı dahil olmak üzere çeşitli frekanslarda yüksek rezonans özellikleri ile gerçekleştirilmiştir. Geniş bant, düşük profil, geniş açı ve son derece ince metayüzey polarizasyon dönüştürücüler mikrodalga alanında dikkatleri üzerine çekmektedir. Metayüzey temelli yansıtıcı ve iletim modlu polarizasyon dönüştürücüler olarak iki gruba ayrılırlar. Yansıtıcı modlu polarizasyon dönüştürücülerde metal sonlandırmalar oluşturulduğu için metayüzeyden yansıyan dalganın polarizasyonunu dönüştürülürken, iletim modlu polarizasyon dönüştürücülerde metal sonlandırma olmadan iletilen dalganın polarizasyonunu dönüştürülür. Ayrıca metayüzey polarizasyon dönüştürücüler, dönüştürme deneylerinde kullanılan dalga polarizasyonunun türüne bağlı olarak dairesel ve lineer olmak üzere çeşitlenmiştir. Lineer polarizasyondan dairesel polarizasyona dönüşüm yapılan (LP-CP) çalışmalarında, polairzasyon dönüştürücüler elektrik alanı dairesel bir yönde yansıtılırken, lineerden lineere dönüşüm yapılan (LP-LP) yansıtıcı çalışmalarında elektrik alanın yönü 90 derece kayar. Metayüzey kullanılarak, LP-LP dönüştürme cihazları için tasarımlar polarizasyon dönüşüm oranı (PCR), bant aralığı, geliş açısı, kalınlık ve mikrodalga frekans bölgesi üzerinde yoğunlaşmıştır. Bu cihazların pratik kullanımı için, tasarımın birim hücre hacimleri ve kalınlıkları çok önemlidir. Ek olarak, LP-LP önemli çok yollu sönümleme, yüksek iyonosferik kayıplardan muzdarip olduğundan ve antenlerin yönüne bağlı olduğundan, LP-CP bazı özel mikrodalga uygulamalarında tercih edilir. Ayrıca, LP-CP dönüştürücüler uydu iletişiminde, anten

yönelimlerinin zorluklarını aşmak ve bu anten yönelimleri olmadan veri akışını sağlamak için kullanılır.

1967'de Moskova fizik ve teknoloji enstitüsünden Sovyet fizikçisi Victor Veselago, metamalzemeler için ilk teorik modeli önerdi. Veselago araştırması, solak malzemelerin ürettiği negatif kırılma fenomenini tahmin etmek için yöntemler üretmenin yanı sıra malzemeler için teorik modelleri keşfetmeyi içeriyordu. Bu malzemeler hem negatif elektriksel geçirgenliğe hem de negatif manyetik geçirgenliğe veya çift negatif geçirgenliğe sahip malzemelerdi.

Önümüzdeki otuz yıl boyunca, metamalzemeleri etkin bir şekilde tasarlamak ve üretmek için gereken kurucu malzemeler ve hesaplama gücü eksik olduğundan, bunlar ağırlıklı olarak soyut kalacaktı. Metamalzemelerin çerçevesi teorik düzeyde geliştirilirken, mikrodalga mühendisliğinin ilgili alanı ve anten tasarımına uygulanması II. Dünya Savaşı'ndan sonra hızla gelişmeye başladı. 1950'lerde ve 1960'larda yapay dielektriklerin gelişimi, özellikle anten tasarımı için mikrodalga radyasyonunu şekillendirmek için yeni yollar açmaya başladı. Yapay dielektrikler, metamalzemelere benzer iletken olmayan bir matriste düzenlenmiş iletken şekil dizilerinden veya parçacıklardan oluşan malzemelerden oluşur. Yapay dielektrikler, bir dielektrik malzeme gibi davranan belirli bir elektromanyetik tepkiye sahip olacak şekilde tasarlanmıştı. 1990'ların sonunda, meta-materyalleri teoriden gerçeğe taşımaya yönelik ilk girişimler ortaya çıkmaya başladı ve bunları oluşturan köklü ilkeler, devam eden araştırmaların odak noktası olmaya devam edecekti.

İngiliz teorik fizikçi John Pendry, kısa sürede MM'lerin özelliklerini kavramdan gerçeğe getirerek çok önemli bir katkıda bulunacaktı. Pendry, malzemenin mikrodalga emiliminin, yapıldığı karbonun kimyasal yapısı tarafından değil, liflerin uzun şekli tarafından yönlendirildiğini keşfetti. Bu gözlemden Pendry, bir malzemenin yerel yapısını belirli bir radyasyon bandından daha küçük ölçeklerde değiştirerek, o malzemenin radyasyonla etkileşimini değiştirebileceğini fark etti. Bu gözlemden metamalzeme terimi, doğal olarak meydana gelenin ötesine geçen özelliklerden dolayı türetilmiştir. Pendry, bu konsepti, geleneksel bir manyetik maddenin özelliklerini taklit edebilecek bir döngülü kompozit malzeme (Yarık Halka Rezenatörleri) fikrini doğurdu. Bu döngüler, boyutlarına ve geometrilerine bağlı olarak belirli manyetik tepkiler yaratarak etkin bir şekilde ayarlanabilir manyetik rezonatörler haline gelmektedir. Pendry'nin ürettiği malzeme, malzeme bilimlerinde daha önce görülmemiş bir şeydi. Bir malzemenin elektriksel ve manyetik tepkisini etkili bir şekilde nasıl manipüle edeceğini anlamıştı ve bu durum ona elektromanyetik radyasyonun bir malzeme içinde nasıl hareket ettiğini tasarlamak için bir yöntem sağladı. Pendry, 1999'da çalışmalarının sonuçlarını yayınlamaya devam edecek ve dünya çapındaki fizikçilerin dikkatini hızla çekecekti.

Bunların yanısıra, San Diego'daki California üniversitesinde deneysel bir fizikçi olan David Smith, Pendry'nin teorik cihazını inşa etmeye ve analiz etmeye çalışmak için meslektaşı Willie Padilla ile birlikte çalışacaktı. Smith ve Padilla çalışmalarında, malzeme bir radyasyon kaynağı tarafından uyarıldığında malzemenin doğal olarak manyetikmiş gibi davrandığı çok küçük bobinler dizisi inşa etmişti. Ayrıca oldukça küçük ince telleri bu dizimlerle yerleştirerek hem elektriksel hemde manyetik geçirgenşliği negatif yapmıştı. Pendry'nin konseptini tam olarak gerçekleştiren ekip, 2000 yılının Mayıs ayında bulgularını yayınlamaya devam edecekti. 2000 yılının sonlarında Pendry, süper bir lens oluşturmak için metamalzemeler kullanma fikrini önerdi. Süper lensler, geleneksel bir lensin kırınım sınırının ötesinde çalışabilen teorik lenslerdir ve bunun bir sonucu olarak genellikle kırınım sınırının bir sonucu olarak bozunan yakın alan ışınlarının dalga boyu altı görüntülemeye izin vererek spot ışığına getirilmesine izin verir. Bu süper lenslerin başlangıçta inşa edilmesinin imkansız olduğu düşünülüyordu. Pendry, bir meta malzemenin negatif kırılma indisi davranışı kullanılarak geliştirilebileceğini teorileştirdi. Bununla birlikte, pratikte, metamalzemelerin yayılan radyasyona yüksek oranda dağılmalarını sağlayan rezonans özellikleri nedeniyle bunun inanılmaz derecede zor bir görev olduğu kanıtlandı. Ayrıca bu lensler bir tasarımı çok dar bir dalga boyu çalışma bandıyla sınırlayan, seçilen kırılma parametrelerine karşı oldukça duyarlıydılar. Ayrıca, ışığın dalga boylarında negatif geçirgenliğe sahip metamalzemelerin üretimi o zamanlar mümkün değildi. 2003 yılında Pendry'nin teorisi, metallerin mikrodalgalara negatif geçirgenliğinden yararlanarak mikrodalga frekanslarında ilk kez laboratuvar tarafından belirlendi. 2005'te iki bağımsız grup, kullanılan dalga boylarından daha az nesnelerin fotoğraflarını sunmak için UV ışığıyla aydınlatılmış ince gümüş katmanları uygulayarak ultraviyole aralığında Pendry'nin süper lensini üretmede başarılı olduklarını bildirmişti. Diğer deneyler, MRI görüntülemesini geliştirmek için metamalzeme mikrodalga süper merceklemenin kullanımını da göstermiştir. Kısa bir süre sonra Berkeley'de fizikçi Zhang Xiang liderliğindeki bir ekip, en iyi optik mikroskoplarınkinden birkaç kat daha iyi bir çözünürlüğe sahip ultra ince bir gümüş tabakasından ilk optik süper lensi yarattı. 2008'in ortalarında Zhang'ın grubu, 21 alternatif gümüş levhadan ve balık ağı olarak adlandırılan cam benzeri maddeden oluşan nano ölçekli bir üç boyutlu optik meta malzeme üreterek optik görünmezlik pelerini yaratmaya yönelik ilk adımları attı. Birkaç ay sonra Pendry ve Smith, altındaki bir nesneyi mikrodalga algılamadan gizleyebilecek bir cihaz oluşturarak mikrodalga gizleme deneylerini daha da geliştireceklerdi. Mikrodalga radyasyonu ile bugüne kadar yapılan araştırmalar ve göreceli başarı, metamalzemeler arasında hareket eden bir metamalzeme içinde ışığın manipüle edilmesinin teknik zorlukları nedeniyle, optik gizleme hala belirsizliğini koruyor.

Birim hücrenin diyagonal yönelimdeki simetrisi nedeniyle, x-polarize gelen düzlem dalga yansımasıyla y-polarize bir düzlem dalga ışıması gerçekleşir. Son zamanlarda geniş bant absorpsiyonunu gerçekleştirmek için nispeten bu diagonal yapı kullanılmıştır, ancak çapraz polarize yansıma dikkate alınmadığından bu yapı gerçekte zayıf bir absorbe edicidir. Simetrik rezonatörden yapılmış bir metal-dielektrik-metal yapı, aynı anda düşük eş polarizasyon ve çapraz polarizasyon yansıması ile etkili bir soğurucu işlevi görür. Rezonatörün simetrisi bozulduğunda eş-polarizasyon yansıması azalsa bile çapraz polarizasyon yansıması önemli ölçüde arttığı gözlemlenmiştir. Son araştırmalar, diagonal yerleştirilmiş bu metamalzeme yapılarını emici olarak gösteren çalışmaların yanlışlıkla mikrodalga emici olarak çalışmadığını raporlamıştır. Asimetrik rezonatörlere sahip bu aygıtlar zayıf emiciler olsalar bile, etkili polarizasyon dönüştürücüler olarak kullanılabileceği raporlanmıştır.

Fedotov 2006 yılında, LP-LP polarizasyon dönüştürücülerinde asimetrik iletim oluşumunun ilk gözlemini yaptı. Ayrıca asimetrik iletim etkisinin gücünün, çok katmanlı MM'ler tarafından arttırıldığı öne sürülmüştür. 2011'de Kang, çelişkili yayılma yönünde 0,8'den fazla iletim dönüştürme verimliliğine ve 6.2 GHz'de doğrusal polarize dalganın asimetrik iletimine sahip S-şekilli bir MM önerdi. 2013 yılında Shi, iki katmanlı bir kiral MM ortaya çıkardı ve y dalgaları gelen dalga için polarizasyonu %90'ın üzerinde bir verimle dönüştürebileceğini belirtti. Wang daha sonra 2015 yılında 0.6’nın üzerinde verimlilikle çapraz şekilli iki katmanlı bir MM yarattı ve merkez dalga boyuna göre %33'e varan asimetrik iletim bant genişliği sağladı. Aynı yıl Mutlu, 1 GHz'den daha düşük bant genişliğine sahip, çok çeşitli frekanslarda gerçekleşebilen, açık, son derece ince bir kiral yapıda bir alt dalga boyu rezonansı getirdi. Basitçe söylemek gerekirse, daha önce önerilen MM tabanlı cihazların asimetrik iletim etkisi, düşük sınırlı bant frekansıdır (genellikle maksimum 0,6'dan fazla değildir). Bu nedenle yüksek verimliliğe ve geniş bant genişliğine sahip bir polarizasyon dönüştürücü oluşturmak ideal olacaktır. Çoklu dönüştürme modları, LP-LP ve LP-CP, son yıllarda geliştirilen çeşitli polarizasyon dönüştürücü türleri arasındadır. 13-15 GHz ve 16-18 GHz bantlarında çalışan polarizasyon dönüştürücü ile Gao önemli ilerlemeler kaydetti. Literatürde LP-LP dönüştürücüler daha fazla dikkat çekmekle birlikte ve LP-CP düzenlemeleri hakkında çok az araştırma yapılmıştır. Akram kısa süre önce hem yansıma hem de iletim modlarında çalışan ultra geniş bantlı bir meta yüzey önerdi, ancak eğik açı hassasiyeti bu çalışmada dikkate alınmadı. 2017'de Huang tarafından 8.16-15.32 GHz frekans aralığında dairesel polarize dalgaların dönüş yönünü kontrol edebilen ve yüksek açı hassasiyeti olan basit bir yapıya sahip bir polarizasyon dönüştürücü sunuldu.

Bu çalışmada, ultra ince metamalzeme temelli yansıma modlu LP-LP ve LP-CP dönüşümü gerçekleştiren mikrodalga polarizasyon dönüştürücüler tasarlanmıştır. Yapılan iki adet metayüzey polarizasyon dönüştürücüler mikrodalga simülasyon programında dizayn edilmiştir. Oluşturulan metayüzey polarizasyon dönüştürücüler kare ve L şekillerinin oluşturduğu bir metayüzey yapısı iler gerçekleştirilmiştir. Her iki dizaynda da alttaş olarak kolay erişilebilir FR-4 malzemesi seçilmiştir. Metayüzey yapısılarının en alt tabakasında bulunan metal plaka ve en üst tabakasında yer alan metayüzey için iletkenliği yüksek bakır seçilmiştir. Yöntem olarak Stokes parametreleri ile polarizasyon kestirim yöntemi ve yansıma katsayıları ile polarizasyon tesbit yöntemi kullanılmıştır. Bu iki analiz yönteminde S11 saçılım parametrelerinin x ve y yönlü yansıma katsayıları kullanılmıştır. Metayüzeye +z yönünde gelen dalganın elektrik alan bileşeninin +y yönünde olduğu kabul edilerek, -z yansıyan dalganın elektrik alan bileşenin +x yönünde yansıması sağlanılarak LP-LP dönüşümü sağlanılmıştır. Ayrıca aynı şekilde gönderilen dalganın dairesel polarize olarak yansıması da sağlanmıştır. Bu haliyle üretilen metayüzey polarizasyon dönüştürücüler hibrit rol üstlenmiştir. Elde edilen sonuçlar aynı bant aralığı için tasarlanan literatürdeki diğer çalışmalar ile açı hassasiyet, kalınlık, hacim, çalışma bant aralığı gibi yönlerden kıyaslanmıştır. Tasarlanan dönüştürücüler aynı şekil yapısına sahiptir ve 1 mm kalınlığa sahiptir. Fakat tasarımların birim hücre boyutları farklı olup, birinci tasarım 5x5 mm kare şekilli MM dönüştürücü ve ikinci tasarım 2x2 mm kare şekilli MM dönüştürücüdür. Tasarım CST simülasyon programı ile gerçekleştirilmiş ve sonuçlar MATLAB tarafından hesaplanmıştır. İlk metamalzeme temelli polarizasyon dönüştürücü için, X ve K mikrodalga frekans bantlarında üç farklı frekans bölgesinde %90'ın üzerinde LP-LP dönüşümü elde edilmiştir. Dolayısıyla 8.55-8.925 Ghz, 12.18-13.33 ve 17-17,4 GHz frekans bant genişliği aralıklarında %90 üzerinde lineer polarizasyon verimliliği sağlanmıştır. Ayrıca bu polarizasyon dönüştürücü 9.6-11 GHz (sol elli) ve 14.68-16 GHz (sağ elli) bant genişliklerinde minumum %99 polarizasyon dönüşüm oranı dairesel polarizasyon gerçekleştirmiştir. Bu aygıtın açı hassasiyeti LP-LP çalıştığı bölgelerde 30^0'e kadar eğik gelen dalgalar için %90 üzerinde polarizasyon dönüşüm oranı performansı sağlarken, LP-CP olarak görev yaptığı frekanslardan 9.6-11 GHz bandında 60^0 ‘ye kadar 14.68-16 GHz bant aralığı için 40^0 ‘ye kadar %99 üzerinde performans göstermektedir. Ayrıca çalışma literatürdeki benzer çalışmalarla kıyaslatıldığında kalınlık, göreceli hacim ve göreceli bant genişliği olarak oldukça ince bir yapıya sahiptir. İkinci metamalzeme temelli polarizasyon dönüştürücü K ve Ka mikrodalga frekans bantlarında 18.6-26.7 GHz frekans bölgesinde %90'ın üzerinde LP-LP dönüşümü elde edilmiştir. Ayrıca 31.8-40.5 GHz frekans bölgesinde ise %99 üzerinde polarizasyon dönüşüm oranı ile LP-CP (sol elli) elde edilmiştir. Önerilen bu metamalzeme polarizasyon dönüştürücü LP-LP çalıştırğı frekans bögesinde eğik açılı geliş için 40^0 ‘ye kadar eğik %90 üzerinde lineer polarizasyon performansı sağlamaktadır. LP-CP bölgesinde ise 30^0 ‘ye kadar gelen eğik açı için %99 üzerinde dairesel polarizasyon dönüşüm sağlamaktadır. Önerilen bu polarizasyon dönüştürücü literatürdeki diğer benzer çalışmalara kıyasla kalınlık, hacim ve göreceli hacim olarak oldukça ince ve kullanılabilir boyuttadır.

TABLE OF CONTENT

LIST OF TABLES

LIST OF FIGURES

LIST OF SYMBOLS AND ABBREVIATIONS

Symbols

ρ	Electric Charge Density
ε_{eff}	Effective Permittivity
μ_{eff}	Effective Permeability
δ_x	Phase Constant for E_x
δ_y	Phase Constant for E_x
B	Magnetic Flux Density
C_0	Speed of Light in Vacuum
D	Electric Displacement Vector
e	Charge of an Electron
E	Electrical Field Vector
E_{ox}	Optical Field Maximum Amplitude in the y Direction
E_{oy}	Optical Field Maximum Amplitude in the y Direction
f_{max}	maximum frequency of the operational bandwidth
f_{min}	minimum frequency of the operational bandwidth
H	Magnetic Field Vector
J	Electric Current Density
K	Wave Propagation Vector
n	Medium Refraction Index
P	Poynting Vector
R	Jones Reflection Coefficient Matrix
R_v	volume of a unit cell
R_{xx}	Co Polarization Reflection Component in the x Direction
R_{xy}	Cross Polarization Reflection Component in the x Direction
R_{yx}	Cross Polarization Reflection Component in the y Direction
R_{yy}	Co Polarization Reflection Component in the y Direction
S_0 or I	Total Propagation Intensity
S_1 or Q	Total Horizontal or Vertical Linear Propagation
S_{11}	First Medium Reflection Parameters
S12	Second Medium Transmission parameters
S_2 or U	Total Diagonal Linear Propagation
S21	First Medium Transmission parameters

S22	Second Medium Refection Parameters
S_3 or V	Total Circular Propagation
S_{L+45P}	Linear +45^0 Polarization Stoke's Parameters
S_{L-45P}	Linear -45^0 Polarization Stoke's Parameters
S_{LCP}	Left-hand Circular Polarization Stoke's Parameters
S_{LHP}	Linear Horizontal Polarization Stoke's Parameters
S_{LVP}	Linear Vertical Polarization Stoke's Parameters
S_{RCP}	Right-hand Circular Polarization Stoke's Parameters
T_v	total volume of a unit cell
ε	Dielectric Permittivity
ε_0	Free-space Permittivity
ε_{metal}	Metal Electric Permittivity
ε_r	Relative Permittivity
λ	Wavelength
λ	wavelength of the operational bandwidth
μ	Magnetic Permeability
μ_0	Free-space Permeability
μ_r	Relative Permeability
σ	Surface per unit area Conductivity
ω	Angular Frequency
ω_p	Plasmon Frequency
δ	Polarization Ellipse Phase

Abbreviations

BW_{CE}	cost-effective bandwidth
CPC	Cross-Polarization Conversion
CST	Computer Simulation Technology
DNG	Double Negative
DPD	Double Positive
EM	Electromagnetic
ENG	Epsilon Negative
EVI	Electric Field Intensity
GHz	Gigahertz
IEEE	Institute of Electrical and Electronics Engineering
ITO	Indium Tin Oxide

L+45	Linear +45^0 Polarization
L-45	Linear -45^0 Polarization
LH	Left-Handed
LHCP	Left-Hand Circular Polarization
LP-CP	Linear Polarization to Circular Polarization
LP-LP	Linear Polarization to Linear Polarization
MM	Metamaterial
MNG	Mu Negative
MS	Metasurface
NIM	Negative Index Material
PCR	Polarization Conversion Ratio
PET	Polyethylene Terephthalate
RBW	relative bandwidth
RF	Resonance Frequency
RH	Right-Handed
RHCP	Right-Hand Circular Polarization
SRR	Split Ring Resonator
TE	Transverse Electric
THz	Terahertz
TM	Transverse Magnetic

INTRODUCTION

The term “electromagnetic wave polarization” characterizes the orientation of the electric field component oscillating at a fixed point in space while taking time into account. The direction of the EM wave could be altered via a polarization converter. Numerous uses of EM wave polarization converters from the microwave to terahertz domains, including the minimization of the radar cross section in stealth systems, antenna design, half and quarter wave plates, have demonstrated their importance. The outcome of a radio link could be increased or decreased by moving the polarization in the pleasant or unpleasant perpendicular orientation because antennas are naturally inclined to polarization. It also applies to monostatic radar, which uses a single antenna for both transmission and reception. Polarization converters are utilized in a variety of industries, including sensors, antenna, radar, optical communication which all require perfect polarization (Zhao et al, 2011).

Traditionally polarization conversion is accomplished with the help of the birefringence phenomenon in naturally occurring crystals and anisotropy is present at the molecular level (Danner et al, 2011). These crystals’ weak anisotropy, bulky volume, angle-dependent polarization response, and significant power loss are preventing them from being used in practical applications. Additionally, these techniques call for specialized equipment for phase calculation and large propagation distances. Light rays separating into two halves is referred to as birefringence by the very definition of the word. This separating, which gives the appearance of a double image, occurs naturally in materials that are birefringent. When a device created using transformation optics is made to perform in dielectrics, birefringence frequently results as an unintended side effect. In dielectrics, on polarization is typically applied while forgoing the other (Leonhadt and PHilbin, 2010). Polarization converters are created utilizing metasurface structures to get around these drawbacks (Chen et al, 2016). MS is a sub-wave periodic structure with narrow volumes that draw attention. MS polarization converters have been developed with high resonance properties in a variety of frequencies, including microwave (Geyi et al 2017), terahertz (Mo et al, 2016), infrared (Zeng et al, 2019), and visible light band (Shi et al, 2012). Broadband, low profile, wide angle, and extremely thin MS polarization converters get interest in the microwave area. Reflective and transmitive are the two main types of MS designs used in converter experiments. While reflecting constructions convert the polarization of the reflected portion from the MS because metal terminals are formed (Nama et al, 2021), transmitting constructions converter the polarization of the transmitted portion without metal terminals. (Wei et al, 2011). In addition, MS polarization converters come in a variety of forms, including circular and linear, depending on the kind of wave polarization used in the conversion experiments (Ozturk G, 2022). In LP-CP works, the electric field is reflected in a circular direction, whereas the electric field's direction shifts by 90 degrees in LP-LP reflective works (CPC). Utilizing MS, designs for LP-LP conversion devices have concentrated on PCR, band gap, incident angle, thickness and microwave frequency region. For the practical use of these devices, the unit cell volumes and thicknesses of the designs development are crucial. Additionally, because LP-LP suffers from significant multi-path fading, high ionospheric losses and is reliant on the orientation of the antennas, LP-CP is favored in some microwave applications. Moreover, LP-CP is used in satellite communication to circumvent the difficulty of antenna orientations and enable data flow without these antennal orientations.

After pioneering mathematical study by Dr. Veselago (VG Veselago, 1967), metamaterials, which are periodic or a periodic structure with extraordinary electromagnetic properties, were created. In experiments, split ring resonator structures and infinite- length wire were subjected to an electric field in order to produce negative permittivity (Pendry et al, 1996) and negative permeability (Pendry et al, 1999). Smith created the first metamaterial with a negative refractive index by combining wires and SRR as a composites (Smith et al, 2000). Antenna (Ziolkwoski and Erentok, 2006), optic lens (Kundts and Smith, 2010), energy harvesting (Chen et al, 2014), sensors (Abbott et al, 2013), cloaking (Pendry et al, 2006), absorber (Wang et al, 2015), and polarization converter (Khan et al, 2019) are a few of the applications that MMs have been employed in. However, polarization converter is the area that we are most interested in this study.

Due to the benefit of its ultrathin thickness and scalable property, MM absorber has attracted significant interest since the ground-breaking work of Landy (Landy et al, 2008). A lot of work has been put into recent years to enhance MM absorber performance, particularly in terms of broadening the absorption band (Liu et al, 2017). Moreover, many additional application, such as metasurface holograms (Wen et al, 2015), need for the broadband characteristic. One method for achieving broadband absorption involves using multi resonance, which involves placing several resonators inside of a single unit cell (Azad, et al, 2016), while another method uses a multilayered structure (Ding et al, 2012). As the standard MM absorber is a periodic array of Metal-Dielectric-Metal resonator, we could define the MM absorber's absorptivity as:

$$A = 1 - {r_{yy}}^2 - {r_{xy}}^2 \quad (1)$$

Where $r_{yy} = |E_{yr}|/|E_{yi}|$ & $r_{xy} = |E_{xr}|/|E_{yi}|$ are reflection coefficients for both co-polarization and cross-polarization correspondingly. Many researchers mistook linear polarization converters for absorbers in numerous earlier experiments. Hue erroneously viewed a cross polarization converter as a broadband absorber (Hoa et al, 2019) by ignoring its cross polarized reflection. Although the proposed designs absorption is less than 20% and the polarization conversion ratio is more than 90%. Fahad Ahmed and Tayyab Hassan corrected this error in Hua's design in 2021(Hoa et al, 2021, scientific reports).

Due to the unit cell's symmetry in the diagonal orientation, a y-polarized plane wave irradiation is taken into consideration in this instance, which is the same as an x-polarized plane wave illumination. A relatively basic structure has lately been used to accomplish broadband absorption, however when cross polarized reflection is taken into account, this structure is really a poor absorber (Wang et al, 2014). A metal-dielectric-metal structure made of symmetric resonator function as effective absorber with low co polarization and cross polarization reflection concurrently. Even if the co polarization reflection is decreased when the symmetry of the resonator is disrupted, the cross polarization reflection increased dramatically. Recent investigations have mistakenly assumed that the structures are effective absorbers because they could only be defined by co polarized antennas. Metal-dielectric-metal devices with asymmetric resonators are attractive prospects for effective polarization converters even if they are poor absorbers.

Fedotov made the first observation of the asymmetric transmission occurrence in LP-LP polarization converters (Fedotov et al, 2006. The strength of the asymmetric transmission effect has now been suggested to be increased by different approaches and structures, like multi-layer MMs (Fedotov et al, 2008). In 2011, Kang proposed an S-shaped MM with a transmission conversion efficiency of more than 0.8 in the contradictory propagation direction and an asymmetric transmission of the linearly polarized wave at 6.2 GHz (Kang et al, 2011). In 2013, Shi revealed a bi-layered chiral MM and indicated that it could convert polarization for y polarized and y waves with an efficiency of above 90%. Wang later created a cross-shaped bi-layered MM in 2015 with a 0.6 efficiency and an asymmetric transmission bandwidth of up to 33% in respect to the center wavelength (Wang et al, 2015). In the same year, Mutlu brought a subwavelength resonance in an open extremely thin chiral structure with a bandwidth of less than 1 GHz that may actualize in a range of frequencies (Mutlu et al, 2015). Simply put, the asymmetric transmission impact of the earlier proposed MMs-based devices is low frequency of limited band (usually the max is not more than 0.6). Therefore, it would be ideal to create a polarization converter with high efficiency and large bandwidth. Multiple conversion modes, LP-LP and LP-CP are among diverse types of polarization converters that have been developed in recent years. Frequency band (13-15) and (16-18) have all seen significant advancement in the work of Gao (Gao et al, 2015). Yet, the LP converter receive the majority of the attention, and there has been little research on LP-CP regulations. Akram recently suggested an ultra-wideband metasurface that operates in both reflection and transmission modes (Akram et al, 2020), but they ignored oblique incidence. One with a straightforward construction that could control the rotation orientation of circularly polarized waves in the frequency range 8.16-15.32 GHz was put out in 2017 by Huang (Huang et al, 2017). The polarization converter, though, is incredibly angle sensitive. The operating bandwidth gets noticeably smaller and the polarization conversion ration falls off quickly when the incident angle is greater than 30^0. The applicability of the device is constrained by the fact that all of the currently available polarization converters can only function under small-angle incidence.

In this study, we tried to solve the above drawbacks and get better results in both the polarization conversion efficiency and the oblique incident propagation. our converter consists of three layers where the upper and lower layers are copper and the mid dielectric layer is FR4. We designed a unique shape that could work in more than one frequency band and could achieve both LP-LP and LP-CP. There are two designs of the same shape with an ultra-thin thickness, the first design works on the operating frequency bands X and Ku, whereas the second works on the frequency bands K and Ka. The X and Ku ultra-thin MM converter could achieve three LP-LP in the frequency ranges 8.55-8.925 Ghz, 12.18-13.33 and 17-17.4 GHZ with PCR more than 90% and two LP-CP in the operating frequency ranges 9.6 -11 GHz (RHCP) and 14.68- 16 GHz (LHCP) with ellipticity more than 99%, and the oblique incident propagation for both is more than 30^0. The K and Ka ultra-thin MM converter could achieve LP-LP in the frequency range 18.55 -26.9 GHz with PCR more than 90% and PCR more than 99% in the frequency range 19.55-24.8 GHz and the LP-CP occurs in the frequency range 31.3-40.5 GHz with ellipticity more than 99%.

THEORETICAL FOUNDATION

History of Metamaterial

The first mention of the properties of metamaterials MMs was in 1904 with the conceptualization of negative wave propagation by British mathematician Horace Lamb (Lamp H, 1904) and British physicist Arthur Schuster (Schuster A, 1905). However, both saw the phenomenon as purely theoretical and did not think it could be practically achieved. Fourteen years later soviet physicist Leonid Mandelson while studying the nature of electromagnetic wave propagation would examine the characteristics of materials demonstrating negative refraction (Mandelson L, 1918). From his experiments he discovered that the phenomena were prevalent in materials composed of crystal lattice. By the later 1960s several research teams would go on to further study the negative propagation properties of crystals as well as the practical implication of the concept of negative permittivity and negative magnetic permeability.

Finally, in 1967 soviet physicist Victor Veselago of the Moscow institute of physics and technology would propose the first theoretical model for a metamaterial (Veselago V, 1967). The Veselago research included producing methods for predicting the phenomena of refraction reversal in which he coined the term left-handed materials as well as exploring theoretical models for materials. That have both negative permittivity and negative permeability or double negative materials.

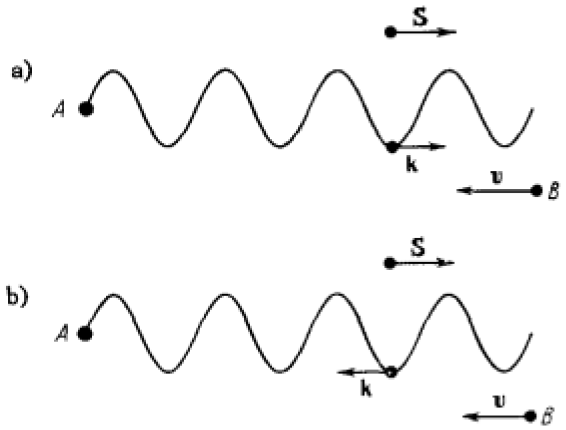

Figure 1. a) Right-handed material’s Doppler effect, b left-handed material’s Doppler effect. Where the source of the radiation is determined by the letter A, and the receiver by letter B.

Over the next three decades these would remain predominantly abstract as the constituent materials and computing power needed to effectively design and experiment with metamaterials were lacking. As the framework for metamaterials was being developed at the theoretical level the related field of microwave engineering and its application to antenna design began to rapidly evolve after world war II. From this the development of artificial dielectrics during the 1950s and 1960s began to open up new ways to shape microwave radiation especially for antenna design. Artificial dielectrics are composed materials made from arranged arrays of conductive shapes or particles supported in a non-conductive matrix similar to metamaterials. Artificial dielectrics are designed to have a specific electromagnetic response behaving as an engineered dielectric material. By the late 1990s the first attempts at migrating metamaterials from theory to reality began to emerge and while the long-established principles that formed them would remain the focal point of ongoing research.

English theoretical physicist John Pendry would soon become a leading contributor to the field by bringing the properties of MMs from concept to reality. Pendry discovered that the microwave absorption of the material did not be driven by the chemical structure of the carbon it was made from but rather the long thing shape of the fibers (Pendry J, 1996). From this observation Pendry realized that by changing a material's domestic structure at scales that were smaller than a specific band of radiation he could alter how that material interacted with it. From this observation the term metamaterial was coined due to the observed properties seemingly going beyond what was naturally occurring. Pendry would explore this concept further with an idea for a composite material that could mimic the properties of a conventional magnetic substance he theorized that such a material could be manufactured from tiny loops of copper wire embedded in a fiberglass substrate as a split ring resonator. These loops would create specific magnetic responses based on their size and geometry effectively becoming tunable magnetic resonators. The implication of Pendry's was something unseen before in material sciences. He had figured out how to manipulate a material's electric and magnetic response effectively allowing him for a method to engineer how electromagnetic radiation moves through a material. Pendry would go on to publish the results of his work in 1999 quickly attracting the attention of physicists worldwide (Pendry J, 1999).

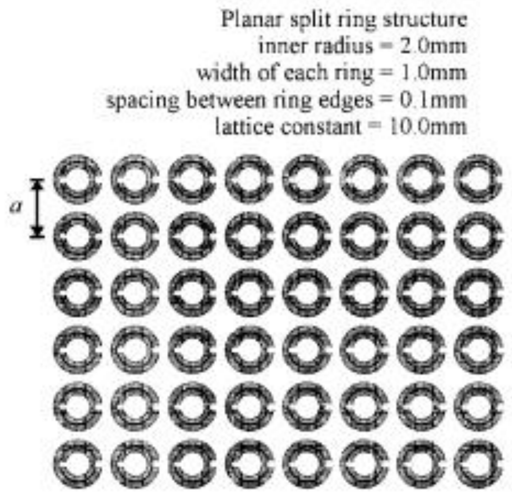

Figure 2. Plain view of an SRR (Split-Ring Structure) in a square array (a is the lattice spacing) (Pendry J,1999)

Among them David smith an experimental physicist at the university of California at San Diego would team up with colleague willie Padilla to attempt to construct and analyze Pendry's theoretical device (Smith and Padilla, 2000). Smith and Padilla had constructed an array of very small coils that can be tuned in such a way that when illuminated by a source of radiation the material behaved as though it were naturally magnetic. Fully realizing Pendry's concept the team would go on to publish their findings in May of 2000. By late 2000 Pendry proposed the idea of using metamaterials to construct a super lens (Pendry J, 2000). Super lenses are theoretical lenses that can operate beyond the diffraction limit of a traditional lens allowing near-field rays that commonly decay as a result to its diffraction limit to be brought into spotlight allowing for sub-wavelength imaging. Those super lenses were initially considered impossible to construct. Pendry theorized that one could be developed employing the negative refractive index behavior of a metamaterial. However, in practice this proved to be an incredibly difficult task due to the resonant features of metamaterials that made them highly dispersive to propagating radiation. They were also highly sensitive to the parameters of refraction chosen which limited a design to a very narrow wavelength band of operation. Furthermore, manufacturing metamaterials that have a negative permeability at the wavelengths of light was not feasible at the time. This limited experimentation on the concept to microwave radiation. By 2003 Pendry's theory was laboratory determined for the first time at microwave frequencies by exploiting the negative permittivity of metals to microwaves. In 2005 two independent groups had reported success at producing Pendry's super-lens at the ultraviolet range applying thin layers of silver illuminated with UV light to deliver photographs of objects less than the used wavelengths. Other experiments had also demonstrated the use of metamaterial microwave super lensing to improve upon MRI imaging. Shortly after a team at

Berkeley led by physicist Zhang Xiang created first optical super lens from an ultrathin layer of silver with a resolution that was several times better than that of the best optical microscopes (Fang et al, 2005) In 2004 at a lecture Pendry had flippantly presented another theoretical implication of the properties of metamaterials that they could be designed for cloaking (Pendry and Smith 2004). Darpa took these ideas very seriously and shortly thereafter David Smith would team up with Pendry under Darpa funding to build a cloaking device from this collaboration. The first functional invisibility cloak that started microwave radiation around the copper cylinder hiding it from detection was constructed in 2006 (Pendry et al 2006). By mid-2008 Zhang's group took the first steps toward creating an optical invisibility cloak by fabricating a nanoscale three-dimensional optical metamaterial composed of 21 alternating sheets of silver and the glass-like substance the material referred to as a fish net caused light to bend in unusual ways as it moves through the alternating layers (Zhang et al 2008). A few months later Pendry and Smith would refine their microwave cloaking experiments further by creating a device that could mask an object beneath it from microwave detection what made this particularly notable was that it operated on a wide band of radiation than their previous attempts despite the ongoing research and relative success with microwave radiation to date optical cloaking still remains elusive due to the technical challenges of manipulating light within a metamaterial light moving through metamaterials typically get absorbed until at some point the energy of the radiation falls off making it a challenge to guide its propagation in a useful way (Pendry et al 2008).

Characteristics of Metamaterial

MMs are artificial materials that couldn't be found in nature, so they are artificially manufactured. The metamaterial word consists of two combined words meta and material. Meta's etymology is a Greek word that means beyond so the total meaning of metamaterial is beyond the material. Its unique characteristics no doubt differ from those in the normal materials.

The electric and magnetic properties of a material could be determined by permittivity and permeability values respectively. We could say also Electric permittivity and magnetic permeability. Almost in all natural materials the permittivity and permeability are positive (except for some metals in UV frequencies where permittivity is negative). If the permittivity and permeability are positive the material could be referred as right-handed material (RHM). While if the pair permittivity and permeability are negative then the material could be referred as left-handed material (LHM) (Pendry J, 1999).

The electric polarization of a dielectric is measured using permittivity. The permittivity is directly proportional to an applied field. The symbol for permittivity is the Greek letter ε (Epsilon). In the simplest scenario, an applied electric displacement field **E** produces an electric displacement field **D** that is (Wiley J and Sons, 2012):

$$\mathbf{D} = \varepsilon \mathbf{E} \quad (2)$$

In which **D** is the electric displacement vector (C/ m^2), $\varepsilon = \varepsilon_0 \varepsilon_r$ & ε_0 is free space's permittivity ($8.85 * 10^{-12}$ F/m), ε_r is the relative permittivity, and **E** is the electric field (V/m).

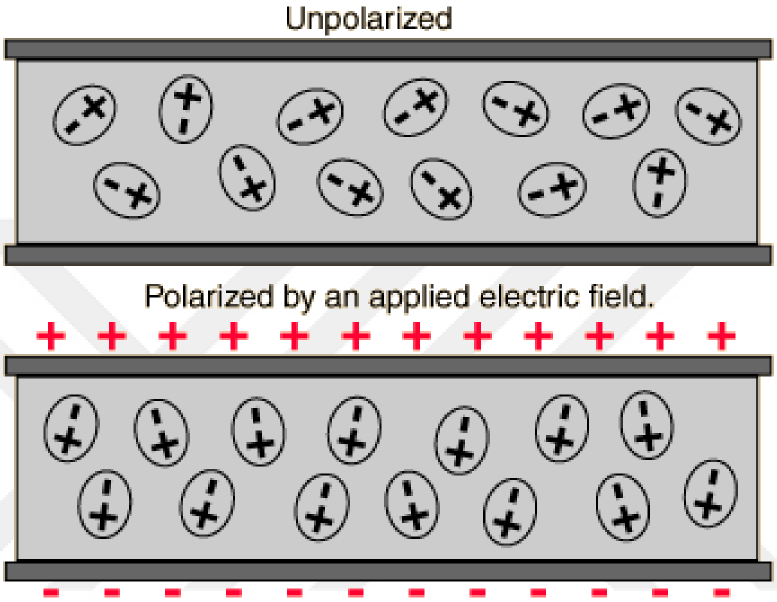

Figure 3. A dielectric medium before and after applying an electric field (Moqadam et al 2017)

A magnetizable substance's permeability is a characteristic that governs how much it affects the magnetic flux in a magnetic field. The symbol for permeability is the Greek letter μ (Mu). In the simplest case, the magnetic flux density **B** resulting from a magnetic field **H** is (Wiley J and Sons, 2012):

$$\mathbf{B} = \mu \mathbf{H} \quad (3)$$

Where B is the magnetic flux density (Tesla or Wb/m^2), $\mu = \mu_0 \mu_r$ & μ_0 is the permeability of the free space ($4*Pi*10^{-7}$ H/m), μ_r is the relative permeability, and H is the magnetic field (A/m).

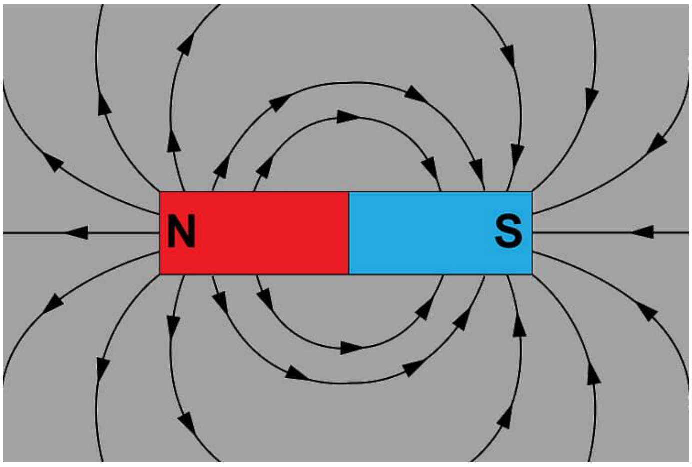

Figure 4. The magnetic field of a dipole magnet

According to the sign of permittivity and permeability of a material we could classify the materials into four different groups as illustrated below:

Transmission Properties of Materials

The magnetic permeability and dielectric permittivity are the main determinant of the transmission properties of a lossless material. So, we start by looking at the negative permittivity phenomenon. Then there is the phenomenon of negative permeability and negative refractive index metamaterials, that do have negative permeability as well as negative permittivity. Maxwell's Equations provide the essential premise for the wide electromagnetic phenomena. Accordingly, we will start analyzing Maxwell’s Equations to understand the characteristic properties of the different categories of the materials (Maxwell J.C, 1865).

Every point in space must have electromagnetic field solutions that fulfill Maxwell's equations, that are represented in the time domain as follows.:

$$\nabla \times \mathbf{E} = -\frac{\partial \mathbf{B}}{\partial t} \qquad \text{(Faraday's Law)} \qquad (4)$$

$$\nabla \times \mathbf{H} = \frac{\partial \mathbf{D}}{\partial t} + \mathbf{J} \qquad \text{(Ampere's Law)} \qquad (5)$$

$$\nabla \bullet \mathbf{D} = \rho \qquad \text{(Gauss's Electric Law)} \qquad (6)$$

$$\nabla \bullet \mathbf{B} = 0 \qquad \text{(Gauss's Magnetic Law)} \qquad (7)$$

For the sake of ease in our analysis, we focused on the homogeneous plane wave stimulation at a specific angular frequency ω. Using the $e^{+j\omega t}$ terminology, the formal definition for the E and H fields of a homogeneous plane wave in phasor domain can be expressed as:

$$\mathbf{E} = \mathbf{E}_0 e^{+j\mathbf{k}\bullet\mathbf{r}} \qquad (8)$$

$$\mathbf{H} = \mathbf{H}_0 e^{+j\mathbf{k}\bullet\mathbf{r}} \quad (9)$$

In which **k** is the propagation vector, **r** is the position vector and the wave is supposed to spread in a lossless, simple (homogeneous, isotropic and linear) and source-free medium having constitutional relations as previously mentioned in Eq. (2) and Eq. (3)

The simplified Maxwell's equations for isotropic, monochromatic plane waves can be expressed as follows in the phasor domain:

$$\mathbf{K} \times \mathbf{E} = -w\mu\, \mathbf{H} \quad (10)$$

$$\mathbf{K} \times \mathbf{H} = w\varepsilon \mathbf{E} \quad (11)$$

Additionally, the shortest dispersion relation for the homogeneous isotropic, and lossless materials could be given as follows:

$$k^2 - w^2 \mu\, \varepsilon = 0 \quad (12)$$

$$k^2 = w^2 n^2 \quad (13)$$

In which n (medium's refractive index), could be determined as:

$$n = \sqrt{\mu\, \varepsilon} \quad (14)$$

and for a composite material supplied by with effective medium parameters μ_{eff} and ε_{eff}, provided by

$$n = \sqrt{\mu_{eff} \varepsilon_{eff}} \quad (15)$$

The electromagnetic wave's propagation in the given substance is controlled by the dispersion relation. We could say that the material's magnetic permeability (μ) and dielectric permittivity (ε) are the typical parameters of the material for the lossless medium as ε and μ are the sole materials properties in Eq. (12). The refractive index(n) contrarily does not alter its sign as both μ and ε go negative according to Eq. (13). The effects of simultaneous negative magnetic permeability (μ) and dielectric permittivity (ε) are, nevertheless, illustrated by Maxwell relations. Different from the typical positive μ and ε materials, the materials with simultaneous negative display special properties.

H, E and **K** make up a right-handed perpendicular coordinate system (RHM) for materials with positive μ and ε as indicated in Eqs. (10) and (11) see fig (5.a). When both μ and ε are negative an unusual situation arises where **H, E** and **K** constitute a left-handed perpendicular coordinate system (LHM) see fig (5.b) (Del Barrio, 2010):

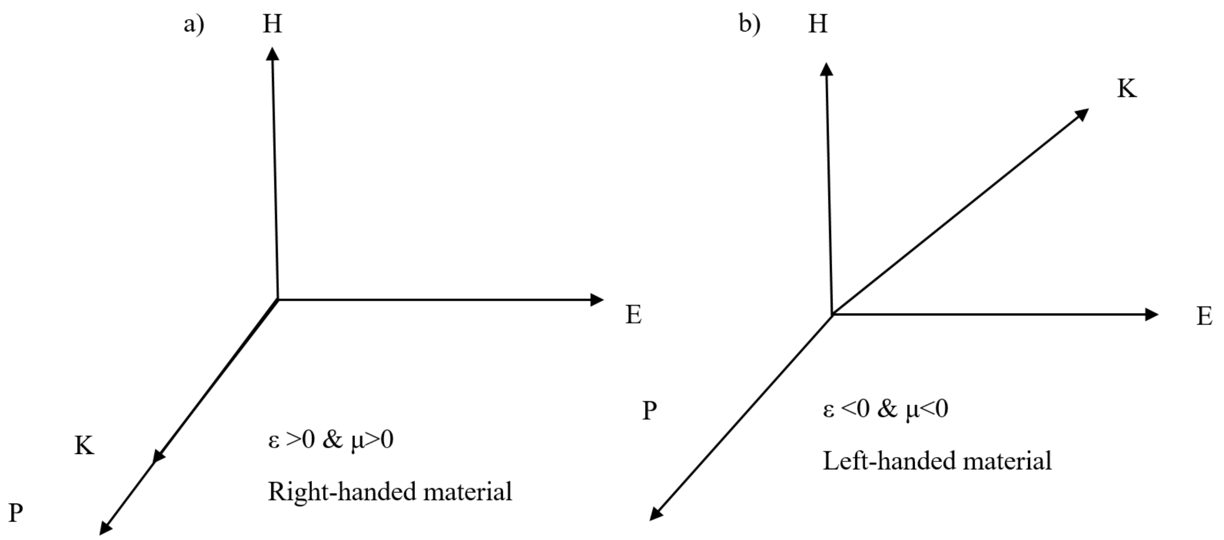

Figure 5. a) Right handed perpendicular coordinate system (μ and ε are positive). b) left handed perpendicular coordinate system (μ and ε are positive).

Moreover, as the sign of Poynting Vector (**P**) irrespective of the sign of μ and ε as it is illustrated in Eq. (16), the orientation of the energy flow is unaffected:

$$\mathbf{P} = \mathbf{E} \times \mathbf{H} \tag{16}$$

Accordingly, the orientation of the power flow won't ever shift unless with left-handed materials. The wave propagation orientation is the polar opposite of the power flow orientation. That reality is, the Cerenkov Radiation and Doppler Shift are reversed, as well as the well-known effects of an antiparallel phase and the group velocity. Moreover, we identified the scenario in which both μ and ε are either positive or negative. Electromagnetic waves are entirely reflected and evanescent waves are produced when the signs of μ and ε are in opposite $\mu\varepsilon < 0$ (Marques R, 2011). The response of the materials for the four different variations of the signs μ and ε is summarized in fig (6):

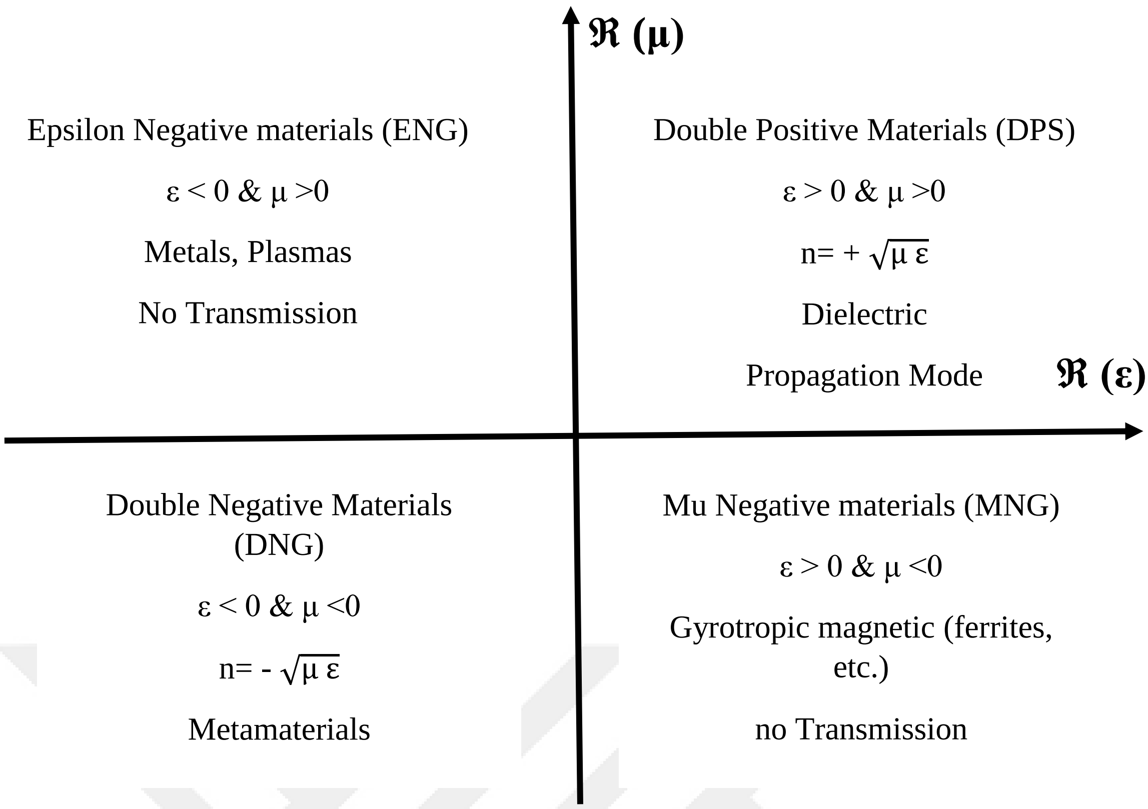

Figure 6. The μ-ε diagram (the four different variations of μ and ε) (Del Barrio, 2010)

The graph's first quadrant in fig (6) represents common materials with positive ε and positive μ. The materials with negative ε and positive μ are represented in the second quadrant of the graph (like plasmas, metals in special cases). Due to the imaginary propagation constant(k), electromagnetic waves become evanescent. Owing to the exceptional electromagnetic properties indicated above, the third quadrant is significant. Although ε and μ are both negative, the wave can still move since εμ>0 (real propagation constant, k). The fourth quadrant, which include materials with positive ε and negative μ polarities, is where anisotropic ferromagnets predominate. In this sector, electromagnetic waves also start to fade away.

Negative Permittivity (Epsilon Negative Materials ENG)

Several metals exhibit properties akin to an electron plasma. Plasma frequency is a particular frequency that can produce negative permittivity. Due to the plasma frequency of metals in optical frequencies, the negative dielectric permittivity predominates in visible light and ultraviolet light frequency. A periodic array of metallic wires is used to achieve negative permittivity in the microwave band. The formula for the permittivity function in metals is (Pendry J, 1996):

$$\varepsilon_{metal}(\omega) = 1 - \frac{{\omega_p}^2}{\omega^2} \tag{17}$$

In which plasma frequency is ω_p. The formula for the metallic thin wire's plasma frequency is:

$$\omega_p = \frac{ne^2}{\varepsilon_0 m} = \frac{2\pi c_0{}^2}{a^2 \ln(a/r)} \tag{18}$$

In which m is the electron mass, n is the electron density, e is the charge on an electron, c_0 is the free space's speed of light, a is the lattice parameters and r is the cylindrical thin wire's radius,. The media for the metallic thin wire structure can be represented utilizing fig (7). By modifying the necessary parameters, such as r and a described above, the design with negative permittivity values could be achieved. According to the previous equation Eq.2.18, rather of using microscopic quantities (n, m, e), the plasma can be represented in the form of the array macroscale properties (a and r).

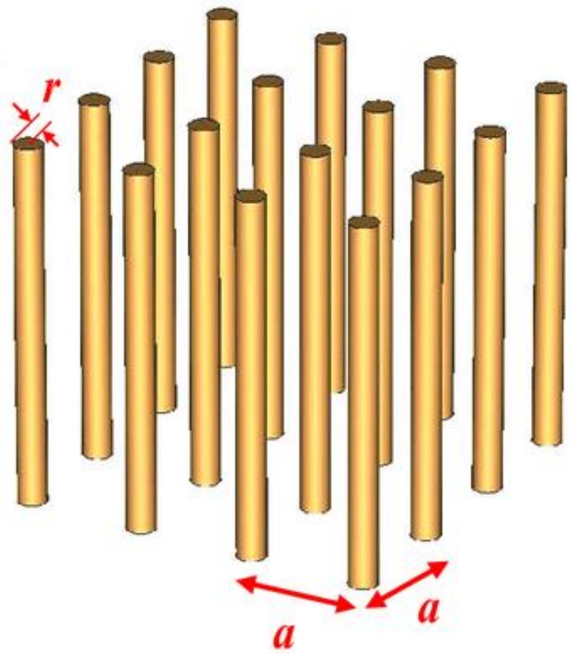

Figure 7. Periodic metallic thin wire (Pendry J, 1998).

The system response could be regarded using the effective medium theory which involve the effective magnetic permeability and the dielectric permittivity of the media, once the distance between the metallic thin wires (a) is arranged less than the wavelength (λ) of the incident wave (λ>>a).

Negative Permeability (Mu Negative Materials MNG)

Finding a material with negative permeability is far more challenging than developing a material with negative electric permittivity because there aren't many free magnetic charges in nature. The thin wire arrays that used in obtaining negative permittivity can't be used to achieve negative permeability. To obtain mu negative materials Pendry et al. developed magnetic resonator architectures in 1999. To pair with one another and produce a strong magnetic response that results in negative permeability, the architectures are arranged in periodic arrays. The SRR (Split Ring Resonator, Spiral Resonator and U-shaped Resonator are the three main typical magnetic resonator structures. Figure (8) displays instances of these formations:

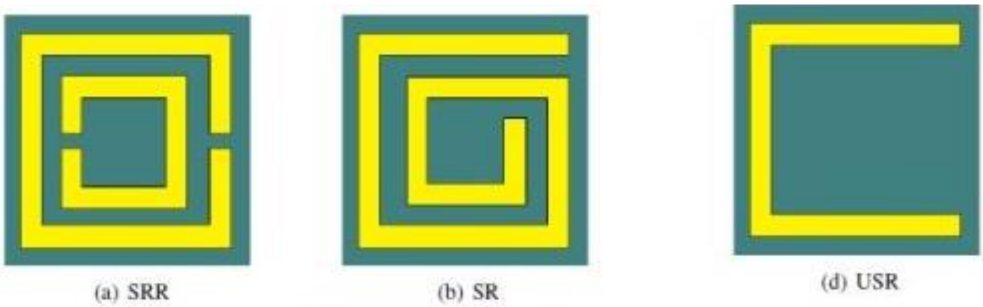

Figure 8. Different Shapes of resonators a) SRR (Split Ring Resonator). b) SR (Spiral Resonator). c) UR (U-shaped Resonator) (Ekmekci R, 2010).

The effective permeability for the Split Ring Resonator (SRR) architecture are deduced as (Pendry J,1999):

$$\mu_{eff} = 1 - \frac{\frac{\pi . r^2}{a^2}}{1 + \frac{2\sigma . j}{\omega r \mu_0} - \frac{3dc^2}{\pi^2 r^3 \omega^2}} \tag{19}$$

In which a is the lattice parameter for a unit cell, μ_0 is the vacuum magnetic permeability, r is the inner ring radius, d is the gap distance separating two metallic surfaces, c is the vacuum speed of light, σ is cylinder surface per unit area’s conductivity. According to the presumption that the metallic rings are composed of a PEC (Perfect Electric Conductor), fig (9) depicts the standard μ_{eff} shape of an SRR as a variation of the angular frequency ω.

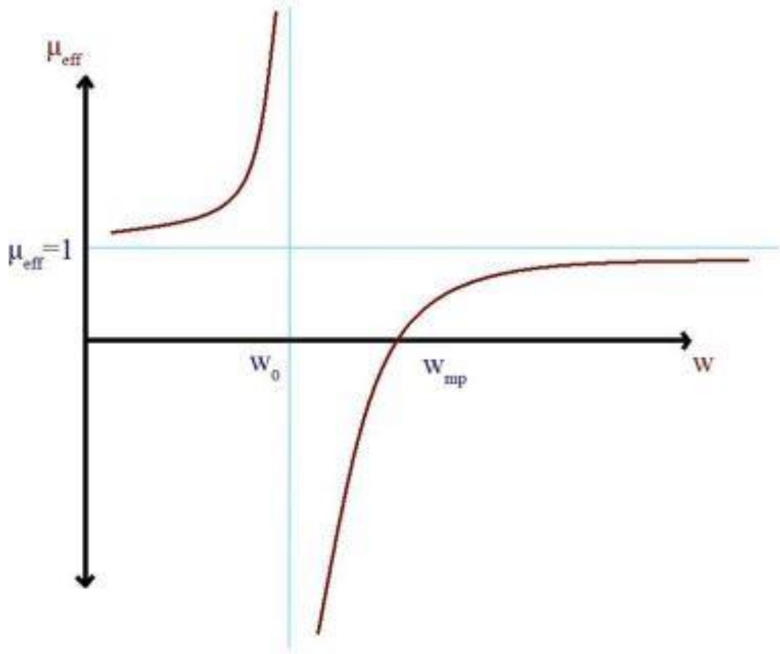

Figure 9. The relationship between SRR Permeability and frequency (Pendry J,1999)

Negative Refraction Index (Double Negative Materials DNG)

The refractive index could be generally formulated as:

$$n = \pm\sqrt{\mu\varepsilon} \tag{20}$$

For the materials found in nature, the positive sign is typically used. The production still remains positive if both the permeability and the permittivity are negative, but the negative sign of the refractive index indicates the wave-vector's path of propagation. Based on Snell's law, that describes the relation between the angle of incidence and the refraction, the refraction and reflection occurrences at the interfaces of two distinct mediums with differing dielectric constants are well known. The distribution on light beam at the interface of a RHM and LHM could also be studied now.

As it is demonstrated in fig (10), the reflected wave is in the opposite direction from what would be anticipated in the traditional materials based on the energy flow in the interaction (Engheta and Ziolkowski, 2006)

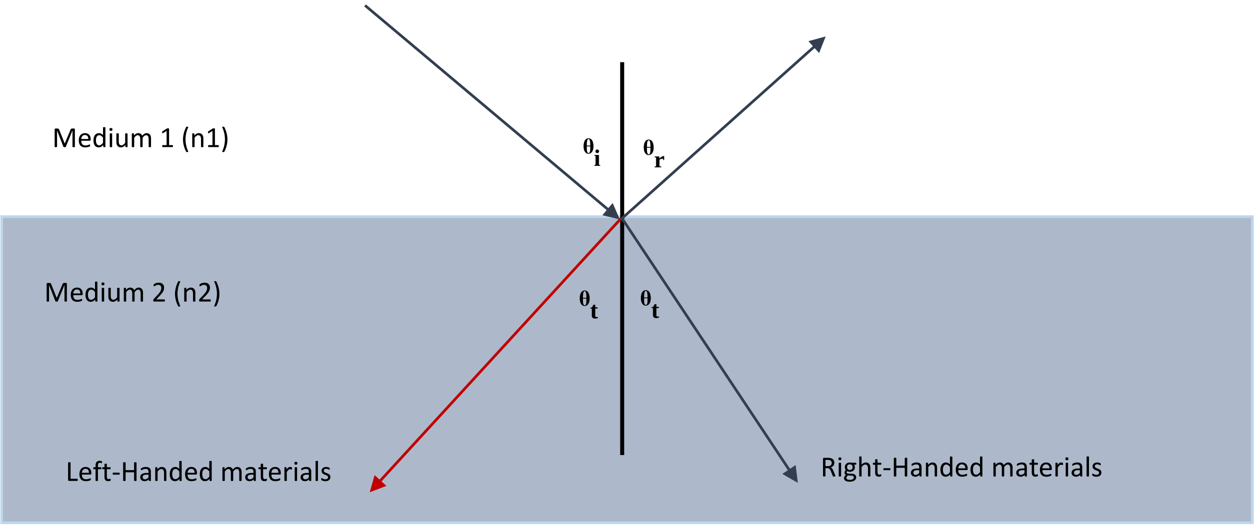

Figure 10. The refraction of a wave on both RHM and LHM

According to Snell's law of reflection, the refracted angle and the incident angle have a correlation that could be provided as:

$$\frac{\sin \theta_1}{\sin \theta_2} = \frac{n_1}{n_2} = \sqrt{\frac{\mu_2 \varepsilon_2}{\mu_1 \varepsilon_1}} \quad (21)$$

In which θ_1 and θ_2 are the incident and the transmitted angles correspondingly, n_1 and n_2 are the refractive index of both the transmitted and refracted medium in respect.

Split Ring Resonator (SRR)

There have been significant efforts to bring the SRR to reality after introducing them in 2000.

So now the first most prevalent type of metamaterial resonator construction is SRR since they can be built to achieve DNG, ENG and MNG form structure. SRRs are useful because, for instance, negative permittivity could be achieved without any need for using thin wire arrays as it was used before. The stimulation methods of SRR must be understood that on may appreciate the electromagnetic material characteristics of SRR metamaterial architecture. Both Electric-magnetic, Electric, magnetic stimulation could all be used to excite SRR structure. The variables of the SRR as illustrated in fig (11), including the gap width (d), the unit cell size (a), spacing distance between adjacent rings(l), and the metal strip width(c), influence the structure resonance frequency, that is often researched in literature. The SRR structures electrical and magnetic responses are dependent on the methods of stimulation. The excitation methods could be electrical and magnetic or only electrical or only magnetic excitation (Smith et al, 2000).

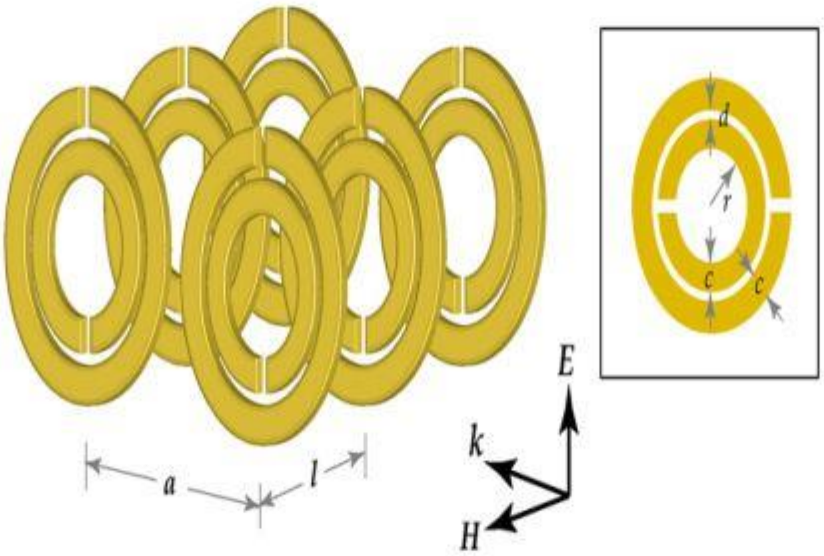

Figure 11. The periodic structures of SRR(Smith et al, 2000).

Based on Faraday's equation of induction, the magnetic stimulation is just possible once the magnetic field intensity **H** is orthogonal to the loops in the SRR. In contrast, electric stimulation occurs only if the electric field strength E is aligned to the ring gaps. Therefore, as illustrated in fig (12.a) only magnetic stimulation occurs, while fig (12.c) illustrates the occurrence of the electric stimulation, fig (12.b) shows electric and magnetic stimulation, fig (12.d) illustrate no evidence of stimulation.

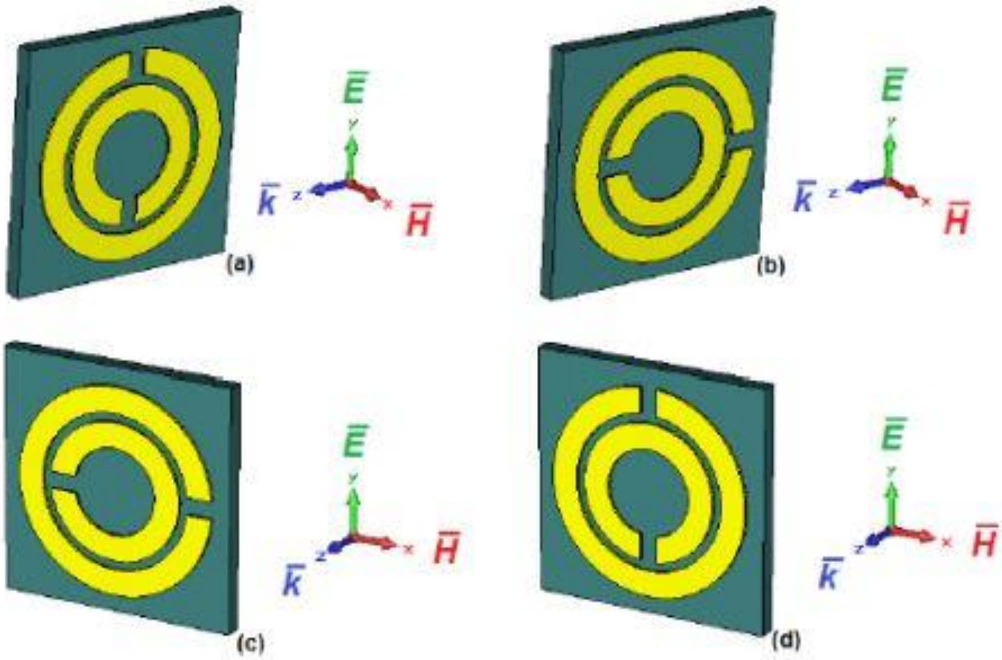

Figure 12. types of stimulation a) magnetic stimulation. b) Electric and magnetic stimulation. c) Electric stimulation. d) No stimulation.

Metamaterial Applications and Research Areas

Due to their tremendous potential, metamaterials offer a wide range of applications and research issues, thus scientists have been motivated to look for and studying these applications. Antennas (metamaterial could enhance the gain and minimize the disadvantage and return loss on a patch antenna), invisible cloaks, filters, diffraction-limit breaking, polarization converters, super lensing, optics, metamaterial absorbers and sensor applications are just a few of the many uses for metamaterials. For the sensors we could increase and improve the resolution and sensitivity of them at the hand of metamaterials. Metamaterial field is a promising field that could be used in a lot of areas. Now uncounted researches arise in so many fields like terahertz metamaterials, seismic metamaterials, acoustic metamaterials, tunable metamaterials, metactronics, power harvesting metamaterials, aerospace metamaterials, tunable metamaterials, frequency selective surface (FSS), photonic metamaterials, etc…

Today metamaterials have been considered in a lot of research areas and maybe in the near future could be involved. We will see below some of the main domains that gives metamaterials increased attention:

Seismic metamaterials

Seismic metamaterials are MMs created to mitigate the negative impacts of seismic waves on man-maid structures found on or near surface. The idea incorporates a layered system of metamaterials, separated by elastic plates in a cylinder arrangement, to provide seismic protection for surface structures. The seismic waves that an earthquake produce could be controlled by seismic metamaterial. It is suggested that using metamaterial as a ring around a building's base may be able to divert the most harmful seismic waves away from the entire structure (Mu D et al, 2020).

Acoustic metamaterials

Acoustic metamaterials are synthetic materials created with the intention of directing, controlling and manipulating sound in the form of sonic waves. Sonic waves could now reach into the region of negative refraction. They could be used on better ultrasound equipment lenses. The material might be used to make soundproof walls for homes or to improve acoustics or steer noise away from specific locations in music halls. Additionally, they could be used in military to develop a new generation of stealth ship and hide submarines from acoustic detection (Cummer et al, 2016).

Tunable metamaterials

Contrary to tunable metamaterial, which has ability to randomly modify frequency variation in the refractive index, normal metamaterial only responds to one frequency or frequency band. The current focus of this domain's research is on negative refractive index materials RHM and the electromagnetic band gap (EBG), also known as the photonic band gap. Researchers are working on a new metamaterial design that will demonstrate the switching feature. Without altering its design, the gadget could transition from a standard flat mirror to a focusing/defocusing mirror. An anisotropic liquid crystal is used in tunable metamaterials to enable frequency tweaking. These metamaterials are used in a variety of electrically adjusted microwave systems for defense, space and business communications (Boardman et al, 2011).

Metactronics

Future nanoscale electronics could be designed using a method called metactronics. Metamaterials' distinctive light-related properties make it possible to create electronic circuitry more quickly and precisely using light. Professor Nader Engheta presented this idea in 2007. A method for modifying, patterning and adjusting optical electric fields is provided by metactronics. The components of clumped Nano-circuits will be represented by nanoparticles. Instead of using electron transport, these optical Nano-electronics will operate on light (Ehgheta et al, 2008).

Power harvesting metamaterials

Metamaterials are idea for harnessing electromagnetic energy. Energy conversion technology is used in power harvesting. The power harvesting metamaterial, according to scientists, might one day be included into a cell phone, enabling wireless recharging of the device when they are not in use. Theoretically, this functionality would enable locals to harvest energy from a neighborhood cell phone tower in locations where there isn't simple access to a regular power outlet. Appliances can consume less energy by wirelessly recovering electricity that is now lost while operating (Hawkes et al, 2013).

Terahertz metamaterials

Materials that interact at terahertz frequencies are referred to as terahertz metamaterials. The frequency range is typically specified as 0.1 to 10 THz for applications and THz research for metamaterials and other materials. This matches to wavelengths 0.03 mm – 3 mm range. Terahertz metamaterials are a mixture of synthetic materials that interact at terahertz frequencies. Passive materials are those metamaterials that can produce the desired magnetic response with negative values of permeability. In order to develop a new response, “tuning” is therefore accomplished by constructing a new material with slightly altered dimensions (Xu et al, 2017).

Now we will see the most useful applications that the metamaterial used in:

Metamaterial antennas

An important class of antennas includes metamaterial-based ones that have negative permittivity with or without negative permeability. Negative permeability or negative permittivity materials could offer an electrically tiny antenna dimensions. Metamaterial antennas could improve the performance of the antenna in terms of bandwidth and efficiency. Variable operating frequency, High directivity, and antenna aligning control are crucial characteristics of metamaterial antennas. The most recent metamaterial antenna emits 95% of the radio signal received at 350 MHz. The smallest experimental metamaterial antenna is only one of five of the wavelength in size.

For instance, the metamaterial CNC-shaped resonator as seen in fig (13) improves the gain and bandwidth for 5.5 GHz frequency (Upadhyaya et al, 2014).

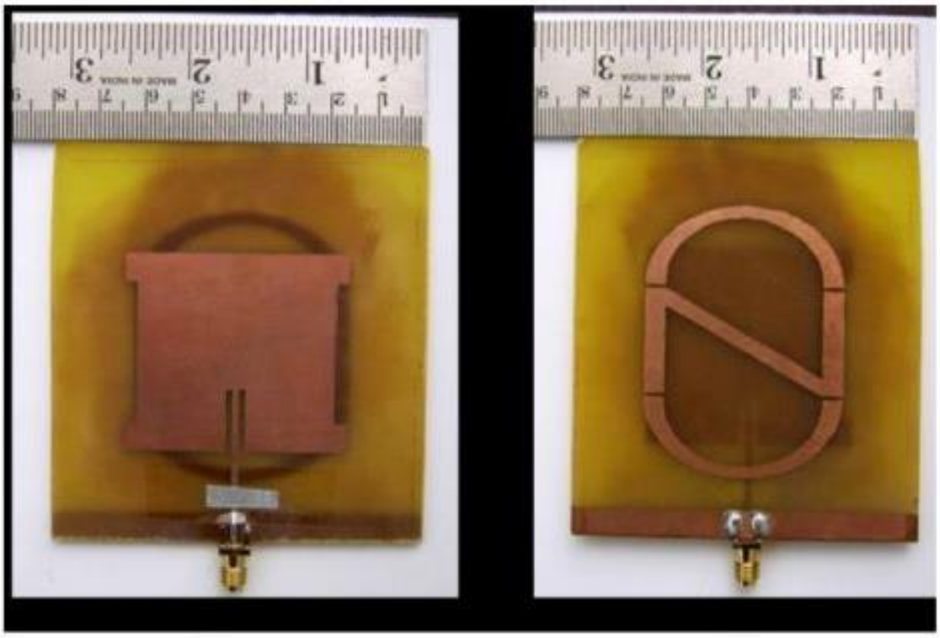

Figure 13. CNC-shaped metamaterial antenna (Upadhyaya et al, 2014)

Metamaterial cloaks

Investigation into cloaking in the 1990s revealed that complete cloaking was not feasible in all incidence directions. After then, starting in 2007, metamaterial cloaking has brought the idea of an object’s invisibility to life. By canceling the magnetic and electric fields that an object produces or by directing the electromagnet wave around the object, cloaking could be accomplished. In order to redirect the wave, the coordinate system must be altered until the electromagnetic field inside the hollow cloak is zero, which causes the area inside the shell to vanish (Pendry et al, 2006).

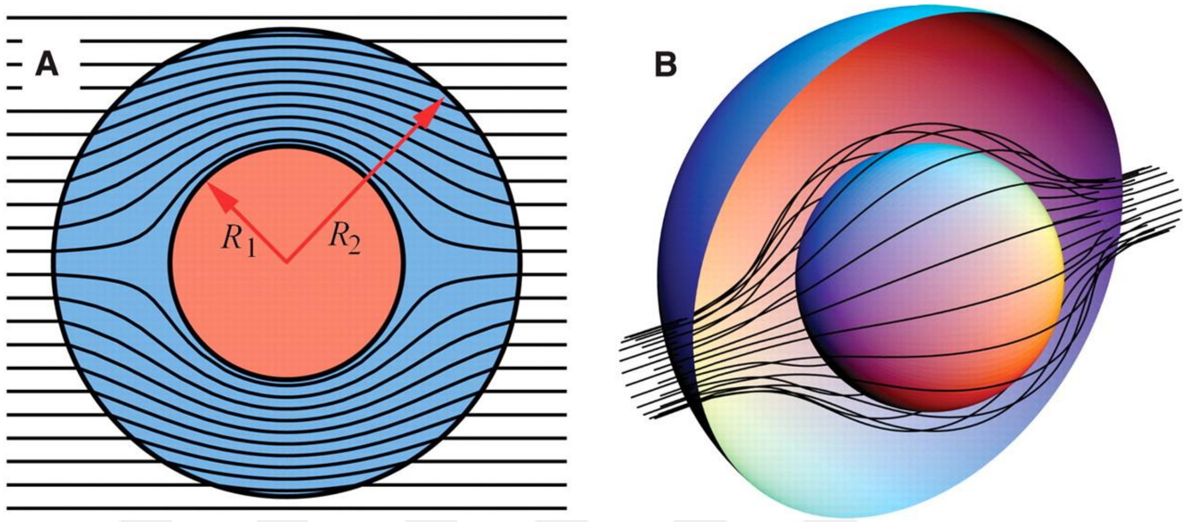

Figure 14. Pendry's invisible metamaterial cloak (Ung B, 2009)

In the case of metamaterial object, incoming light from the rear side of the object slides around it and move to the front side. As a result, incoming light from the item's rear side is the only light that could be seen by a human observer on the front side of the object. Despite the fact that the object is present physically, incident wave from the backside overpowers whatever light it reflects, rendering it optically invisible.

Superlens

With the use of superlens made of metamaterials, the diffraction-based image resolution limitation of conventional lenses could be overcome. A superlens, that counteracts wave fading and improves image quality, is realized in the work of (Pendry, 2000).

The superlens' operational concept is shown in fig (15). A metamaterial media with a low refractive index twist the incoming wave in the opposite direction. The wave here converges to a point despite the fact that it would be normally diverge from a point because of the negative refractive index in the case of right handed materials.

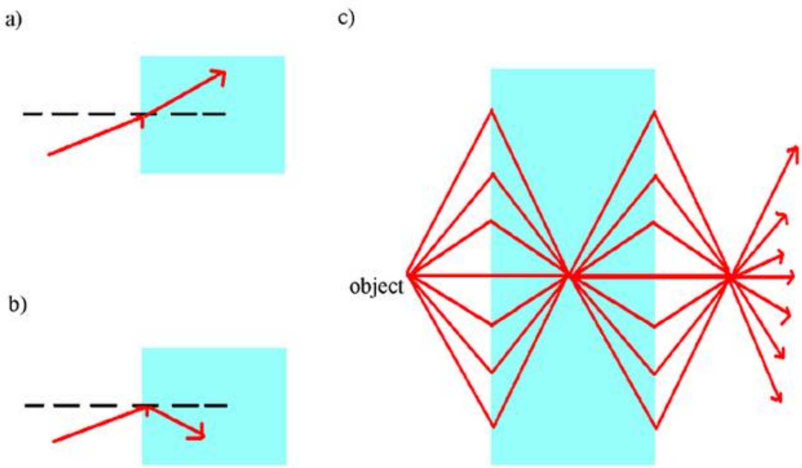

Figure 15. Superlens a) positive refraction index. b) negative refractive index. c) Refraction of wave in superlens.

Metamaterial absorber

An effective way to absorb electromagnetic waves is via a metamaterial absorber. Metamaterials that are intended to function as absorbers provide advantages over traditional absorbers, like wider adaptability, further miniaturization and increased efficacy. Photodetectors, emitters, sensors, infrared camouflage, spatial light modulators, wireless communication, usage in solar photovoltaics and thermophotovoltaics are some of the potential uses for the metamaterial absorbers.

Landy created the first metamaterial absorber in 2008, which has three layers, one dielectric and two metallic, and exhibits a simulated absorptivity of 99% at 11.48 GHz frequency, see fig (16)

Experimentally, Landy was successful in achieving only 88% of absorptivity due to fabrication errors (Landy et al, 2008).

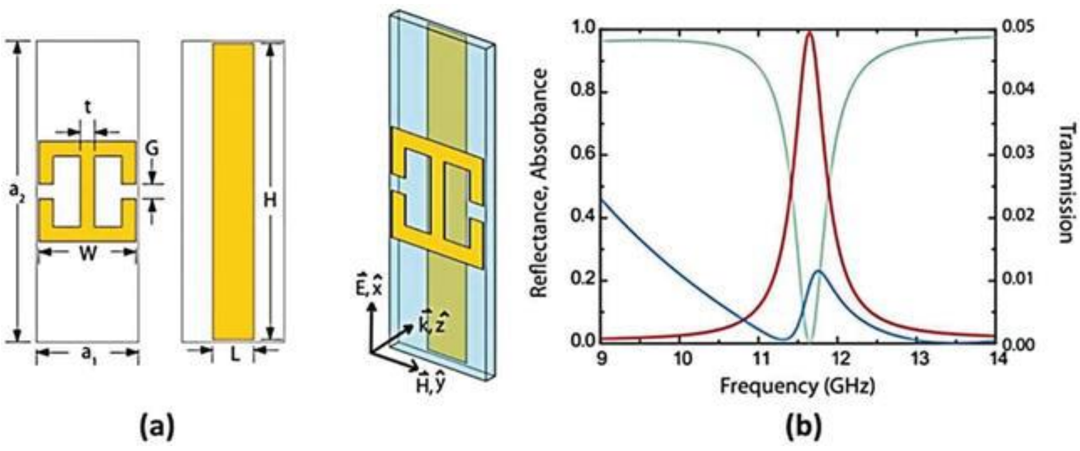

Figure 16. Landy's absorber a) the unit cell and its components b) the simulation results

Metamaterial converter

The study of electromagnetic metamaterials has grown recently. Electromagnetic wave amplitude, propagation direction and phase difference can all be successfully controlled by metamaterials. The could be used to do a variety of amazing tasks that conventional materials couldn't or be fulfilled with ease. One of the crucial aspects of electromagnetic radiation is polarization. Application of electronic information including sensing, imaging and optical communication require the ability to manipulate polarization.

The used metamaterial converters could differ in a lot of aspects like the bandwidth or the material that made from or the number of layers stuck together to build it, if the converter could be used to maintain LP or CP or both…

The MM converters have two main advantages compared with the conventional ones which are the efficiency and the small size. Some MM converter could convert with an efficiency more than 99% in 10*10 cm^2 in size.

In 2018, Khan and Tahir made a MM converter with a thickness of 2.4 that work in the range of 5-15 and could achieve both LP-LP and LP-CP with efficiency of more than 90% (Khan and Tahir, 2018). In 2019, Fu et.al found an MM converter with a thickness of 3 mm that could achieve a PCR of more than 98.2% in the range of 9.38 -13.36 GHz (Fu et al. 2019). In 2019 Zhao et.al found an MM converter with a thickness of 3 mm that work from 8.44 – 24.96 GHz with a PCR more than 90% (Zhao et al, 2019).

In 2021, Tutar and Ozturk make an MM converter (see fig. (17)) that could achieve both linear and circular polarization with a PCR than 90% in the range of 4.61-4.85 GHz and 6.86-7.78 GHz, the RHCP is more than 97% in the range of 5353-5.94 GHz and the LHCP is more than 97% in the range of 8.88-12.03 GHz. The MM unit has a 10 mm length and width and a depth of 2.8 mm (Tutar and Ozturk, 2021).

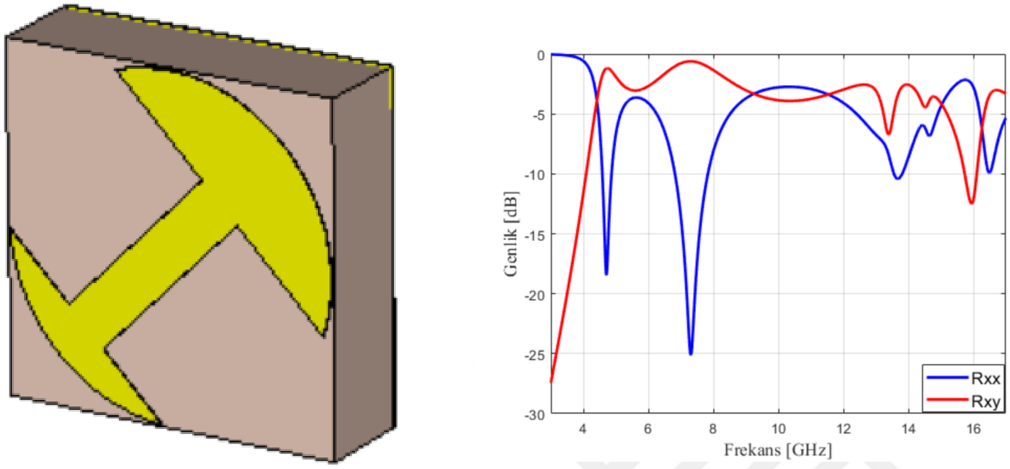

Figure 17. Linear and circular polarization converter that could work in both c and x bandwidth (Tutar and Ozturk 2021)

In our study, as we will see later, we were able to achieve good results in both linear and circular polarization with more than 99% of polarization.

MATERIAL AND METHOD

Polarization

Since almost sources of ligh are made of a choatic mixture of waves with various spatial properties, phases, frequencies and polarization staters, they are typically categorized as incoherent and unpolarized sources of light. Coherent plane waves, which are sinusoidal radiations with a specific direction, phase, direction and polarization state, make understanding electromagentic waves and polarization specific.

Phisics states that the wave nature of electromagnetic radiation causes the phenomenon known as polarization. Since sunlight passes through the vacuum to reach the our planet, it serves as an illustration of elelctromagnetic waves. Because of the interaction between the magnetic field **B** and the electric field **E**, these waves are known as electromagnetic waves.

Ther are a lot of uses of polarization in many fields like for instance 3D movies, Radio reception and transmission, sky polarization and photography, polarized sunglasses, infrared spectroscopy, in chemistry, display technologies,…

It is recommended to start by merely thinking about pure polarization and a coherent sinusoidal signal at a certain optical frequency in order to understand polarization.

The first two figures below (fig (18)) show the linear polarization's electric field vector across a full cycle for to two distinct inclination; each of them is thout of as seperates SOP (State Of Polarization). It shoud be noticed that the linear polarization at 45^0 can also be viewed as the combination of horizontally polarized wave with the same phase and amplitude as the vertically one (as displayed in the second shape).

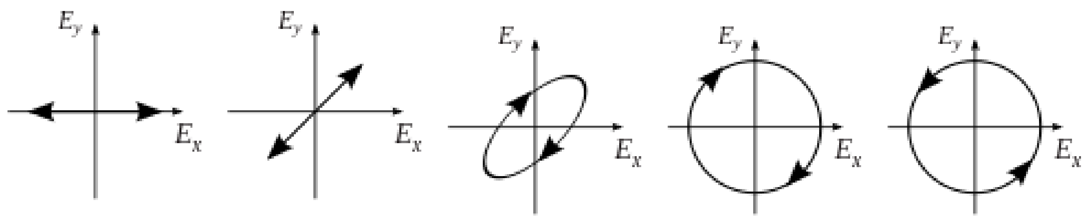

Figure 18. Types of polarization (Linear, Elliptical and Circular Polarization)

Now, if a phase shift were to be added between those horizontal and vertical polarization components, elliptical polarization would typically result, as seen in the third shape. Circular polarization is created when the phase shift is precisely 90^0 as illustrated in the fourth and fifth shape. In order to introduce such a phase shift, a quarter-wave plate is used to start with linearly polarized light and construct circular polarization from there. Noting that the rotation of the field during circular polarization or elliptical polarization might occur either clockwise or counterclockwise. If the rotation is in the clockwise direction then according to the direction of propagation the direction is in a left-hand direction, and in contrast if the rotation is in the counterclockwise direction then the propagation is in a right-hand direction (Garg et al, 2011).

Linear polarization

A light wave is known to be linearly polarized if an electric field swings in a straight line orthogonal to the wave axis. The advancing axis and the electric field's direction are both orthogonal to the magnetic field, which is oscillating in that direction. The oscillation of the electric field is thought to occur in the direction of polarization. Any other direction perpendicular to the wave axis could experience polarization. A rationally different state is not produced by 180^0 of polarization shift (Balanis C.A, 2012).

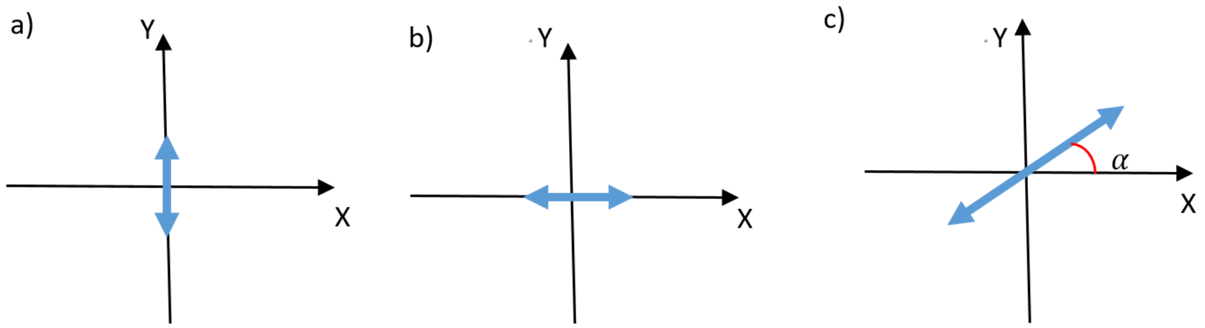

Figure 19. LP-LP where the blue line is the electric field variation over time a) Vertical LP b) Horizontal LP c) Arbitrary-Angle LP

In the previous diagram the direction of the propagation is out of the page to us.

We could define the equations for the vertical and horizontal linear polarization as below (see fig (19.a and 19.b):

$$\mathbf{E_x}(\mathbf{r}, t) = \mathrm{Re}\{E_0 \hat{y} e^{j(kz-\omega t)}\} \quad (22)$$

$$\mathbf{E_y}(\mathbf{r}, t) = \mathrm{Re}\{E_0 \hat{x} e^{j(kz-\omega t)}\} \quad (23)$$

If the angle is 45^0 between the x axis and the E field then we could consider the wave propagation consists of two components $\mathbf{E_x}$ and $\mathbf{E_y}$ as follow:

$$\mathbf{E_x}(z, t) = \mathrm{Re}\{E_0 e^{j(kz-\omega t)}\} \quad (24)$$

$$\mathbf{E_y}(z, t) = \mathrm{Re}\{E_0 e^{j(kz-\omega t)}\} \quad (25)$$

And the total wave propagation is:

$$\mathbf{E}(z,t) = E_x\hat{x} + E_y\hat{y} \tag{26}$$

In general, if the angle between the x axis and the E field is α then we could write the equations of the propagation as follow:

$$\mathbf{E_x}(z,t) = \mathrm{Re}\{E_0\cos(\alpha)e^{j(kz-\omega t)}\} \tag{27}$$

$$\mathbf{E_y}(z,t) = \mathrm{Re}\{E_0\sin(\alpha)e^{j(kz-\omega t)}\} \tag{28}$$

And the total wave propagation is also:

$$\mathbf{E}(z,t) = E_x\hat{x} + E_y\hat{y} \tag{29}$$

If we will define the polarization state as a 2D vector (Jones vector) that contain two complex amplitudes:

$E = \begin{vmatrix} E_x \\ E_y \end{vmatrix}$ or as relative values $E/E_x = \begin{vmatrix} 1 \\ E_y/E_x \end{vmatrix}$ or $E/E_y = \begin{vmatrix} E_x/E_y \\ 1 \end{vmatrix}$ then we could specify all the above results like:

0^0 linear polarization: E_y/E_x=0 then $E/E_x = \begin{vmatrix} 1 \\ 0 \end{vmatrix}$

90^0 linear polarization: E_x/E_y=0 then $E/E_y = \begin{vmatrix} 0 \\ 1 \end{vmatrix}$

45^0 linear polarization: E_x/E_y=1 then $E/\sqrt{2}E_x = \begin{vmatrix} 1 \\ 1 \end{vmatrix}$

Arbitrary linear polarization: $\frac{E_y}{E_x} = \frac{\sin\alpha}{\cos\alpha} = \tan\alpha$

Circular polarization

In this case, the electromagnetic field’s strength is consistent throughout. However, the direction spins at a fixed rate in a plate that is orthogonal to the direction of the path. A circularly polarized wave could spin in just one of two directions: either the electric field vector rotates in a left-hand direction or in a right-hand direction, depending on the propagation’s direction. Since Light behaves as a two-dimensional transverse wave, the phenomenon of polarization occurs.

So if the magnitudes of both E_x and E_y are equal, but with a phase shift of 90^0 then the circular polarization occurs.

There are an LHCP waves or an RHCP waves depending on the rotation's direction. If the wave rotates from the source in clockwise direction in the x-y plane, then the phase difference between x and y angles is -90^0. we could say in this case that the wave is left-hand circularly polarized. And Vice versa, if the wave rotates from the source in counter clockwise direction in the x-y plane, then the phase difference between x and y angles is +90. We could say in this case that the wave is right-handed circularly polarized.

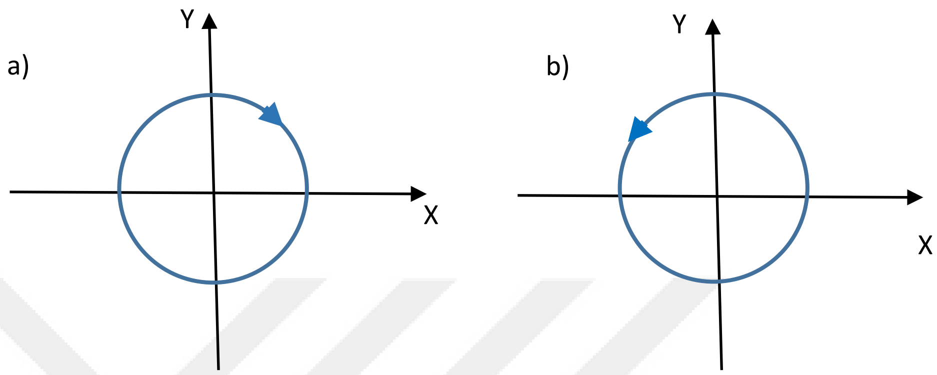

Figure 20. Circular Polarization. a) LHCP wave. b) RHCP wave.

If the light is left-handed circular polarization, as the phase difference between the x and y electric field is: Φ_x- Φ_y=+90^0, we could write (Balanis C.A, 2012):

$$\mathbf{E_x}(z,t) = \mathrm{Re}\{E_0 e^{j(kz-\omega t)}\} = E_0 \cos(kz - wt) \tag{30}$$

$$\mathbf{E_y}(z,t) = \mathrm{Re}\{E_0 j e^{j(kz-\omega t)}\} = -E_0 \sin(kz - wt) \tag{31}$$

And the actual electric field will be:

$$\mathbf{E}(z,t) = E_0\hat{x} \cos(kz - wt) - E_0\hat{y} \sin(kz - wt) \tag{32}$$

In the case of the right-handed circular polarization, as the phase difference between the x and y electric field is Φ_x-Φ_y=-90^0, we could write:

$$\mathbf{E_x}(z,t) = \mathrm{Re}\{E_0 e^{j(kz-\omega t)}\} = E_0 \cos(kz - wt) \tag{33}$$

$$\mathbf{E_y}(z,t) = \mathrm{Re}\{-E_0 j e^{j(kz-\omega t)}\} = +E_0 \sin(kz - wt) \tag{34}$$

And the actual electric field will be:

$$\mathbf{E}(z,t) = E_0\hat{x} \cos(kz - wt) + E_0\hat{y} \sin(kz - wt) \tag{35}$$

Elliptical polarization

As the point of the electric field vector crosses any fixed plane and forms an ellipse orthogonal to the orientation of propagation, this kind of polarization happens (Elliptical

Polarized wave). the elliptical polarization is the general case of the circular polarization where the difference between the E_x phase and E_y phase is any angle not necessarily $\pm 90^0$:

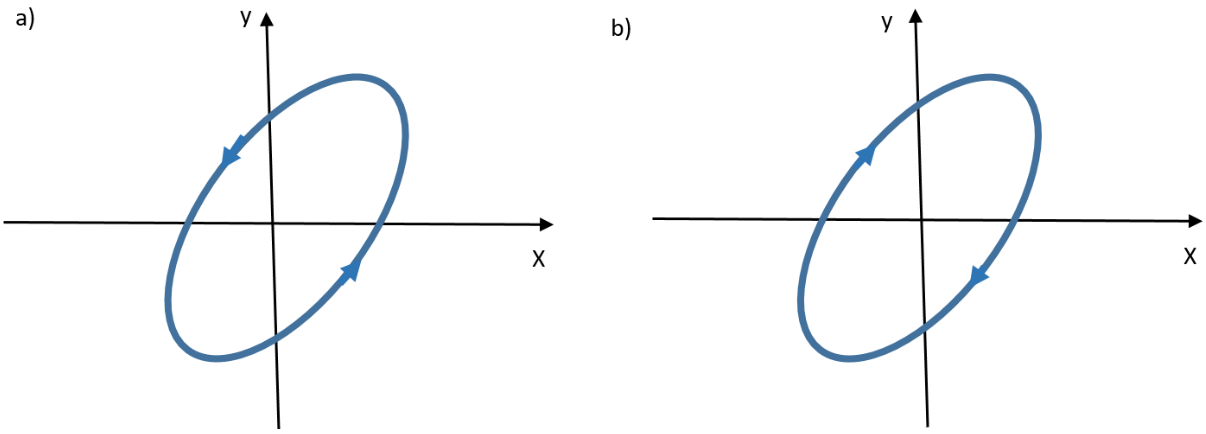

Figure 21. Elliptical polar a) right-hand elliptical polarized wave. b) left-hand elliptical polarized wave.

For the left-hand or right-hand elliptical polarization detection, we should consider the rotation of the wave. The polarization is a left-hand elliptically polarized wave if the rotation is in the clockwise direction. In opposite, the polarization is a right-hand elliptically polarized wave if the rotation is in the counter clockwise direction.

Let's consider the phase difference between the x and y angle of the electric field θ as $\theta = \Phi_x - \Phi_y$ thus we could write the elliptical equations as (Balanis C.A, 2012):

$$\mathbf{E_x}(z,t) = \mathrm{Re}\{E_{0x}e^{j(kz-\omega t)}\} = E_{0x}\cos(kz - wt) \quad (36)$$

$$\mathbf{E_y}(z,t) = \mathrm{Re}\{E_{0y}e^{j(kz-\omega t-\theta)}\} = E_{0y}\cos(kz - wt - \theta) \quad (37)$$

And the actual electric field will be:

$$\mathbf{E}(z,t) = E_{0x}\hat{x}\cos(kz - wt) + E_{0y}\hat{y}\cos(kz - wt - \theta) \quad (38)$$

Where E_x and E_y are different and the relative phase in nonzero, the wave is propagation in the z direction, the polarization rotates in the x-y plane. For the linear polarization could be found if the phase difference θ between Ex and Ey is set to zero, while the circular polarization corresponds to $\theta = \pm 90^0$ and $E_x = E_y$.

Scattering Parameters

Using matched impedances, scattering parameters or S parameters are utilized to describe electrical networks. In this context, scattering refers to the impact of transmission line discontinuity on the propagating currents or voltages. S parameters make it possible to simulate a system without having to deal with the intricate aspects of its actual construction by treating a device as a black box with resulting outputs and inputs.

The explanation of s parameters is divided into two sections; the first part will present the background information necessary to grasp the notion of s parameters. The second section will show us how to use s parameters in EMC measurement and testing.

Two-Port network theory

The circuit analysis method that differs from the bulk of other methods is called two-port network theory. Kirchhoff's rules, superposition, node mesh/voltage current method and other circuit analysis techniques all offer a mechanism to calculate currents and voltages in every circuit. Treating the network as a two-port circuit will allow us to describe the circuit in terms of the two terminals. In a lot of electrical circuits acquiring currents and voltages at the input and output ports, rather than any point in the circuit, is more practical and convenient. This means that the only variables that matter in a two-port circuit analysis are the terminal variables (output voltage or current and input voltage or current).

The two-port network analysis in EMC is often conducted in a sinusoidal steady state, where the current and voltage are sinusoids and are therefore defined by their phase and amplitude at every frequency.

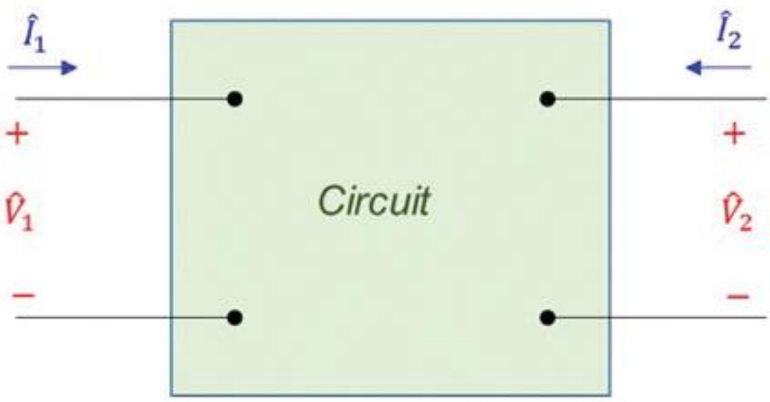

Figure 22. Two port network

Only two of the four terminals variables $(\widehat{V_1}, \widehat{I_1}, \widehat{V_2}, \widehat{I_2})$ are independently varying. The placed hat above the variables refers to the complexity of the variables. From now we won't put these hats in the equation, but for simplicity in all the following equations the variables V_1 I_1 V_2 and I_2 are complex values. There are six different ways to describe the variables above that are (Adamczyk B, 2017):

$$V_1 = z_{11}I_1 + z_{12}I_2 \qquad V_2 = z_{21}I_1 + z_{22}I_2 \tag{39}$$

$$I_1 = Y_{11}V_1 + Y_{12}V_2 \qquad I_2 = Y_{21}V_1 + Y_{22}V_2 \tag{40}$$

$$V_1 = a_{11}V_2 + a_{12}I_2 \qquad I_1 = a_{21}V_2 + a_{22}I_2 \tag{41}$$

$$V_2 = b_{11}v_1 + b_{12}I_1 \qquad I_2 = b_{21}v_1 + b_{22}I_1 \tag{42}$$

$$V_1 = h_{11}I_1 + h_{12}v_2 \qquad I_2 = h_{21}I_1 + h_{22}v_2 \tag{43}$$

$$I_1 = g_{11}v_1 + g_{12}I_2 \qquad V_2 = g_{21}v_1 + g_{22}I_2 \tag{44}$$

The parameters of the two network are the coefficients in each set of equations in the previous six coupled equations. We will refer to each couple as the letter that contains for instance, Z parameters, y parameters, b parameters, etc… the information about a network is the same for each parameter couple, and any set could indeed be calculated in terms of any other set. We need to know how to get a specific set of parameters.

Let's start with z parameters, as it is cleared from the Eq. (39) we will extract the z parameters as:

$$z_{11} = \frac{v_1}{I_1}\bigg|_{I_2=0} \quad z_{12} = \frac{v_1}{I_2}\bigg|_{I_I=0} \quad z_{21} = \frac{v_2}{I_1}\bigg|_{I_2=0} \quad z_{22} = \frac{v_2}{I_2}\bigg|_{I_1=0} \tag{45}$$

Thus the z parameters could be gained from the current and voltage measurements if we apply open-circuit for each port.

From the eq. (40) the y parameters are derived as:

$$y_{11} = \frac{I_1}{v_1}\bigg|_{v_2=0} \quad y_{12} = \frac{I_1}{V_2}\bigg|_{V_I=0} \quad y_{21} = \frac{I_2}{V_1}\bigg|_{V_2=0} \quad y_{22} = \frac{I_2}{V_2}\bigg|_{V_1=0} \tag{46}$$

Thus the y parameters could be gained from the current and voltage measurements if we apply short-circuit on each port.

From the eq. (41) the y parameters are derived as:

$$a_{11} = \frac{v_1}{v_2}\bigg|_{I_2=0} \quad a_{12} = -\frac{v_1}{I_2}\bigg|_{v_2=0} \quad a_{21} = \frac{I_1}{V_2}\bigg|_{I_2=0} \quad a_{22} = -\frac{I_1}{I_2}\bigg|_{V_2=0} \tag{47}$$

Thus the a parameters could be gained from the current and voltage measurements if we apply both open-circuit and short-circuit on port 2.

From the eq. (42) the y parameters are derived as:

$$b_{11} = \frac{v_2}{v_1}\bigg|_{I_1=0} \quad b_{12} = -\frac{v_2}{I_1}\bigg|_{V_1=0} \quad b_{21} = \frac{I_2}{V_1}\bigg|_{I_1=0} \quad b_{22} = -\frac{I_2}{I_1}\bigg|_{V_1=0} \tag{48}$$

Thus the b parameters could be gained from the current and voltage measurements if we apply both open-circuit and short-circuit on port 1.

From the eq. (43) the y parameters are derived as:

$$h_{11} = \left.\frac{v_1}{I_1}\right|_{V_2=0} \quad h_{12} = \left.\frac{v_1}{V_2}\right|_{I_1=0} \quad h_{21} = \left.\frac{I_2}{I_1}\right|_{V_2=0} \quad h_{22} = \left.\frac{I_2}{V_1}\right|_{I_1=0} \tag{49}$$

Thus the b parameters could be gained from the current and voltage measurements if we apply open-circuit on port 1and short-circuit on port 2.

From the eq. (44) the y parameters are derived as:

$$g_{11} = \left.\frac{I_1}{V_1}\right|_{I_2=0} \quad g_{12} = \left.\frac{I_1}{I_2}\right|_{V_1=0} \quad g_{21} = \left.\frac{V_2}{V_1}\right|_{I_2=0} \quad g_{22} = \left.\frac{V_2}{I_1}\right|_{V_1=0} \tag{50}$$

Thus the b parameters could be gained from the current and voltage measurements if we apply open-circuit on port 2 and short-circuit on port 1.

It is essential to have a basic understanding of transmission line theory in order to comprehend the idea of S parameters. The maximal power transfers at high frequencies is correlated with the impedance of the power source Z_S and the impedance of load $Z_{L.}$ Waves of current, voltage and power from a source with impedance Z_S are transmitted via a transmission line with impedance Z_C to load with impedance Z_L. Total power is transmitted from the source to the load if $Z_L= Z_C$. if $Z_L \neq Z_C$ then the maximum power transfer is prevented because some power is reflected from the load back to the source. The reflection coefficient Γ, denoted by the complex number, which include phase and amplitude information about the signal, describes the connection between the reflected and incident waves.

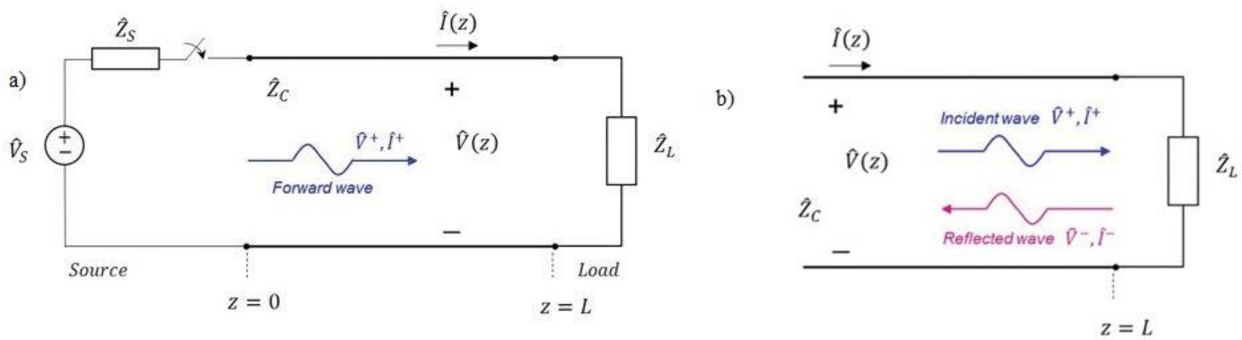

Figure 23. transmitted and reflected waves a) Forward wave b) reflection at the load

If Z_L and Z_C perfectly match, there are no reflection and Γ=0. With all power reflected back to Z_S if Z_L is typically not exactly equal to Z_C in passive systems. Since reflection coefficients Γ are a function of the impedances being taken into account may be expressed as:

$$\Gamma_L = \frac{Z_L - Z_C}{Z_L + Z_C} \tag{51}$$

S parameters

S parameters are used to describe high-frequency circuits because they relate traveling voltage waves that occur when a two-port system is introduced into a transmission line and are incident, transmitted and reflected waves as illustrate in figure (24) (Adamczyk B, 2017).

The incident waves (that result in the transmitted and reflected waves) can be impacting one of the ports 1 and 2. Let’s use the symbols a_1 and a_2 to represent the waves hit ports 1 and 2 correspondingly. The reflected waves from the port 1 and 2 will be denoted as b_1 and b_2 respectively (see figure (24))

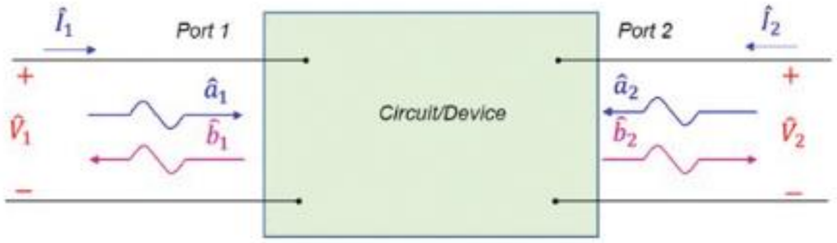

Figure 24. Reflected and Incident waves at port 2 and port 1

For a two port system, the reflected and incident waves are used to provide the S parameters. The two-port equations in terms of the S parameters are:

$$b_1 = S_{11}a_1 + S_{12}a_2 \qquad\qquad b_2 = S_{21}a_1 + S_{22}a_2 \qquad (52)$$

Similar to how the two-port parameters sets covered before were obtained, we derive the four S parameters as:

$$S_{11} = \frac{b_1}{a_1}\bigg|_{a_2=0} \quad S_{12} = \frac{b_1}{a_2}\bigg|_{a_1=0} \quad S_{21} = \frac{b_2}{a_1}\bigg|_{a_2=0} \quad S_{22} = \frac{b_2}{a_2}\bigg|_{a_1=0} \qquad (53)$$

We can’t apply the open or short circuited that used in the two-port system as they aren’t real at frequencies that are high. As it is illustrated in fig (25.a) the incident wave a_1 reaches port 1 in which it creates a transmitted wave b_2 and a reflected wave b_1. Where the reflected wave will come back to the source. Now if $Z_L = Z_C$ then all the incident wave will pass through the system and no reflection will occur. For the incident wave a_2 we could apply the same method (see fig (25.b))

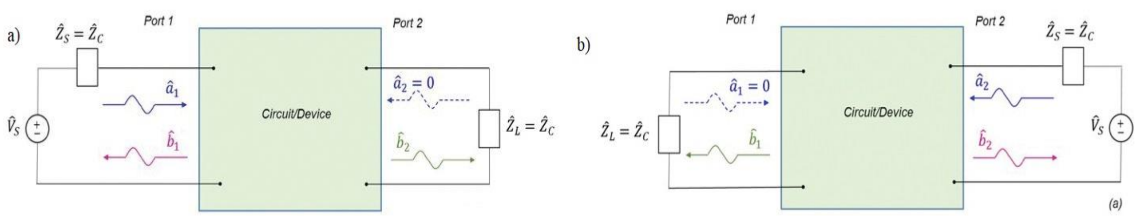

Figure 25. a) the determination circuit for S11 and S21 b) The determination circuit for S22

and S12

We could also talk about the incident, reflected and transmitted power when applying the S parameters. We could connect these S parameters to the incident, reflected and transmitted power. The incident power at port 1 could be mathematically expressed as a_1^2 and at port 2 as a_2^2, while for the reflected power form port 1 the math expression is b_1^2 and for port 2 is b_2^2.

For the gains and losses in dB, they could be expressed as a definition of S parameters. The far more typical EMC losses are:

$$\text{Return loss}_{dB} = 10 \log(a_1^2/b_1^2) = -20 \log(S_{11}) \quad (54)$$

$$\text{Insertion loss}_{dB} = 10 \log(a_1^2/b_2^2) = -20 \log(S_{21}) \quad (55)$$

Stokes Parameters

In addition to fully and elliptically polarized light, partially polarized light and unpolarized light are also described by the Stokes Parameters. When the optical beam is made up of two separated perpendicular components with varying phase and amplitude, E_x (z, t) and E_y (z, t), polarization occurs. In order to make the propagation direction in the z-direction, the perpendicular components could be assumed to be along the y and x axes. We could describe this attitude as the equations below (Papas C.H, 2014):

$$E_x(z,t) = E_{ox}cos(\omega t - kz + \delta_x) \quad (56)$$

$$E_y(z,t) = E_{oy}cos(\omega t - kz + \delta_y) \quad (57)$$

In which t stands for time. The optical field maximal amplitude are E_{oy} and E_{ox}, the wave number k is defined as k=2π/ λ, ω which is the angular frequency could be defined as $\omega = 2\pi f$, the phase constants for E_x and E_y are δ_x and δ_y respectively.

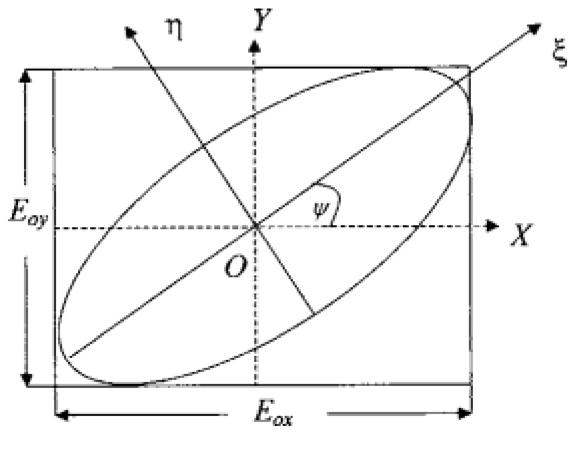

Figure 26. Elliptical polarization along the x-axes and the y-axes

If we define $\delta = \delta_x - \delta_y$ as the polarization ellipse (since it explains the optical field polarization), and taking advantage of the mathematical relation :

$cos(x - y) = cos\, x\, cos\, y + sin\, x\, sin\, y$, then we could reach to the equation:

$$\frac{{E_x}^2(z,t)}{{E_{ox}}^2} + \frac{{E_y}^2(z,t)}{{E_{oy}}^2} - \frac{2E_x(z,t)E_y(z,t)}{E_{ox}E_{oy}} cos\delta = sin^2\delta \qquad (58)$$

Solving the previous equation is complex so we need to transform it to the intensity domain by taking the time average of the variables as: $<E_x(z, t)^2> = \frac{1}{2} E_{ox}$, $<E_y(z, t)^2> = \frac{1}{2} E_{oy}$ and

$<E_x(z, t)E_y(z, t)> = \frac{1}{2} E_{ox} E_{oy} \cos \delta$. By multiplying the Eq.3.35 by $4{E_{ox}}^2{E_{oy}}^2$and applying the previous transformation we could write 3. As:

$$\left(2{E_{ox}}^2{E_{oy}}^2\right) + (2{E_{ox}}^2{E_{oy}}^2) - (2E_{ox}E_{oy}cos\, \delta)^2 = (2E_{ox}E_{oy}sin\, \delta)^2 \qquad (59)$$

Applying the relation: $(4xy= (x + y)^2 – (x-y)^2$ to the previous equation we could reach to our final equation:

$$({E_{ox}}^2 + {E_{oy}}^2)^2 - ({E_{ox}}^2 - {E_{oy}}^2)^2 - (2E_{ox}E_{oy}cos\, \delta)^2 = (2E_{ox}E_{oy}sin\, \delta)^2 \qquad (60)$$

Which also could be written as:

$$ {S_o}^2 = {S_1}^2 + {S_2}^2 + {S_3}^2 \qquad (61)$$

$$ S_o = I = {E_{ox}}^2 + {E_{oy}}^2 \qquad (62)$$

$$ S_1 = Q = {E_{ox}}^2 - {E_{oy}}^2 \qquad (63)$$

$$ S_2 = U = 2E_{ox}E_{oy}cos\, \delta \qquad (64)$$

$$ S_3 = V = 2E_{ox}E_{oy}sin\, \delta \qquad (65)$$

The wave intensity is determined by the parameter I or S_0 while Q, U and V or S_1 S_2 and S_3 depend on the characteristic of linear or circular polarization, respectively. The parameter Q equals to + 1 for the 100% horizontal linearly polarized wave, and equals to -1 for the 100% vertical linearly polarized wave. U vector equals to +1 for the 100% diagonal (+45) linearly polarized wave, and equals to -1 for the 100% diagonal (-45) linearly polarized wave. V vector equals to +1 for the 100% right-hand circularly polarized wave, and equals to -1 for the 100% left-hand circularly polarized wave. We could set the most useful set of polarization states as (Papas C.H, 2014):

$$S_{LHP} = \begin{pmatrix} S_o \\ S_1 \\ S_2 \\ S_3 \end{pmatrix} = \begin{pmatrix} 1 \\ 1 \\ 0 \\ 0 \end{pmatrix} \qquad S_{LVP} = \begin{pmatrix} S_o \\ S_1 \\ S_2 \\ S_3 \end{pmatrix} = \begin{pmatrix} 1 \\ -1 \\ 0 \\ 0 \end{pmatrix} \tag{66}$$

$$S_{L+45P} = \begin{pmatrix} S_o \\ S_1 \\ S_2 \\ S_3 \end{pmatrix} = \begin{pmatrix} 1 \\ 0 \\ 1 \\ 0 \end{pmatrix} \qquad S_{L-45P} = \begin{pmatrix} S_o \\ S_1 \\ S_2 \\ S_3 \end{pmatrix} = \begin{pmatrix} 1 \\ 0 \\ -1 \\ 0 \end{pmatrix} \tag{67}$$

$$S_{RCP} = \begin{pmatrix} S_o \\ S_1 \\ S_2 \\ S_3 \end{pmatrix} = \begin{pmatrix} 1 \\ 0 \\ 0 \\ 1 \end{pmatrix} \qquad S_{LCP} = \begin{pmatrix} S_o \\ S_1 \\ S_2 \\ S_3 \end{pmatrix} = \begin{pmatrix} 1 \\ 0 \\ 0 \\ -1 \end{pmatrix} \tag{68}$$

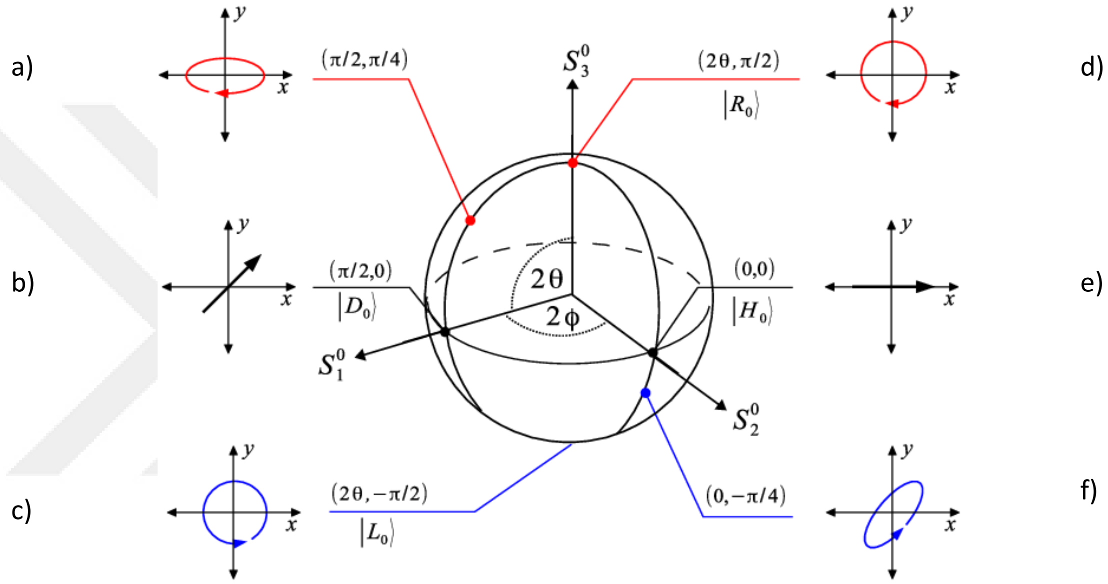

Figure 27. Plane wave polarization states represented by a Poincare sphere a) & f) represent elliptical polarization. b) & e) represent linear polarization c) & d) represent circular polarization.

In addition to totally polarized waves, the Stokes parameters describe also the partially polarized or unpolarized waves. In order to understand these extra polarization states, we need to modify the Eq. (61) as:

$$S_o{}^2 \geq S_1{}^2 + S_2{}^2 + S_3{}^2 \tag{69}$$

If the sign in the previous equation is equal then all the light is polarized, but if the signal greater than then there is unpolarized light or partially polarized one.

The degree of polarization indicated by P is another significant metric. If p equals to one, thus the light is completely polarized and if p equals to 0 thus the light is completely unpolarized. We could define the degree of polarization as below:

$$P = \frac{I_{ELP}}{I_{TOT}} = \frac{\sqrt{{S_1}^2 + {S_2}^2 + {S_3}^2}}{S_o} \quad (70)$$

Ellipticity

We could find the ellipticity from Stoke's parameters by dividing S_3 by S_0 as in the equation below (Khan et al, 2019):

$$\text{Ellipticity} = \frac{S3}{S0} = \frac{2E_{ox}E_{oy}\sin\delta}{{E_{ox}}^2 + {E_{oy}}^2} \quad (71)$$

As it is clear from the Eq. 3.48 in order to achieve maximal ellipticity (Circular polarization) there should be two conditions: The first condition is $E_{ox} = E_{oy}$ and the second condition is $\delta = \mp\frac{\pi}{2}$. for the second condition if the polarization ellipse angle is $+\frac{\pi}{2}$ then the circular polarization is left-hand and V=-1, vice versa if the polarization ellipse angle is $-\frac{\pi}{2}$ then the circular polarization is right-handed and V=+1.

Polarization Conversion Ratio (PCR)

Each and every electromagnetic wave that is reflected from a metasurface typically contains two field components: a cross-polarized reflected field, which has polarization that is perpendicular to the incident wave, and a co-polarized reflected field, which has the same polarized as the incident wave. Using a Cartesian basis, the Jones reflection coefficient matrix R will be utilized to analyze co and cross polarization:

$$R = \begin{pmatrix} R_{xx} & R_{xy} \\ R_{yx} & R_{yy} \end{pmatrix} \quad (72)$$

For the incident waves E_{ix} or E_{iy}, they will be reflecting in two directions x and y as E_{rx} and $E_{ry.}$ so we could define the four reflection components of Jones' reflection matrix R as:

$$R_{xx} = \frac{E_{rx}}{E_{ix}} \quad (73)$$

$$R_{xy} = \frac{E_{rx}}{E_{iy}} \quad (74)$$

$$R_{yx} = \frac{E_{ry}}{E_{ix}} \quad (75)$$

$$R_{yy} = \frac{E_{ry}}{E_{iy}} \quad (76)$$

We could determine from the previous equations that R_{xx} and R_{yy} are the co polarized reflection components while R_{xx} and R_{yy} are the cross-polarized reflection components. So for the E field in x direction (E_{ix}) then it will reflect in the x and y direction E_{rx} and $E_{ry,}$ in which $E_{ix} = E_{rx} + E_{ry}$, so for all cases the summation of R_{xx} and R_{yx} equals to 1: $R_{xx} + R_{yx}=1$. We could apply the same method for the field in y direction (E_{iy}) as $R_{yy} + R_{yx}=1$.

Polarization Conversion ratio (PCR) is a useful indicator of cross-polarization and co-polarization, and could be defined for x incident wave in x and y direction respectively as follows (Ahmed et al, 2020):

$$\mathrm{PCR} = \frac{{R_{yx}}^2}{{R_{yx}}^2 + {R_{xx}}^2} \tag{77}$$

$$\mathrm{PCR} = \frac{{R_{xy}}^2}{{R_{xy}}^2 + {R_{yy}}^2} \tag{78}$$

In the case of electric field in the x direction if all the incident wave reflected in the y direction then the PCR in Eq. (77) is maximum and equals to one, in this case the cross-polarization is maximum. But if all the incident wave reflected in the same direction x, then the PCR is minimal and equal to 0, in this case the co-polarization is maximum. If the incident wave reflects in both x and y direction, then the elliptical polarization occurs. The circular polarization is a special case of the ellipse polarization where the reflected waves in x and y directions are equal and the phase difference between them equals to 90^0. For the E_{iy} wave, the same method should be applied.

Reflection Coefficient

We will divide the y-polarized incident EFI of the wave travelling in the z-axis into the u-v axes for the sake of comprehending the physical process of the suggested metasurface polarization converter. The portion of the incident EFI that is reflected in the +u orientation must be in the +u orientation, for the reflected EFI in the x – orientation. The portion of the incident EFI that is in the +v orientation should be reflected in the –v orientation (see figure (28). The incident wave in this scenario could be written as:

$$\mathbf{E}_i = \hat{y}E_i e^{-jkz} = \hat{u}E_{iu}e^{-\left(jkz+\frac{\pi}{4}\right)} + \hat{v}E_{iv}e^{-\left(jkz-\frac{\pi}{4}\right)} \tag{79}$$

And the reflected wave could be written as:

$$\mathbf{E}_r = \hat{X}E_i e^{-jkz} = \hat{u}E_{iu}e^{-\left(jkz+\frac{\pi}{4}\right)} - \hat{v}E_{iv}e^{-\left(jkz+\frac{3\pi}{4}\right)} \tag{80}$$

$$\mathbf{E}_r = \hat{u}(r_{uu}E_{iu}e^{j\varphi_{uu}} + r_{uv}E_{iv}e^{j\varphi_{uv}}) + \hat{v}(r_{vv}E_{iv}e^{j\varphi_{vv}} + r_{vu}E_{iu}e^{j\varphi_{vu}}) \tag{81}$$

The following matrix format is used to acquire incident and reflected waves in the u and v directions.

$$\mathbf{E}_r = \begin{bmatrix} \mathbf{E}_{ru} \\ \mathbf{E}_{rv} \end{bmatrix} = \begin{bmatrix} r_{uu} & r_{uv} \\ r_{vu} & r_{vv} \end{bmatrix} \begin{bmatrix} \mathbf{E}_{iu} \\ \mathbf{E}_{iv} \end{bmatrix} \quad (82)$$

The cross and co polarized reflection coefficients are represented in the Eq.82 by the letters r_{uu}, r_{vu}, r_{uv} and r_{vv} correspondingly. The phase of the cross and co-polarized reflection coefficients are φ_{uu}, φ_{vu}, φ_{uv}, and φ_{vv} correspondingly. Where $r_{uu} = E_{ru}/E_{iu}$, $r_{vu} = E_{rv}/E_{iu}$, $r_{uv} = E_{ru}/E_{iv}$, and $r_{vv} = E_{rv}/E_{iv}$ are the cross and co-polarized reflection coefficients. For the cross polarized conversion, the incoming wave in the +u orientation should reflect in the exact same amplitude in the +u orientation and the incoming wave in the +v orientation should be reflected with the same amplitude in the –v orientation so that the reflected wave becomes polarized in the x orientation as illustrated in fig (28). Therefore, it is evident that for cross polarization $|r_{uu}| = |r_{vv}|$ and the phase difference is: $\varphi_{uu} - \varphi_{vv} = \mp\pi$. Equivalently, for LP-CP of the incoming wave in the u-v direction $|r_{uu}| = |r_{vv}|e^{\mp j\pi/2}$. As a result, for circular polarization $|r_{uu}| = |r_{vv}|$ and $\varphi_{uu} - \varphi_{uv} = \mp\pi/2$, where an RHCP is carried out for $+\pi/2$ state, and an LHCP is carried out for the $-\pi/2$ state. Furthermore, by assuming that the following of the suggested polarization converter for the converter for the y-polarized incoming wave could be assessed:

$$\eta = \sqrt{|R_{yy}|^2 + |R_{xy}|^2} \quad (83)$$

Due to the losses experienced during the polarization conversion, the Eq. 82 is calculated to be less than one. Switching the indicators u and v will result in the identical situation under x polarized electric field intensity case.

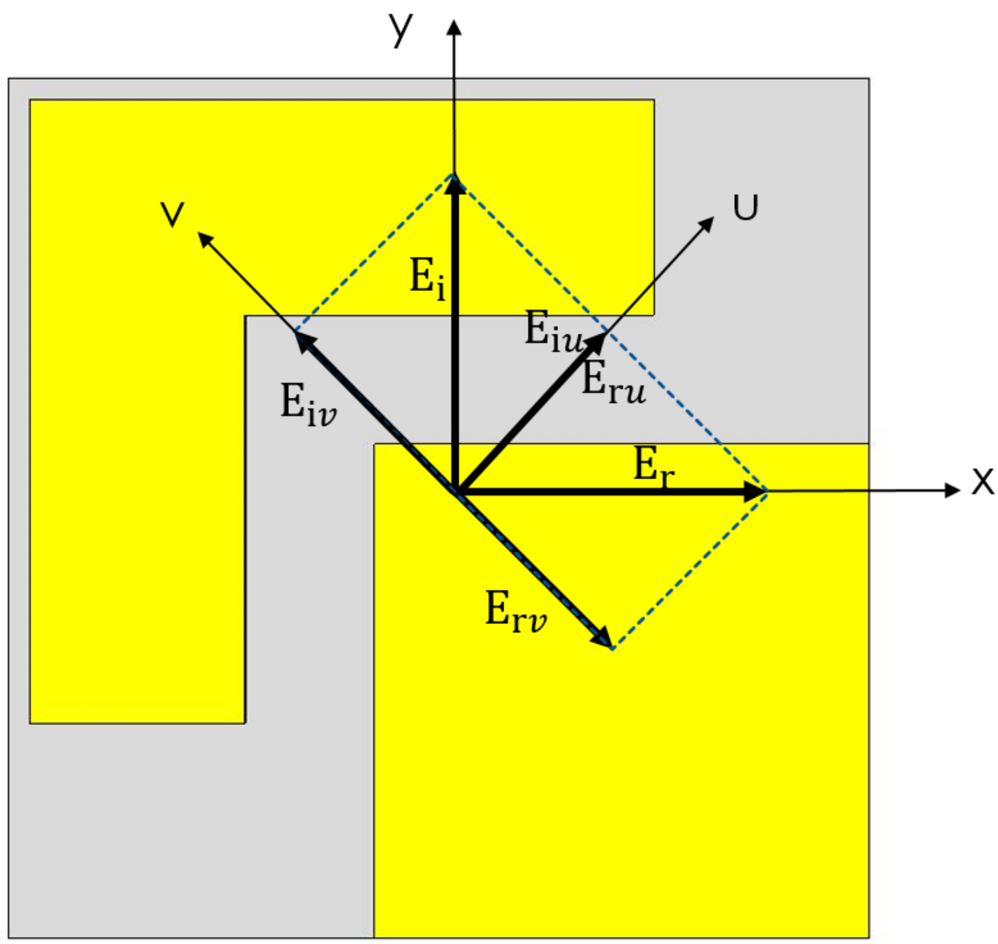

Figure 28. Two orthogonal components of the incident E field along the y-axis and the reflected E field along the x-axis are separated along the u-v axis.

RESEARCH RESULTS AND DISCUSSION

This thesis describes an ultra-thin metamaterial converter that converts with efficiency more than 99% in both LP-LP and LP-CP. The unit cell contains three layers, two metallic layers (copper) and one rectangular dielectric layer (FR4) with a thickness of 1 mm. This section portrays the converters we created for circular and linear polarization as well as their uses. The converter's dimensions will determine in which domains it can operate. Later on, we'll see a converter that could operate in the X and Ku bands, followed by a converter that could operate in the K and Ka bands. The first design's converter operates in a range of frequencies from 8.5 GHz to 17.5 GHz, where it can accomplish three linear conversion with PCR efficiency levels of more than 90% and up to 99% at frequency 12.75. For ellipticity, there are RHCP and LHCP with conversion efficiency exceeding 99%. The second design's converter operates in a range of frequencies from about 18 GHz to more than 40 GHz, where it can accomplish linear and circular polarizaiton with an efficiency more than 99% in both. The program used in this design is CST with the highest accuracy 1e-12.

X and Ku Bands Ultra-thin MM Converter

This converter (see figure (29)) consists of two metallic layer and a dielectric layer in between. The metal used her is copper and the dielectric is FR4.

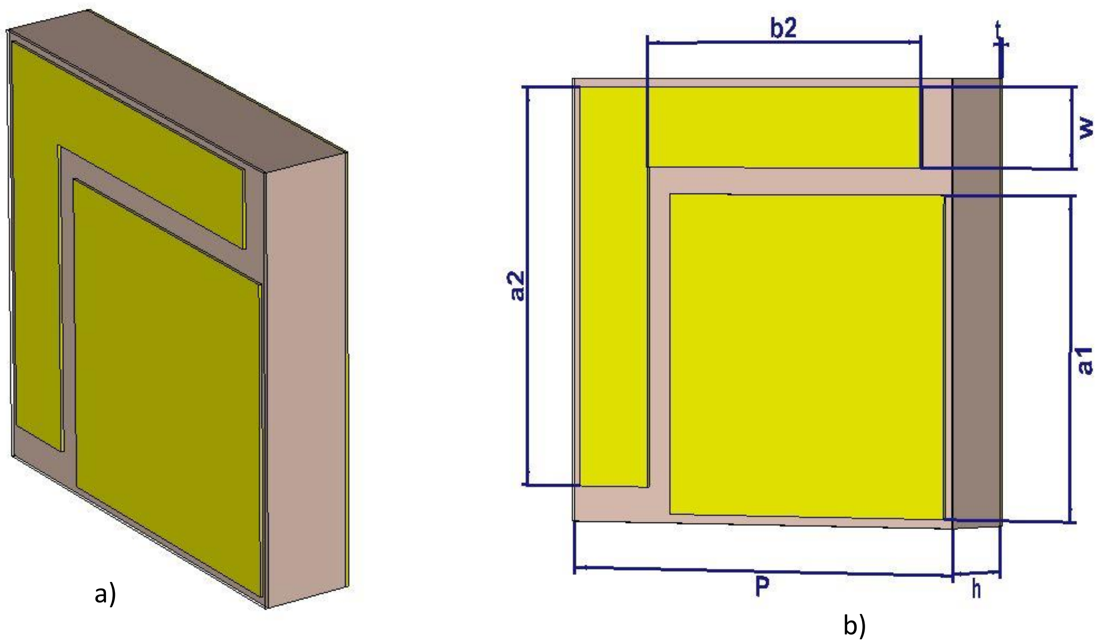

Figure 29. a) X and Ku Bands ultra-thin MM Converter. b) X and Ku ultra-thin MM Converter's dimensions

Figure 29 illustrates the converter's design where the rectangular ground layer is copper. The in between rectangular dielectric layer is FR4. The upper layer is copper and consists of a recangular segment and a gamma Γ shaped segment. The distance between the rectangular or gamma segments and the edges is 0.1 mm. The other dimensions appeared in figure 28.b are: The periodic array P=5 mm, the thickness of the copper layers t=0.035, the thickness of the dielectric is h=1 mm, the upper layer's dimensions are: a1=3.6 mm, a2=4.5 mm, b2= 3.6 mm, w=0.9 mm.

Reflection coefficients

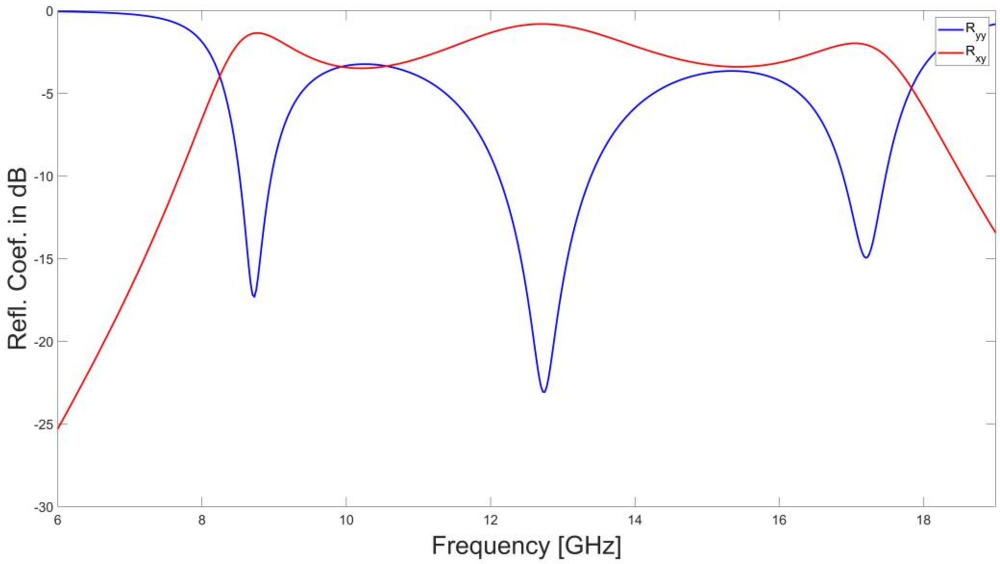

Figure 30. X and Ku Bands ultra-thin MM converter's reflection coefficients in dB.

For the MM converter's reflection coefficients in dB as it is noticed from figure 30 that there could be three LP-LP and two LP-CP. The converter's reflection coefficients in linear will be analyzed in (figure 31) to confirm both LP-LP and LP-CP, while the figure 32 will analyze the polarization ellipse to confirm the LP-CP.

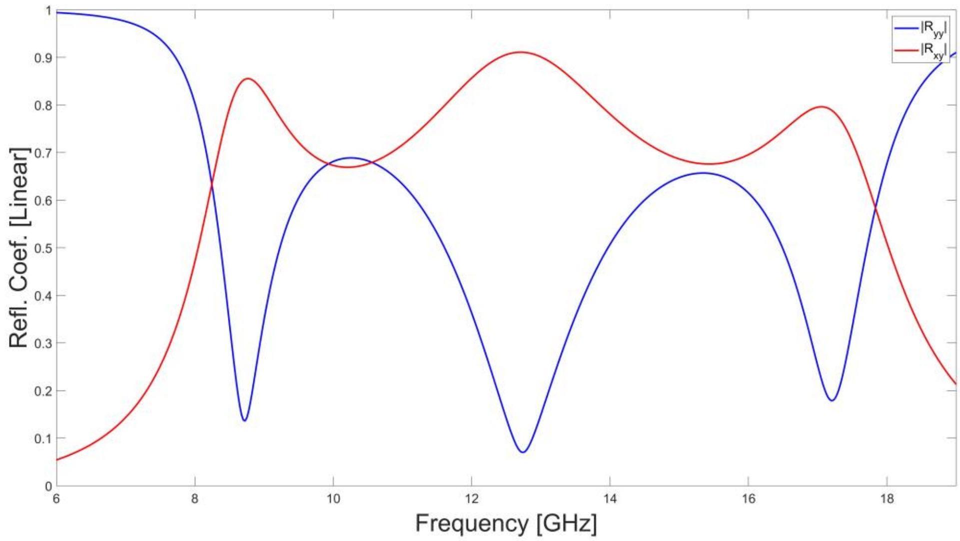

Figure 31. X and Ku Bands ultra-thin MM converter's reflection coefficients in linear.

We will divide the reflection coefficient s in figure 31 into 5 regions where we will compare the values of R_{yy} and R_{xy} to determine the possibilities of linear and circular polarization occurances. (Table 1)

Table 1. Polarization's Oppurtunity of the X and Ku Bands ultra-thin MM Converter.

Frequency band	R_{yy}	R_{xy}	LP-LP opportunity	LP-LP opportunity
8.5-9 GHz	Less than 0.33	More than 0.8	high	x
9.5-11 GHz	0.6-0.69	0.66-0.73	x	High
12-13.4 GHz	Less than 0.33	More than 0.85	High	x
14.7-16 GHz	0.6-0.66	0.67-0.71	x	high
17-17.4 GHz	Less than 0.27	More than 0.75	high	x

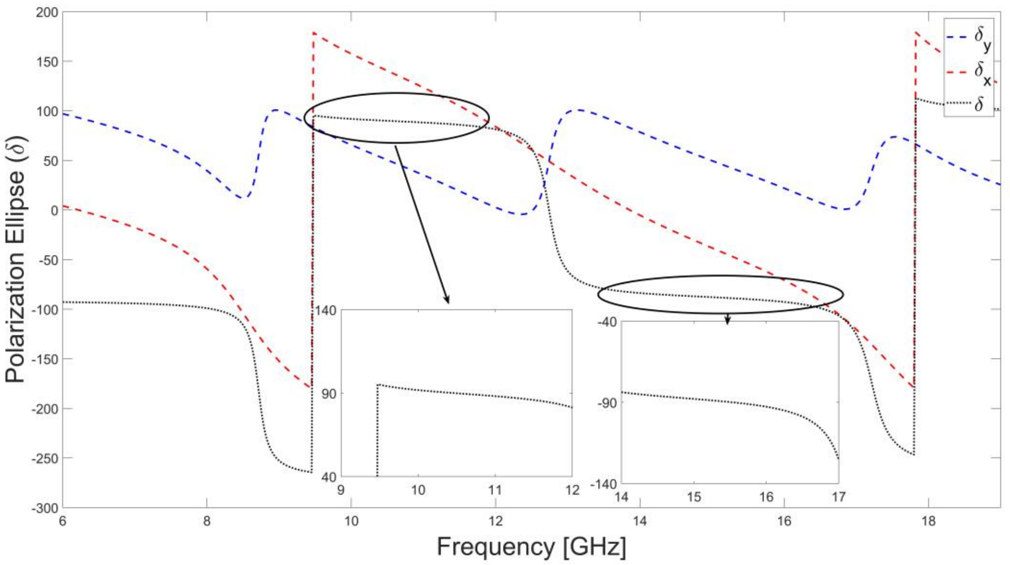

Figure 32. X and Ku Bands ultra-thin MM converter’s polarization ellipse.

To evaluate the occurence of circular polarization there is two conditions: the first condition is that the amplitude of the x and y electric field sould be almost equat. The second condistion is that the polarization’s ellipse angle should be almost 90^0. As it is observed from figure 32, the phase differnce between R_{yy} and R_{xy} is about 90^0 in the frequency ranges 9.5-11 GHz and 14.7-16 GHz.

We will inspect now the PCR and Ellipticity in details to verify the conversion occurence.

PCR

Figure 33 illustrates the PCR of our converter, where the first LP-LP conversion is more than 90% in the frequency band 8.55-8.925 Ghz and could reach to more than 95%, he second LP-LP conversion is more than 90% in the frequency band 12.18-13.33 GHz and could reach to about 99%, he third LP-LP conversion is more than 90% in the frequency band 17-17.4 GHz and could reach to about 95%.

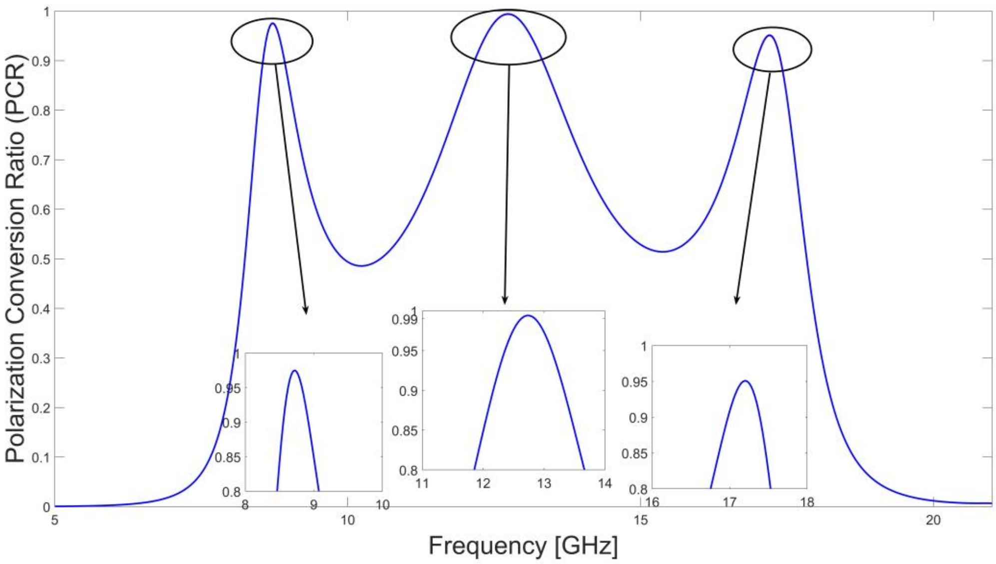

Figure 33. X and Ku Bands ultra-thin MM converter's PCR with normal incidence wave.

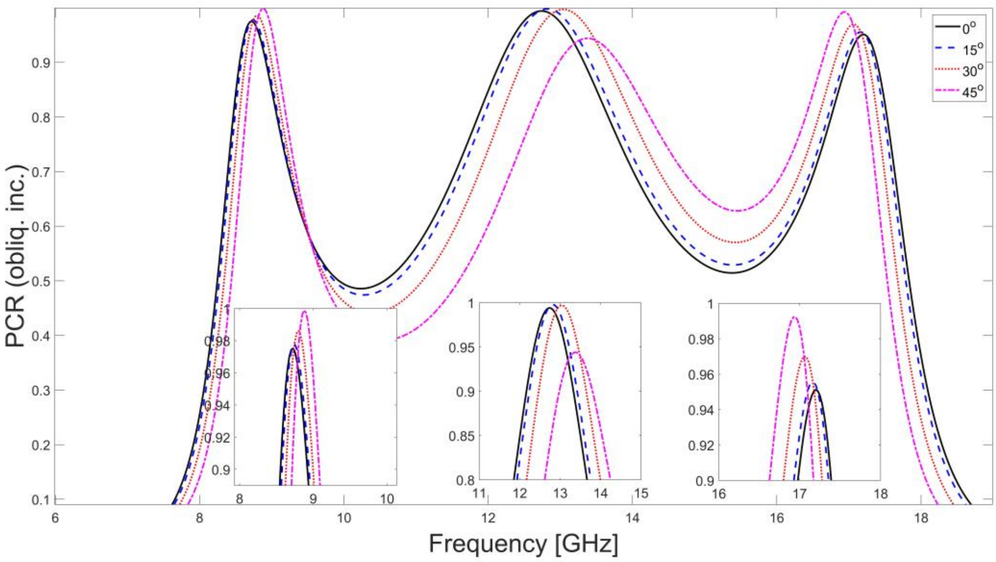

Figure 34. X and Ku Bands ultra-thin MM converter's PCR with oblique incident wave.

For the oblique incident propagation (figure 34), we discussed four propagation oblique incident angles: 0^0, 15^0, 30^0, 45^0 . the results that could be observed from the first region is that the more incident the better PCR, but there is a frequency shifting to the right. In the case of the second and third regions, the more incident wave the less PCR and there is also a frequency shifting to the right.

Ellipticity

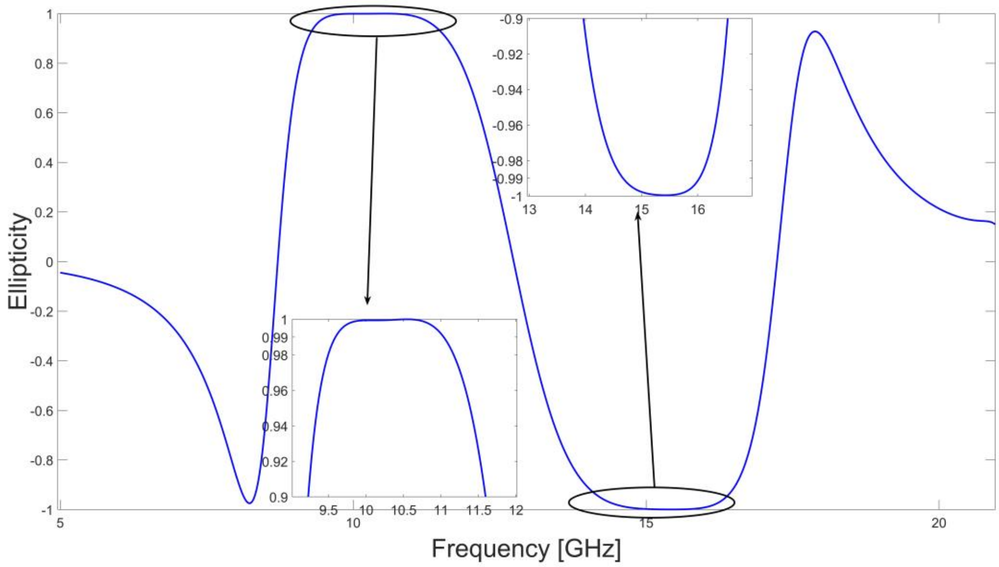

Figure 35. X and Ku Bands ultra-thin MM converter's ellipticity.

Figure 35 illustrates the ellipticitity of the ultra-thin converter, where there is two LP-CP frequency bands. In the first band there is RHCP whith an effiency more than 99% in the region from 9.6 GHz to 11 GHz, while inthe second band there is LHCP with the same results in the region from 14.68- 16 GHz (figure 31).

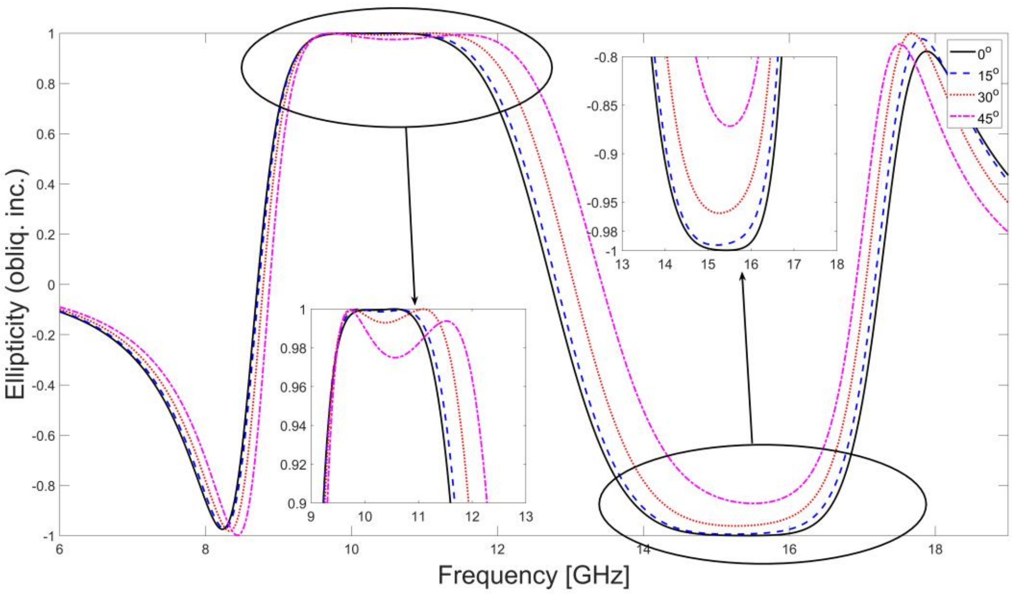

Figure 36. X and Ku Bands ultra-thin MM converter's ellipticity with oblique incident propagation.

For the oblique incident propagation (see figure 36),as in the PCR scenario, we discussed the four propagation oblique incident angles: 0^0, 15^0, 30^0, 45^0. In the case of RHCP, the efficiency still more than 99% in the case of 15^0 and 30^0, but the ellipticity could decline to less than 98% in the case of 45^0. In the LHCP region, the declining is more than before, where in the case of 15^0 the efficiency is about 98%, 30^0 the effiency is less than 95%, 45^0 the efficiency is less than 90%.

AR in dB

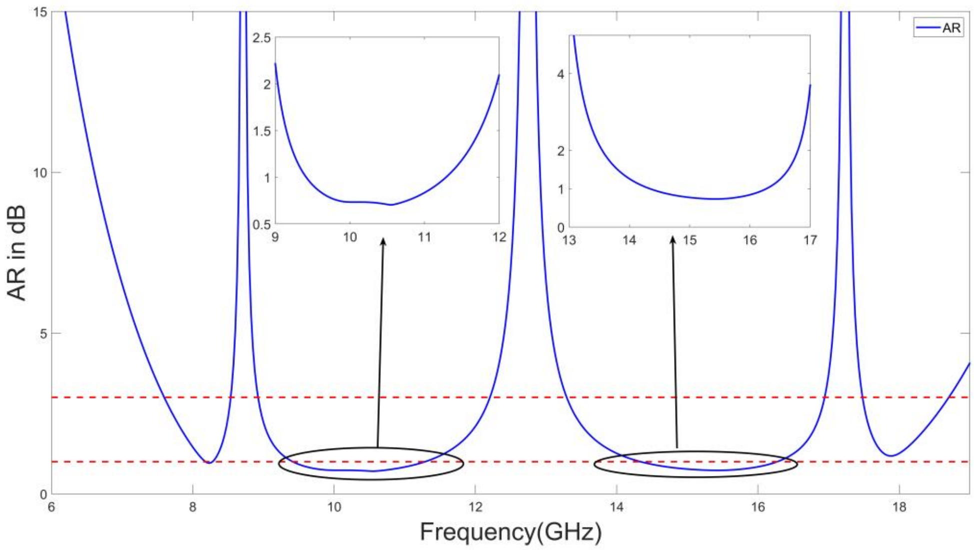

Figure 37. X and Ku Bands ultra-thin MM converter's AR in dB

We will use 1 dB as our reference for AR, even if in antenna and some application if the value of AR in dB less than 3 dB it means that there is LP-CP. As it is illlustrated from figure 37 the AR is below than 1 dB in the range 9.6-11 GHz and 14.7-16 GHz.

Reflection coefficients in u-v axes

Figure 38 illustrates that in the X and Ku bands, in which LP-LP and LP-CP persist, both $|r_{uu}|$ and $|r_{vv}|$ almost equal one. And at the same time the reflection coefficient also almost equals one. The phase angles of the reflection coefficient in the u and v orientations as well as the phase difference of the reflection coefficient will determine the type of the polarization (see fig 39). The LP-LP occurs if the amplitudes of the u-v components are equals and the phase difference of the reflection coefficient is $\mp\pi$ while the LP-CP occurs if the amplitudes of the u-v components are equals and the phase difference of the reflection coefficient is $\mp\pi/2$, in which if the angle is $+\pi/2$ then the polarization case here is RHCP and if the angle is $-\pi/2$ then the polarization case here is LHCP. The LP-LP occurs in three regions: the first region is 8.55-8.92 GHz in which the phase difference is in the range [-148^0,-210^0] and the frequency difference in the resonance frequency (8.72 GHz) is equal to exactly 180^0, the second region is 12.18-13.33 GHz in which the phase difference is in the range [$+144^0$,$+215^0$] and the frequency difference in the resonance frequency (12.73 GHz) is equal to exactly 180^0, the third region is

17-17.4 GHz in which the phase difference is in the range [-150^0, -206^0] and the frequency difference in the resonance frequency (17.21 GHz) is equal to 177^0. The LP-CP occurs in two regions: the first region is 9.6-11 GHz in which the phase difference is in the range [+88^0, +97^0] which means that the polarization here is RHCP, while the second region is 14.68-16 GHz in which the phase difference is in the range [-91^0, -97^0] which means that the polarization here is LHCP.

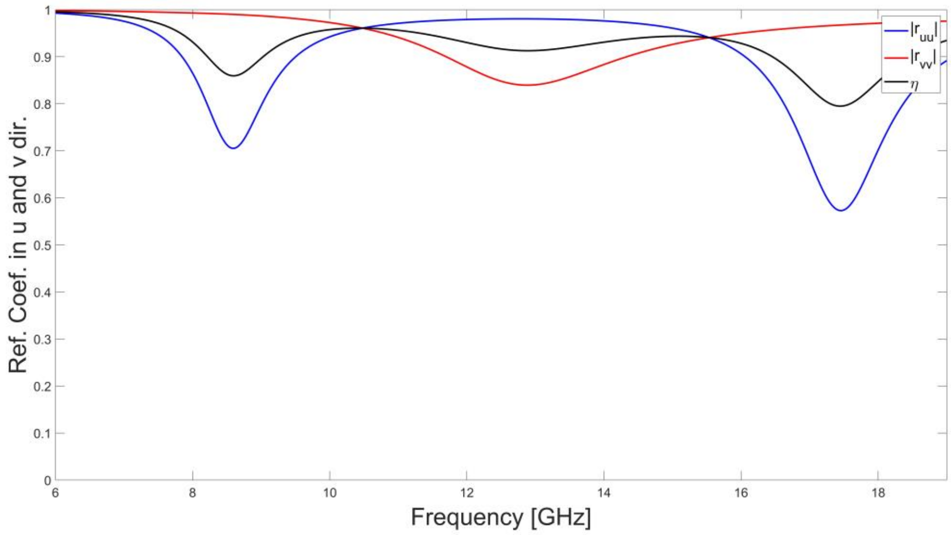

Figure 38. X and Ku Bands ultra-thin MM converter's reflection coefficients in u-v dir.

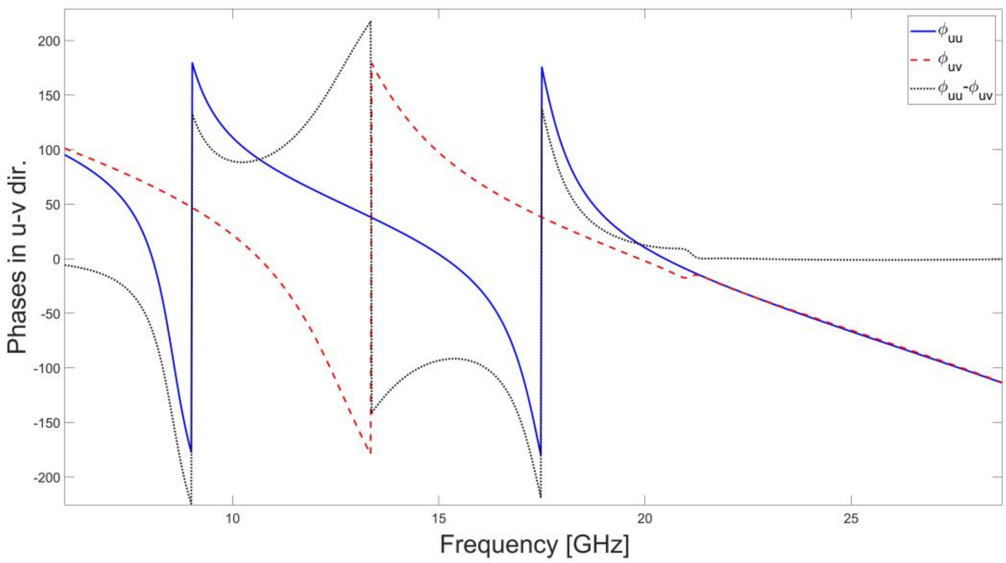

Figure 39. X and Ku Bands ultra-thin MM converter's reflection coefficients phase in u-v dir.

Surface current analysis

Examining the surface current in the upper and lower surfaces of the projected metamaterial converter is yet another analysis to better understand the working mechanism. For this reason, all resonant frequencies (8.72, 12.73, and 17.21 GHz) of the converter's resonating metal were studies. The magnetic and electric fields and the polarization effect are related in the way shown below:

$$\begin{bmatrix} J \\ M \end{bmatrix} = i\omega \begin{bmatrix} \alpha_{ee} & \alpha_{em} \\ \alpha_{me} & \alpha_{mm} \end{bmatrix} \begin{bmatrix} E \\ M \end{bmatrix} \quad (84)$$

Where the vectors **J** and **M** represents the current density of both electricity and magnetism, correspondingly. In addition, the self and linked electric and magnetic polarizations are denoted by the letters α_{ee} , α_{em}, α_{me} and α_{mm} . the surface current densities at the upper and lower surfaces are depicted in figure 40 at the three resonance frequencies (8.72, 12.73, and 17.21 GHz). Furthermore, in fig 40, the color bar's blue and red hues stands for the lowest and highest surface current densities, correspondingly. As it is demonstrated, the current densities on the metal terminal surface and metasurface are going in the opposite orientations. There is magnetic resonance at these three RFs because the surface current arrangementof the two RFs is anti-parallel.

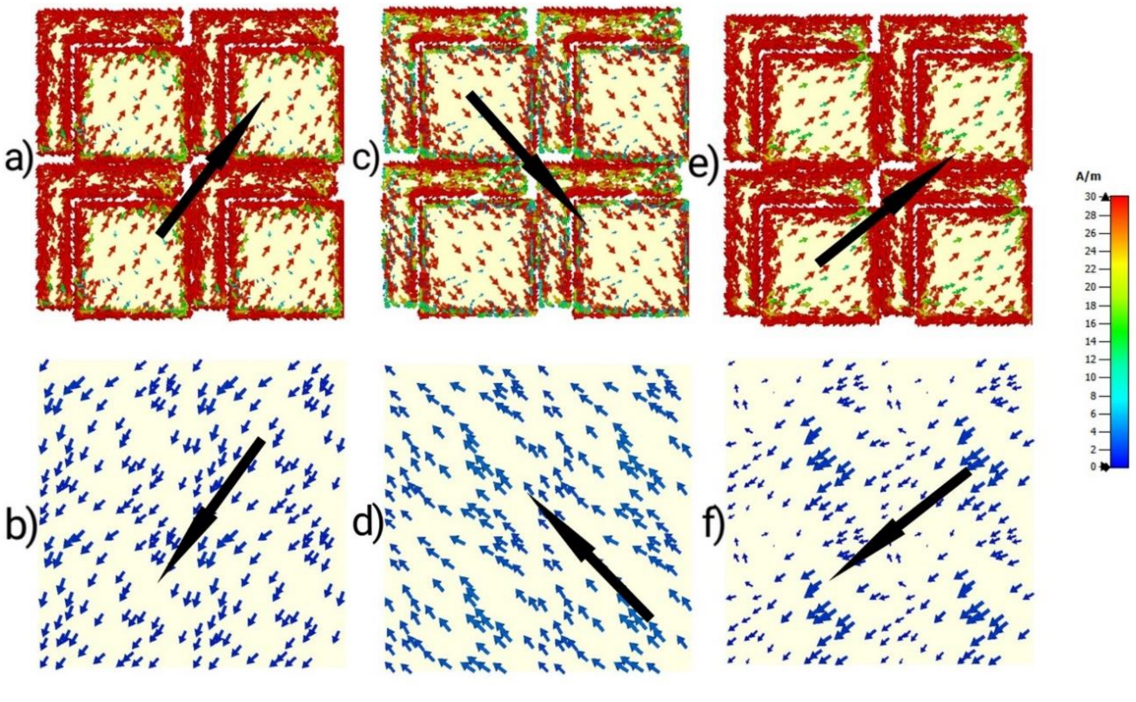

Figure 40. X and Ku Bands ultra-thin MM converter's surface current intensity.

K and Ka Bands Ultra-Thin MM Converter

In this MM converter we maintained the same design and the same thickness but we changed the period of the unit to be 2 mm. by this adjustment , as we will see later, the polarization shifted from X and Ku bands to K and Ka band. The LP-LP here is more than 90% in the frequency band 18.55-26.7 GHz and more than 99% in the frequency band from 19.55-24.8 GHz. The LP-CP here is more than 99% in the frequency band from 31.8-40.45 GHz.

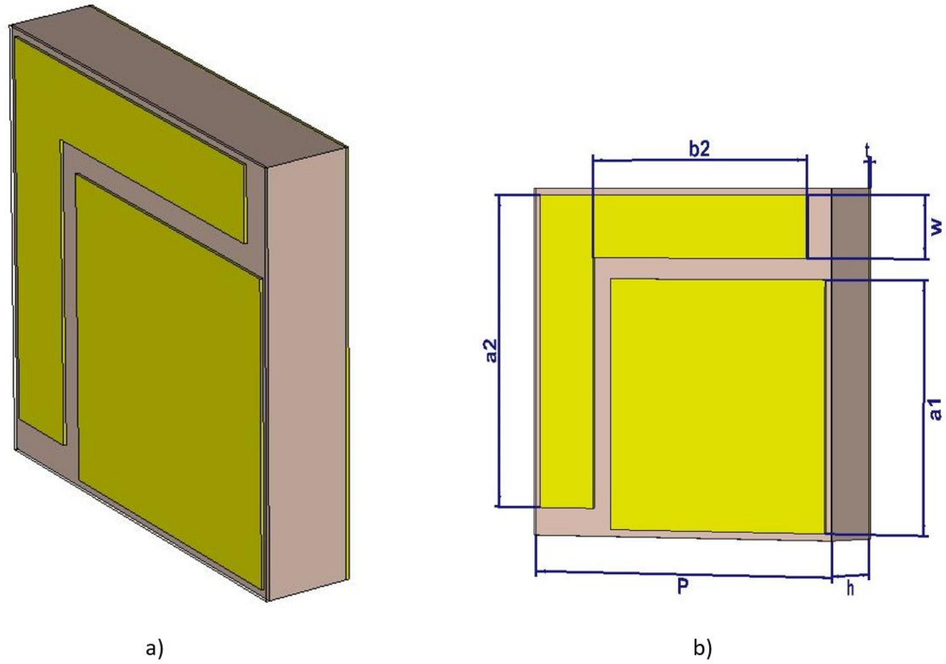

Figure 41. a) K and Ka Bands ultra-thin MM converter. b) K and Ka ultra-thin MM converter's dimensions

The rectangular base layer of the converter is made from copper, as shown in figure 41. FR4 serves as the rectangular dielectric in the middle layer. The upper layer is copper and consists of a recangular segment and a gamma Γ shaped segment. The distance between the rectangular or gamma segments and the edges is 0.1 mm. The other dimensions appeared in figure 28.b are: The periodic array P=5 mm, the thickness of the copper layers t=0.035, the thickness of the dielectric is h=1 mm, the upper layer's dimensions are: a1=1.05 mm, a2=1.7 mm, b2= 1.55 mm, w=0.15 mm.

Reflection coefficients

Figure 42 shows that there is LP-LP polarization and there could be LP-CP polarization. we will analyze linear values of reflection coefficients will be examined in figure 43 to validate the LP-LP and LP-CP occurrence, whereas figure 44 will calculate the polarization ellipse to validate the LP-CP existence.

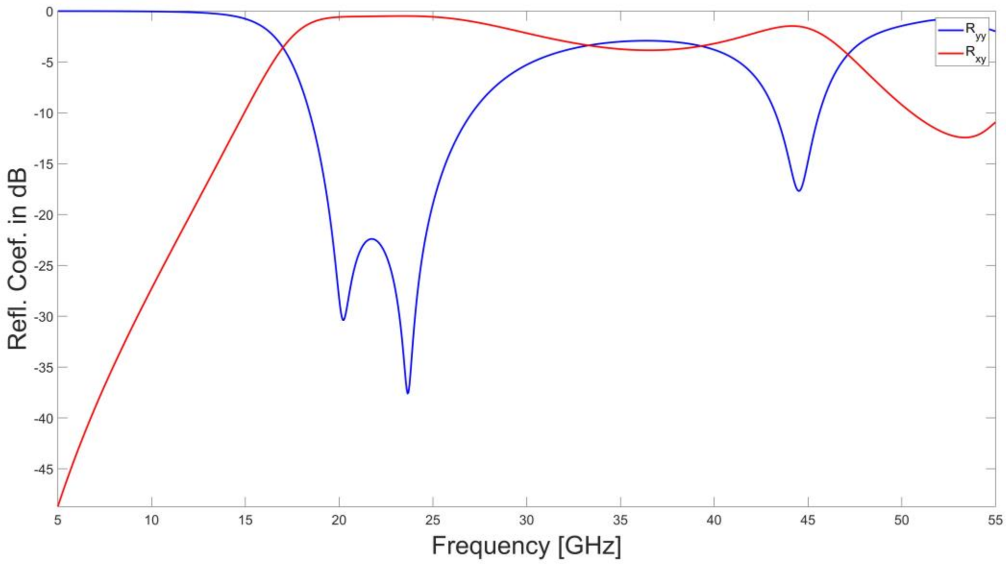

Figure 42. K and Ka Bands ultra-thin MM converter's reflection coefficients in dB.

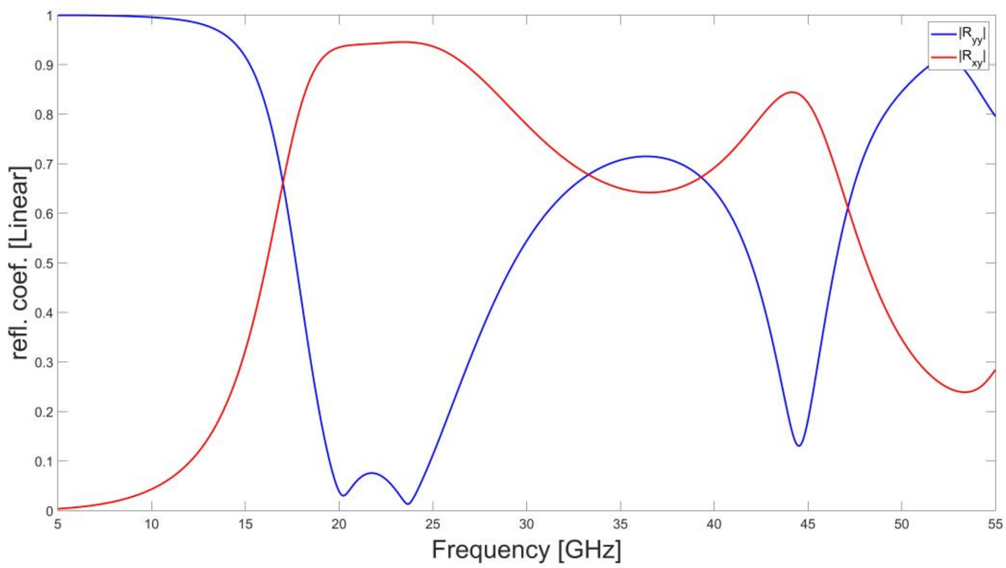

Figure 43. K and Ka Bands ultra-thin MM converter's reflection coefficients in Linear.

It could be estimated from figure 43 that there could be LP-LP in the frequency band 18-27 GHz in which the R_{yy} is less than 0.3 and R_{xy} is more than 0.8, and in the frequency range 19.5 to 25 the R_{yy} is less than 0.1 and R_{xy} is more than 0.9. we could also estimate from figure 39 that there could be LP-CP in the frequency range 31-41 GHz.

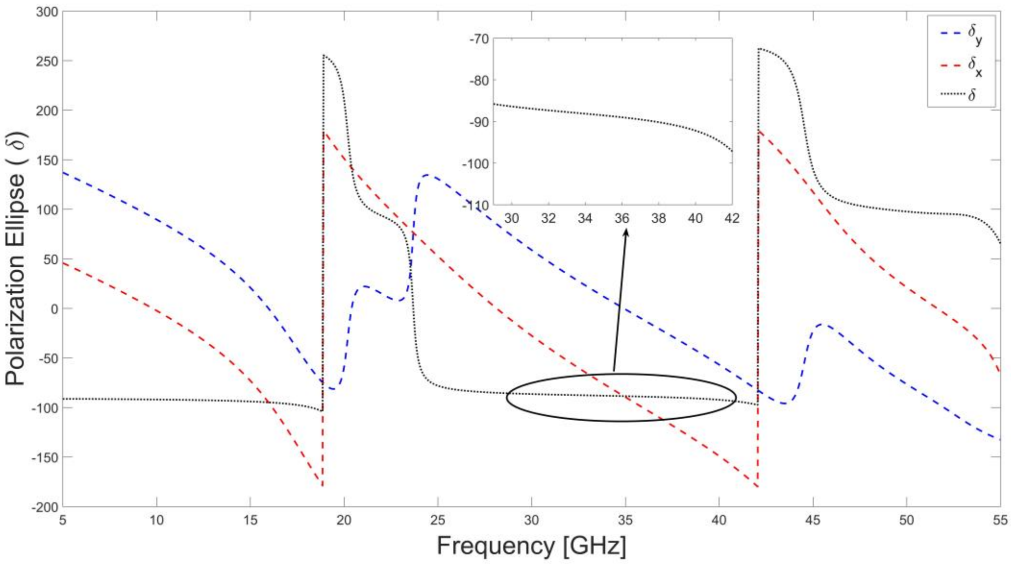

Figure 44. K and Ka Bands ultra-thin MM converter's polarization ellipse.

Two requirements must be met in order to determine the occurrence of circular polarzation: first, the amplitues of the x and y electric field must almost be equal. second the ellipse angle should be 90^0. Figure 44 shows that the the phase differnce between R_{yy} and R_{xy} is about 90^0 in the range 31-41 GHz.

After analyizing the reflection coefficients we will inspect the PCR, ellipticity and AR to verify the conversion existence.

PCR

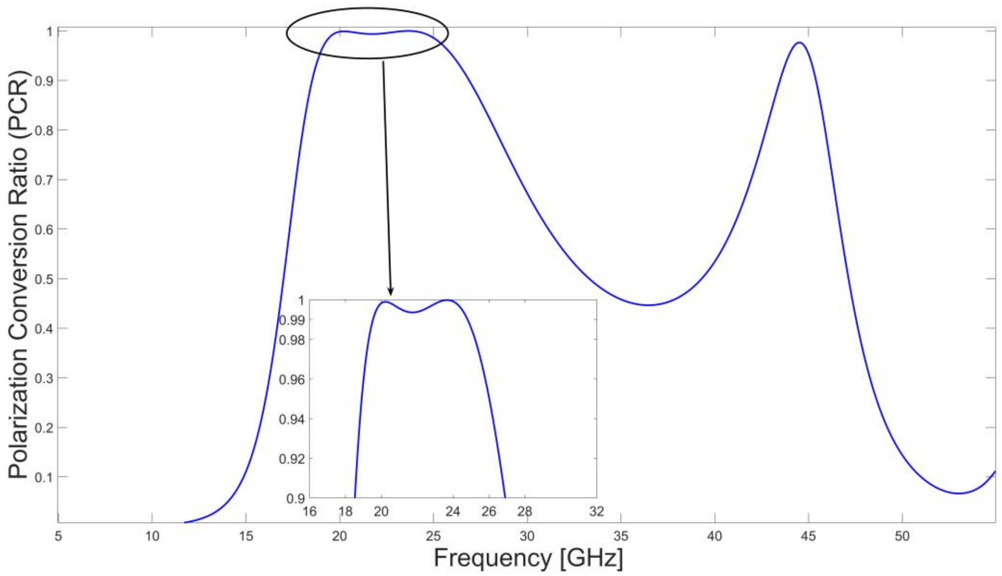

Figure 45. K and Ka Bands ultra-thin MM converter's PCR with normal incidence wave.

The PCR of the previouse specified converter is shown in figure 45, where there is LP-LP in the frequency range from 18.55 -26.9 GHz with a PCR more than 90%, whereas in the frequency range 19.55-24.8 GHz the PCR is more than 99%. We see that the LP-LP covered almost all of the K band frequency and in more than 5 GHz of the 8 GHz K band range the PCR is more than 99% which considered perfect result.

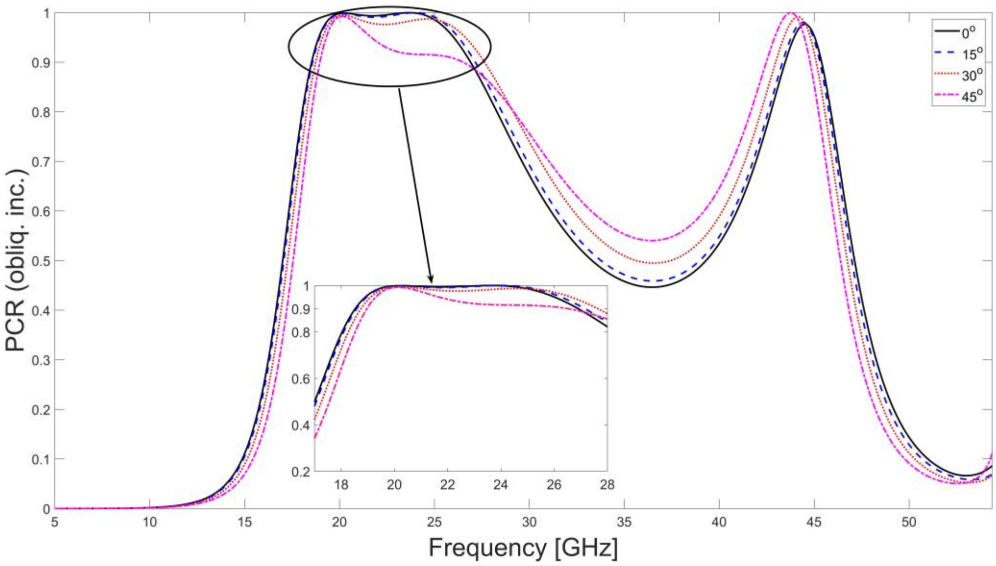

Figure 46. K and Ka Bands ultra-thin MM converter's PCR with oblique incident propagation.

Four oblique incident angles (0^0, 15^0, 30^0, 45^0) were considered for the oblique incident transmission (figure 46). For the 15^0oblique incident waves , we could say that there is almost no differnce from the direct incident, for the 30^0 the LP-LP efficency is more than 90% in the range 18.75-27.6 GHz and more than 97% in the range 19.35-26 GHz, anf for 45^0 oblique incident wave, the LP-LP efficency is above 90% in the frequency range 19-26.45 GHz and could reach to 99% in the frequency 20 GHz.

Ellipticity

we could notice from the figure 47 that the LP-CP occurs with more than 99% efficiency in the frequency range 31.8-40.45 GHz which covers more than half of the Ka band. As the ellipticity is almost -1, there is LHCP here.

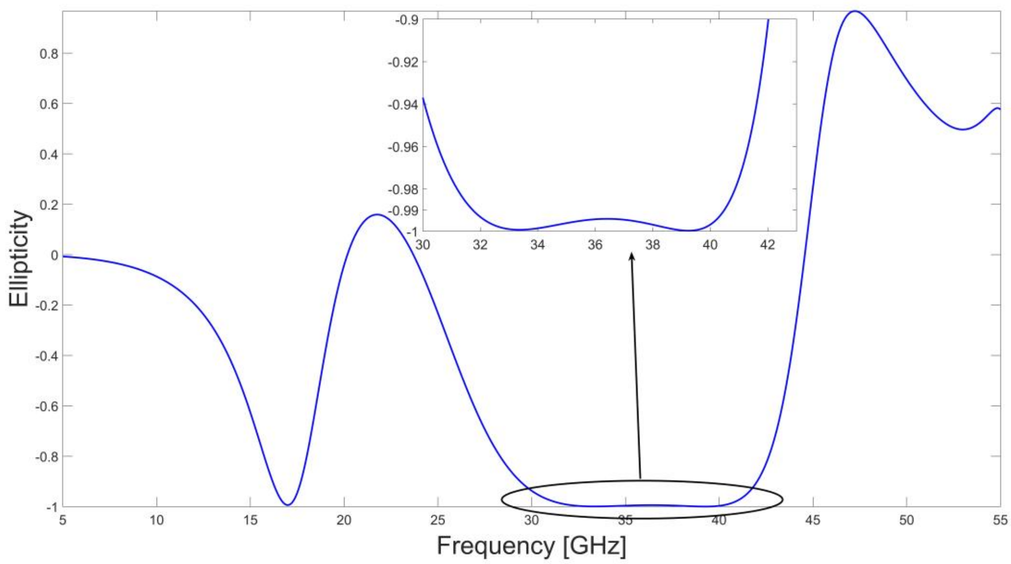

Figure 47. K and Ka Bands ultra-thin MM converter's ellipticity.

As in the PCR situation, we explored the four propagation oblique incident: 0^0, 15^0, 30^0, 45^0 (see figure 48). For the 15^0 incident wave, the LP-CP efficiency is almost more than 99% in the frequency range 32.15-38.9 GHz. For the 30^0 incident wave the LP-CP efficiency is more than 90% in the frequency range 31.3-40.5 GHz and more than 95% in the range 33.15 -38 GHz. For the 45^0 incident wave, the LP-CP efficiency is more than 80% in the range 33.3-40.3 GHz and it couldn't exceed 85%.

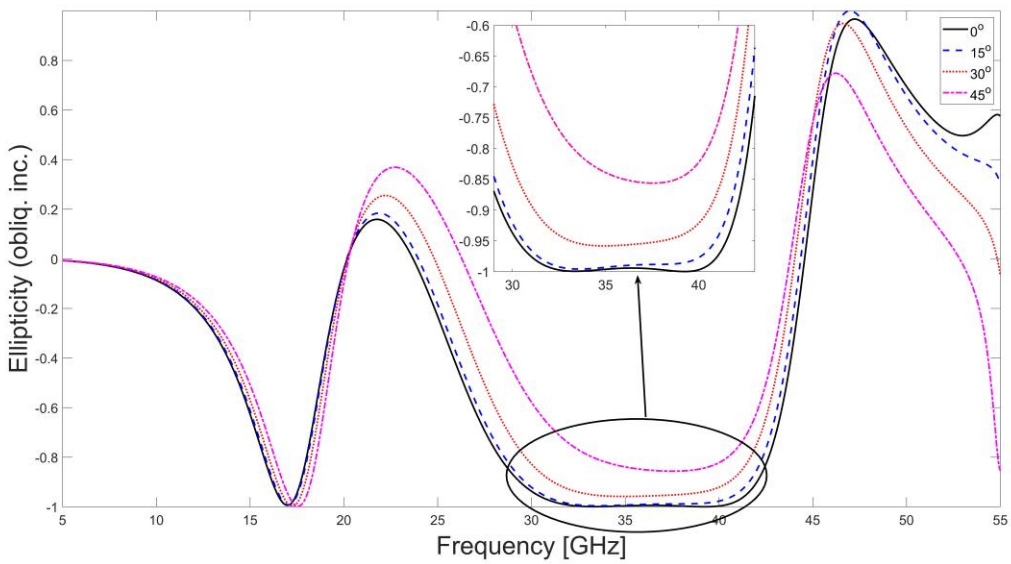

Figure 48. K and Ka Bands ultra-thin MM converter's ellipticity with oblique incident wave.

AR in dB

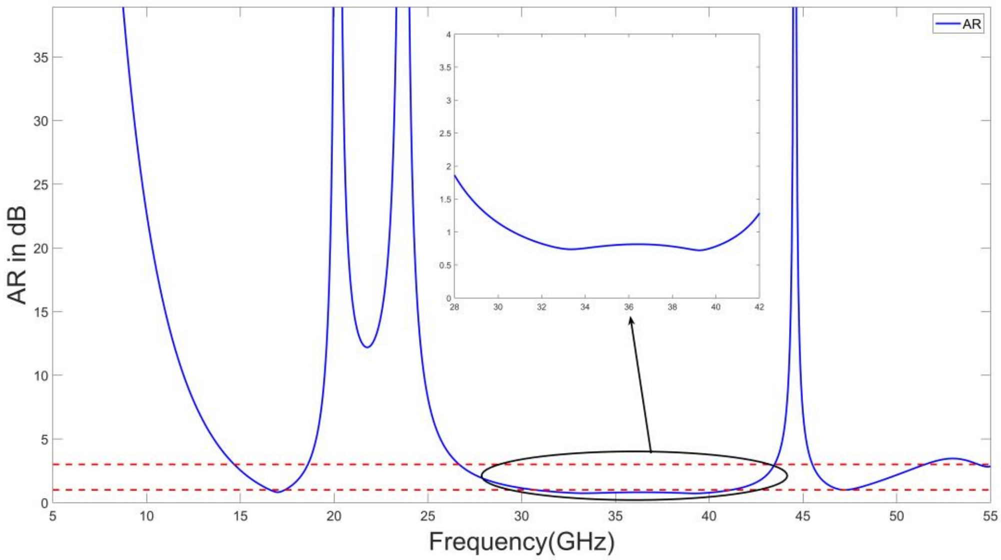

Figure 49. K and Ka Bands ultra-thin MM converter's AR in dB

We will consider here also AR equals 1 as our reference of the LP-CP existence. As it is illustrated from the figure 49, AR less than 1 in the frequency range between 30.8- 41.45 GHz which means that the polarization existence oppurtunity is high in this range.

Reflection coefficients in u-v axes

Figure 50 illustrates that in the K and Ka bands, in which LP-LP and LP-CP persist, both $|r_{uu}|$ and $|r_{vv}|$ almost equal one. And at the same time the reflection coefficient also almost equals one. The phase angles of the reflection coefficient in the u and v orientations as well as the phase difference of the reflection coefficient will determine the type of the polarization (see fig 51). The LP-LP occurs if the amplitudes of the u-v components are equals and the phase difference of the reflection coefficient is $\mp\pi$ while the LP-CP occurs if the amplitudes of the u-v components are equals and the phase difference of the reflection coefficient is $\mp\pi/2$, in which if the angle is $+\pi/2$ then the polarization case here is RHCP and if the angle is $-\pi/2$ then the polarization case here is LHCP. The LP-LP occurs in the frequency region 18.55 -26.9 GHz. in which the phase difference is in the ranges [-144^0, -163^0] and [$+170^0$, $+217^0$] where the frequency difference in the resonance frequencies 20.24 GHz and 23.66 GHz are equal to exactly 180^0. The LP-CP occurs in the region 31.3-40.5 GHz in which the phase difference is in the range [-83^0, -100^0] which means that the polarization here is LHCP.

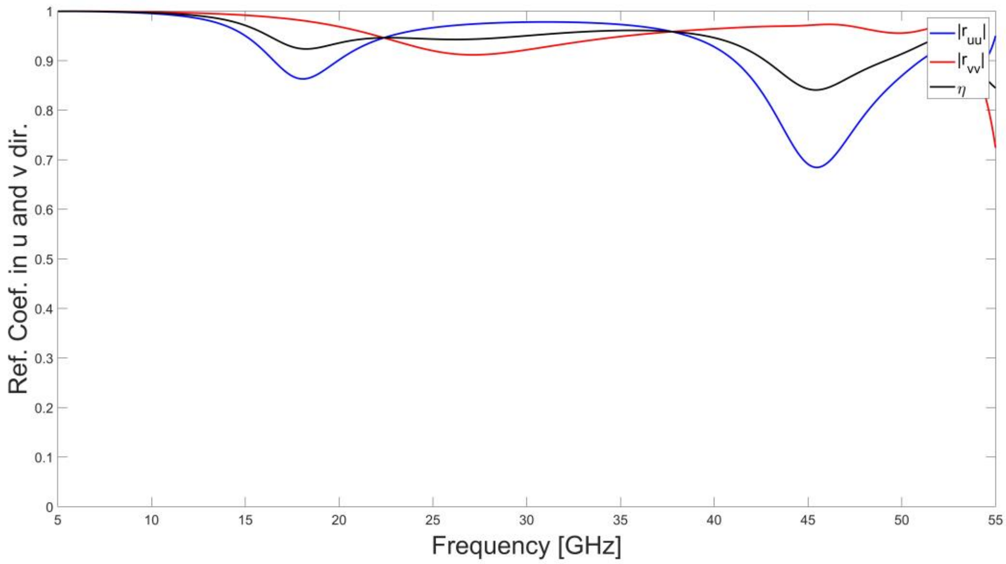

Figure 50. K and Ka Bands ultra-thin MM converter's reflection coefficients in u-v dir.

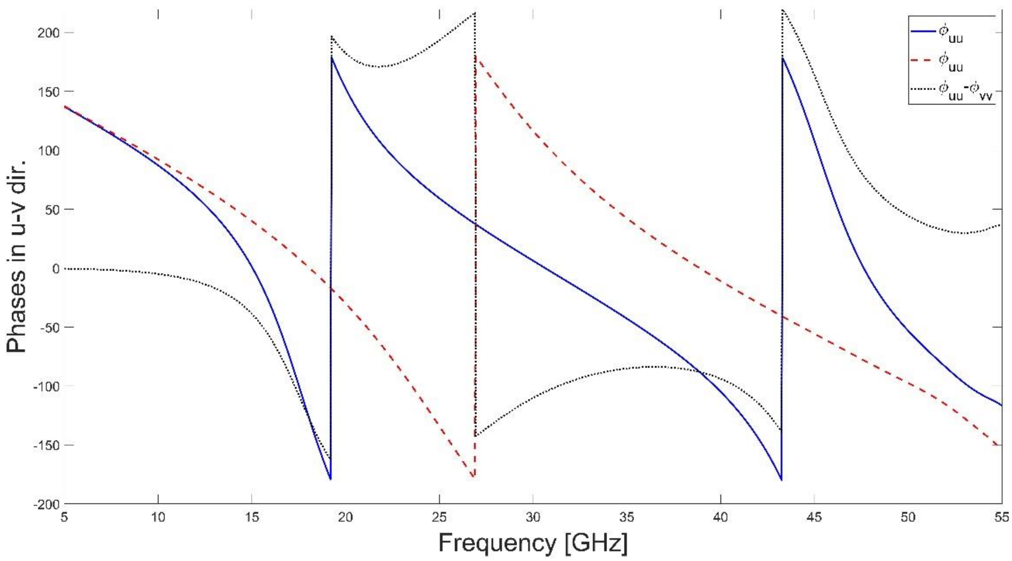

Figure 51. K and Ka Bands ultra-thin MM converter's reflection coefficients phase in u-v dir.

Surface current analysis

Examining the surface current in the upper and lower surfaces of the projected metamaterial converter is yet another analysis to better understand the working mechanism. For this reason, all resonant frequencies (20.24 and 23.66 GHz) of the converter's resonating metal were studies. The magnetic and electric fields and the polarization effect are related in the eq. 82. the surface current densities at the upper and lower surfaces are depicted in figure 52 at the two resonance frequencies 20.24 GHz and 23.66 GHz. Furthermore, in fig 52, the color bar's blue and red hues stands for the lowest and highest surface current densities, correspondingly.

As it is demonstrated, the current densities on the metal terminal surface and metasurface are going in the opposite orientations. There is magnetic resonance at these two RFs because the surface current arrangement of the two RFs is anti-parallel.

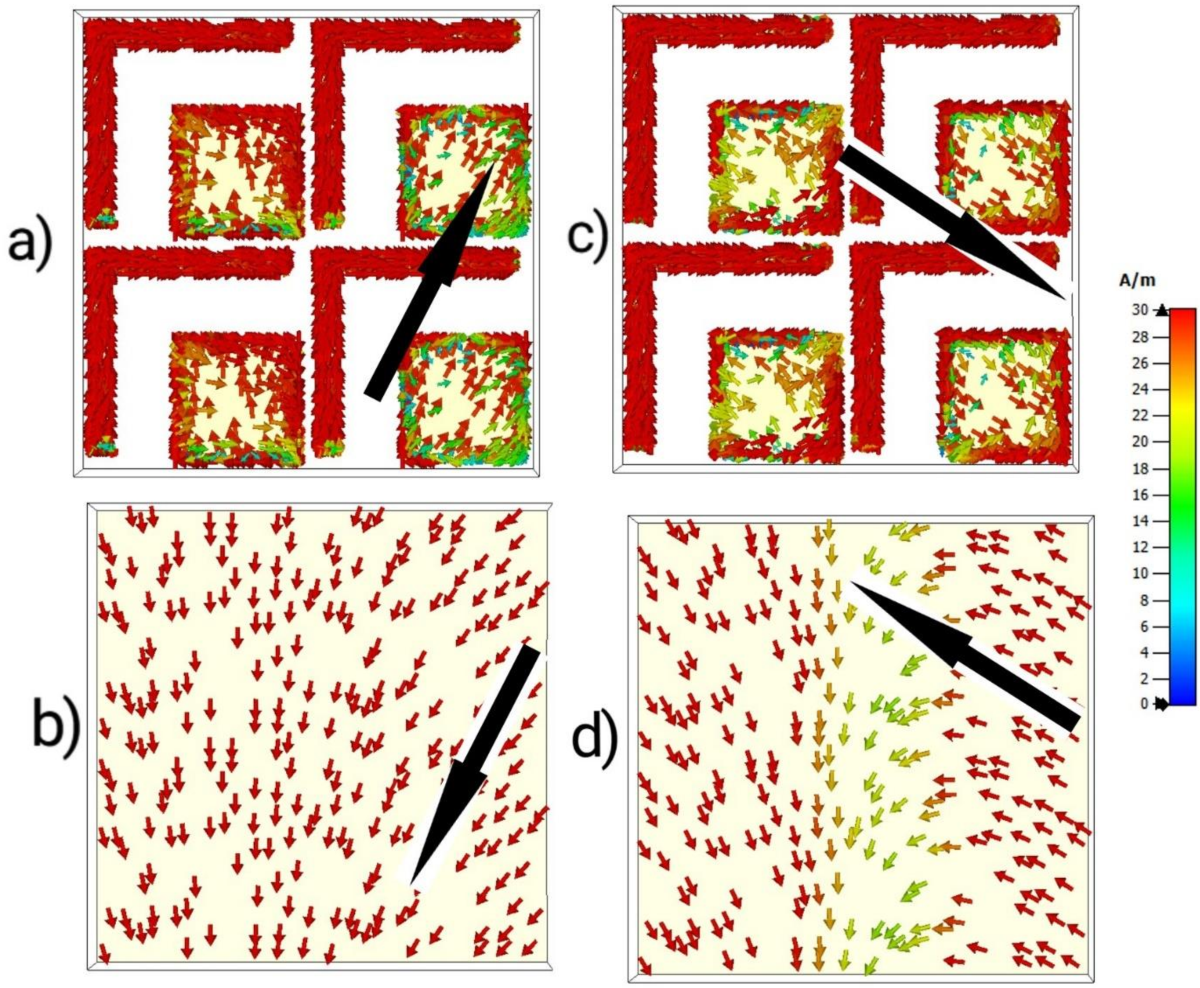

Figure 52. K and Ka Bands ultra-thin MM converter’s surface current intensity.

Comparisons

We will compare our results with the previous results in a lot of aspects. First of all, we will choose the wavelength λ in the center of each operational bandwidth. The performance of the proposed X and Ku MM converter and some previously reported polarization converters are listed in Table2. Moreover, for a more comprehensive comparison, we introduce cost-effective bandwidth, as represented below:

$$BW_{\mathrm{CE}} = \frac{\mathrm{RBW}}{R_{\mathrm{v}}} \quad (85)$$

Where RBW is the relative bandwidth and equals to $2*(f_{max} - f_{min})/ (f_{max} + f_{min})$, $Rv=T_v/\lambda^3$ is the volume of a unit cell, T_v is the total volume of a unit cell.

Table 2. Comparison of the Proposed X, Ku Ultra-Thin MM Converter With Several Reported Polarization Converters

MM Converter	Operating Bandwidth (GHz)	Conversion Type + efficiency	Angular Stability with PCR or ellipticity >0.9	Relative Thickness	Relative Period of the unit	Relative Volume	BW_{CE}
Han et al, 2018	6.7-17.1	LP-LP+90%	0^0	0.14 λ	0.48 λ	0.031	28
Chi et al, 2020	9.8-18.9	LP-LP+90%	30^0	0.08 λ	0.3 λ	0.007	56
Vu et al, 2021	12-18	LP-LP+90%	30^0	0.1 λ	0.23 λ	0.005	120
Deng et al, 2018	6.5-12.1	LP-LP+87%	0^0	0.1 λ	0.25 λ	0.006	99
	13.7-15.6	LP-CP+97%	30^0	0.15 λ	0.4 λ	0.02	5.5
Ozturk and Corapsiz, 2022	12-17.9	LP-LP+90%	30^0	0.06λ	0.33λ	0.0065	59
	11.3-11.5	LP-CP+90%	0^0	0.05λ	0.25λ	0.003	6
X, Ku MM converter	8.55-8.93	LP-LP+90%	30^0	0.03λ	0.15λ	0.0006	70
	12.18-13.33	LP-LP+90%	30^0	0.04λ	0.21λ	0.002	47
	17-17.4	LP-LP+90%	30^0	0.06λ	0.29λ	0.005	5
	9.6-11	LP-CP+99%	60^0	0.03λ	0.17 λ	0.001	134
	14.68-16	LP-CP+99%	40^0	0.05λ	0.26λ	0.003	26

The above table (Table 2) makes evident that our converter produces better outcomes than other converters. Our converter provides many outcomes for the relative thickness, with the best result perhaps being 0.03, while the other's best result is 0.05. (Ozturk and Corapsiz,2022). Our best result for the relative period of the unit is 0.15, whereas the best result for the other is 0.23. (vu et al, 2021). Our best result for the Relative volume is 0.0006, while the other's is 0.005. Our best result for the most cost-effective bandwidth is 134, whereas the other's is 120. The proposed converter may efficiently convert up to 60^0 for the oblique incident waves in the case of RHCP, whereas the other's best result is 30^0. In terms of PCR, the suggested converter could achieve more than 99%, while the others could produce results that were comparable. In terms of ellipticity, our converter provides us with more than 99% in the working bandwidth whereas the other's is, at most, more than 97%.

Table 3. Comparison of the Proposed k, Ka Ultra-thin MM Converter With Several Reported Polarization Converters

MM Converter	Operating Bandwidth (GHz)	Conversion Type + efficiency	Angular Stability with PCR or ellipticity >0.9	Relative Thickness	Period of the unit	Relative Volume	BW_{CE}
Rohde et al, 2021	18-40	LP-LP+92%	40^0	0.12λ	0.34 λ	0.0133	57
Couto et al, 2021	13.8-40	LP-LP+94%	30^0	0.18 λ	0.32 λ	0.019	51
Fahad et al, 2020	25.4-31.4	LP-CP+90%	25^0	0.02 λ	0.67 λ	0.013	16.5
	35.4-42.4	LP-CP+90%	25^0	0.04 λ	0.9 λ	0.033	5.5
Coskun et al, 2022	16.2-16.7	LP-CP+90%	-	0.07	0.19	0.002	14
	17.9-43.2	LP-LP +75%	30^0	0.12λ	0.34λ	0.014	59
k, Ka MM converter	18.6-26.7	LP-LP+90%	40^0	0.075λ	0.15λ	0.0017	210
	31.8-40.5	LP-CP+99%	30^0	0.12λ	0.24λ	0.007	34

The preceding table (Table 3) clearly shows that our converter outperforms other converters in terms of results. Only for the relative thickness, some of the other results are better, with our greatest result perhaps being 0.075 and the best result from the other being 0.02. (Fahad et al, 2020). Our best outcome for the unit's relative period is 0.15, whereas the best outcome for the other is 0.32 (Couto et al, 2021). Our top Relative volume result is 0.0017, whereas the other's is 0.013 (Fahad et al, 2020). In comparison to the other, our top result for the most cost-effective bandwidth is 210, while theirs is 57. For the oblique incident waves in the case of LP-CP, the proposed converter can effectively convert up to 40^0, whereas the other's best result is 40^0. With regard to PCR, the indicated converter could obtain more than 99% in almost all the working frequency, while the others could deliver about 94%. In terms of ellipticity, our converter offers us more than 99% in the working bandwidth whereas the other's is, at most, more than 97%.

CONCLUSION AND RECOMMENDATION

In this study, LP-LP and LP-CP conversion was performed based on ultra-thin metamaterial converter. the MM converter could work in more than one frequency band depending on the period of the array diemnsion. The designed converters has the same shape structure and thickness of 1 mm but different period of unit dimension, where the first design is 5x5 mm rectangular shaped MM converter and the second design is 2x2 mm recatngular shaped MM converter. The design was carried out with the CST simulation program and the results was calculated by MATLAB For the first metematerail converter, a good result was obtained in the X and K frequency bands, where there are three LP-LP conversion regions with more than 90% linear polarization efficiency in the frequency bandwidth ranges 8.55-8.925 Ghz, 12.18-13.33 and 17-17.4 GHz and two LP-CP conversion regions with circular polarization efficiency more thand 99% and AR less than 1 dB in the frequency bandwidth ranges 9.6 -11 GHz (RHCP) and 14.68- 16 GHz (LHCP). For the oblique incident waves in the LP-LP state, the results still good till 30^0, and for the 45^0 the results not bad but there is a frequency shift in the working frequency regions, whereas the results in the oblique incident wave in the LP-CP state still perfect in the RHCP region up to 30^0 and good up to 45^0, and for the LHCP results is good in the 15^0 case, acceptable in the 30^0 case, not acceptable in the 45^0. In the second metamaterial converter, the results is perfect in the K and Ka frequency bands with a conversion ratio more than 99% for both LP-LP in the frequency band region 19.55-24.8 GHz and LP-CP in the frequency band region 31.8-40.45 GHZ. In the cases of LP-LP, the polarization efficiency is more than 90% in the frequency range 18.55 -26.9 GHz and more than 99% in the frequency ragne 19.55-24.8 GHz, whereas in the LP-CP case the AR is less than 1 dB and the efficency is more thant 99% in the frequency range 31.8-40.45 GHZ. For the LP-LP oblique incident wave, the conversion efficiency results for 15^0, $30^0$and 45^0 are 99%, 97% and 90% respectively with a phase change in the 45^0 case. For the LP-CP oblique incident wave, the conversion efficiency results are: more than 99% in the 15^0 case, more than 90% in the frequency range 31.3-40.5 GHz in the 30^0 case and less than 85% in the 45^0 case. At last we made a comarison between the two proposed two converters several reported polarization converters each in its operating bandwidth. The results for the X, Ku MM converter was greater than the others in all of the compared aspects. For the most important aspect (BW_{CE}) we could accomplish 134 while the other's is 120. For the K, Ka MM converter the results were also good and better than the others' in all the aspects except for the relative thickness. However, we accomplished the greatest result in the most important aspect (BW_{CE}), we achieved 210 while the others' is 57.

REFERENCES

Adamczyk, B. (2017). Foundations of Electromagnetic Compatibility: with Practical Applications. John Wiley & Sons.

Ahmed, A., Abutarboush, H. F., Ahmed, F., & Tahir, F. A. (2020, March). An Efficient Anisotropic Metasurface for Linear and Circular-Polarization Conversion Applications. In 2020 14th European Conference on Antennas and Propagation (EuCAP) (pp. 1-3). IEEE.

Balanis, C. A. (1999). Advanced engineering electromagnetics. John Wiley & Sons.

Balanis, C. A. (2012). Advanced engineering electromagnetics. John Wiley & Sons.

Boardman, A. D., Grimalsky, V. V., Kivshar, Y. S., Koshevaya, S. V., Lapine, M., Litchinitser, N. M., ... & Shalaev, V. M. (2011). Active and tunable metamaterials. Laser & Photonics Reviews, 5(2), 287-307.

Chen, H. T., Taylor, A. J., & Yu, N. (2016). A review of metasurfaces: physics and applications. Reports on progress in physics, 79(7), 076401.

Coskun, A., Hasar, U. C., Ozmen, A., & Ertugrul, M. (2022). Easy-to-Implement Ultra-Thin, Wide-Band, and Multi-Functional Polarization Converter for K and Ka Band Applications. Advanced Theory and Simulations, 5(4), 2100543.

Couto, M. M., Silva, M. W. B., & Campos, A. L. P. S. (2021). A novel ultra-wideband reflective cross-polarization converter based on anisotropic metasurface. Journal of Electromagnetic Waves and Applications, 35(12), 1652-1662.

Cummer, S. A., Christensen, J., & Alù, A. (2016). Controlling sound with acoustic metamaterials. Nature Reviews Materials, 1(3), 1-13.

Danner, A. J., Tyc, T., & Leonhardt, U. (2011). Controlling birefringence in dielectrics. Nature Photonics, 5(6), 357-359.

Del Barrio, S. C. (2010). Enhancement of electrically small antennas prop-erties with metamaterials.

Deng, G., Sun, H., Lv, K., Yang, J., Yin, Z., & Chi, B. (2020). An efficient wideband cross-polarization converter manufactured by stacking metal/dielectric multilayers via 3D printing. Journal of Applied Physics, 127(9), 093103.

Ekmekci, R., & Ekmekçi, A. (2010). Sport marketing. Pamukkale Journal of Sport Sciences, 1(1), 23-30.

Engheta, N. (2008, May). Metactronics: Optical circuits and information processing in nanoworlds. In Proc. of META 08, NATO Advanced Research Workshop (p. 533).

Engheta, N., & Ziolkowski, R. W. (Eds.). (2006). Metamaterials: physics and engineering explorations. John Wiley & Sons.

Eonhardt, U. & Philbin, T. G. Geometry and Light: The Science of Invisibility (Dover, 2010).

Fahad, A. K., Ruan, C., Ali, S. A., Nazir, R., Haq, T. U., Ullah, S., & He, W. (2020). Triple-wide-band ultra-thin metasheet for transmission polarization conversion. Scientific Reports, 10(1), 1-12.

Fang, N., Lee, H., Sun, C., & Zhang, X. (2005). Sub-diffraction-limited optical imaging with a silver superlens. science, 308(5721), 534-537.

Fu, C., Sun, Z., Han, L., Liu, C., Sun, T., & Chu, P. K. (2019). High-efficiency dual-frequency reflective linear polarization converter based on metasurface for microwave bands. Applied Sciences, 9(9), 1910.

Garg, A., Sharma, R., & Dhingra, V. (2011). Polarization studies in a computer based laboratory. Latin-American Journal of Physics Education, 5(1), 17.

Hawkes, A. M., Katko, A. R., & Cummer, S. A. (2013). A microwave metamaterial with integrated power harvesting functionality. Applied Physics Letters, 103(16), 163901.

Hoa, N. T. Q., Tuan, T. S., Hieu, L. T., & Giang, B. L. (2021). Facile design of an ultra-thin broadband metamaterial absorber for C-band applications (Retraction of Vol 9, art no 468, 2019).

Hoa, N. T. Q., Tuan, T. S., Hieu, L. T., & Giang, B. L. (2021). Retraction Note: Facile design of an ultra-thin broadband metamaterial absorber for C-band applications. Scientific Reports, 11(1), 1-1.

Jiang, Y., Zhao, H., Wang, L., Wang, J., Cao, W., & Wang, Y. (2019). Broadband linear-to-circular polarization converter based on phosphorene metamaterial. Optical Materials Express, 9(5), 2088-2097.

Khan, M. I., & Tahir, F. A. (2018). A broadband cross-polarization conversion anisotropic metasurface based on multiple plasmon resonances. Chinese Physics B, 27(1), 014101.

Khan, M. I., Khalid, Z., & Tahir, F. A. (2019). Linear and circular-polarization conversion in X-band using anisotropic metasurface. Scientific reports, 9(1), 1-11.

Lamb, H. (1904). I. on the propagation of tremors over the surface of an elastic solid. Philosophical Transactions of the Royal Society of London. Series A, Containing papers of a mathematical or physical character, 203(359-371), 1-42.

Landy, N. I., Sajuyigbe, S., Mock, J. J., Smith, D. R., & Padilla, W. J. (2008). Perfect metamaterial absorber. Physical review letters, 100(20), 207402.

Marqués, R., Martin, F., & Sorolla, M. (2011). Metamaterials with negative parameters: theory, design, and microwave applications. John Wiley & Sons.

Maxwell, J. C. (1865). VIII. A dynamical theory of the electromagnetic field. Philosophical transactions of the Royal Society of London, (155), 459-512.

Moqadam, A. N., Pourziad, A., & Nikmehr, S. (2017). Radiation Forces on a Cluster of Spherical Nanoparticles in Visible Light Spectrum. Progress In Electromagnetics Research C, 75, 99-109.

Mu, D., Shu, H., Zhao, L., & An, S. (2020). A review of research on seismic metamaterials. Advanced Engineering Materials, 22(4), 1901148.

Nguyen, T. Q. H., Nguyen, T. K. T., Nguyen, T. Q. M., Cao, T. N., Phan, H. L., Luong, N. M., ... & Vu, D. L. (2021). Simple design of a wideband and wide-angle reflective linear polarization converter based on crescent-shaped metamaterial for Ku-band applications. Optics Communications, 486, 126773.

Ozturk, G., & Corapsiz, M. F. (2022). Ultra-thin reflective linear and circular polarization converter for Ku band applications. Optics Communications, 516, 128268.

Papas, C. H. (2014). Theory of electromagnetic wave propagation. Courier Corporation.

Pendry, J. B. (2000). Negative refraction makes a perfect lens. Physical review letters, 85(18), 3966.

Pendry, J. B. (2000). Negative refraction makes a perfect lens. Physical review letters, 85(18), 3966.

Pendry, J. B., & Smith, D. R. (2004). Reversing light with negative refraction. Physics today, 57, 37-43.

Pendry, J. B., Holden, A. J., Robbins, D. J., & Stewart, W. J. (1998). Low frequency plasmons in thin-wire structures. Journal of Physics: Condensed Matter, 10(22), 4785.

Pendry, J. B., Holden, A. J., Robbins, D. J., & Stewart, W. J. (1999). Magnetism from conductors and enhanced nonlinear phenomena. IEEE transactions on microwave theory and techniques, 47(11), 2075-2084.

Pendry, J. B., Holden, A. J., Stewart, W. J., & Youngs, I. (1996). Extremely low frequency plasmons in metallic mesostructures. Physical review letters, 76(25), 4773.

Rahm, M., Schurig, D., Roberts, D. A., Cummer, S. A., Smith, D. R., & Pendry, J. B. (2008). Design of electromagnetic cloaks and concentrators using form-invariant coordinate transformations of Maxwell's equations. Photonics and Nanostructures-fundamentals and Applications, 6(1), 87-95.

Schurig, D., Mock, J. J., Justice, B. J., Cummer, S. A., Pendry, J. B., Starr, A. F., & Smith, D. R. (2006). Metamaterial electromagnetic cloak at microwave frequencies. Science, 314(5801), 977-980.

Schuster, A. (1905). Radiation through a foggy atmosphere. The astrophysical journal, 21, 1.

Shi, L. (2012). Thermal and thermoelectric transport in nanostructures and low-dimensional systems. Nanoscale and Microscale Thermophysical Engineering, 16(2), 79-116. Shi, L. (2012). Thermal and thermoelectric transport in nanostructures and low-dimensional systems. Nanoscale and Microscale Thermophysical Engineering, 16(2), 79-116.

Shukoor, M. A., Dey, S., Koul, S. K., Poddar, A. K., & Rohde, U. L. (2021). Broadband linear-cross and circular-circular polarizers with minimal bandwidth reduction at higher oblique angles for RCS applications. International Journal of RF and Microwave Computer-Aided Engineering, 31(7), e22693.

Smith, D. R., Padilla, W. J., Vier, D. C., Nemat-Nasser, S. C., & Schultz, S. (2000). Composite medium with simultaneously negative permeability and permittivity. Physical review letters, 84(18), 4184.

Smith, D. R., Padilla, W. J., Vier, D. C., Nemat-Nasser, S. C., & Schultz, S. (2000). Composite medium with simultaneously negative permeability and permittivity. Physical review letters, 84(18), 4184.

Tutar, F., & Ozturk, G. (2022). An effective metasurface-based linear and circular polarization converter for C-and X-band applications. Optical Materials, 128, 112355.

Ung, B. (2009). Metamaterials: a metareview. Ecole Polytechnique of Montreal: http://www. polymtl. ca/phys/doc/art_2_2. pdf, 1.

Upadhyaya, T. K., Kosta, S. P., Jyoti, R., & Palandoken, M. (2014). Negative refractive index material-inspired 90-deg electrically tilted ultra wideband resonator. Optical Engineering, 53(10), 107104.

Valentine, J., Zhang, S., Zentgraf, T., Ulin-Avila, E., Genov, D. A., Bartal, G., & Zhang, X. (2008). Three-dimensional optical metamaterial with a negative refractive index. nature, 455(7211), 376.

Veselago, V. G. (1967). Electrodynamics of substances with simultaneously negative and. Usp. fiz. nauk, 92(7), 517.

Xu, J., Li, R., Wang, S., & Han, T. (2018). Ultra-broadband linear polarization converter based on anisotropic metasurface. Optics Express, 26(20), 26235-26241.

Xu, W., Xie, L., & Ying, Y. (2017). Mechanisms and applications of terahertz metamaterial sensing: a review. Nanoscale, 9(37), 13864-13878.

Yu, Y., Xiao, F., He, C., Jin, R., & Zhu, W. (2020). Double-arrow metasurface for dual-band and dual-mode polarization conversion. Optics express, 28(8), 11797-11805.

Zhao, Y., & Alù, A. (2011). Manipulating light polarization with ultrathin plasmonic metasurfaces. Physical Review B, 84(20), 205428.

Zhao, Y., Qi, B., Niu, T., Mei, Z., Qiao, L., & Zhao, Y. (2019). Ultra-wideband and wide-angle polarization rotator based on double W-shaped metasurface. AIP Advances, 9(8), 085013.

Zheng, Q., Guo, C., & Ding, J. (2018). Wideband metasurface-based reflective polarization converter for linear-to-linear and linear-to-circular polarization conversion. IEEE Antennas and Wireless Propagation Letters, 17(8), 1459-1463.

CURRICULUM VITAE

Kişisel Bilgiler	
Name Surname :	Fadi ALAHMED ALBASY
Birth date :	
Birth place :	
Nationality :	
Address :	
Tel :	
E-mail :	
Education	
High school :	Alfurat (Syria)
Bachelor :	Damascus University
Language Knowledge	
English :	Professional
Turkish :	Professional
Arabic :	Native
Membership Professional Organizations	